STRUCTURAL INSIGHTS INTO THE MODULATION OF BACTERIAL PEPTIDOGLYCAN SYNTHASE ACTIVITY

by

Nathanael Adam Caveney

B.Sc., The University of Victoria, 2015

A THESIS SUBMITTED IN PARTIAL FULFILLMENT OF

THE REQUIREMENTS FOR THE DEGREE OF

DOCTOR OF PHILOSOPHY

in

THE FACULTY OF GRADUATE AND POSTDOCTORAL STUDIES

(Biochemistry and Molecular Biology)

THE UNIVERSITY OF BRITISH COLUMBIA

(Vancouver)

July 2020

The following individuals certify that they have read, and recommend to the Faculty of Graduate and Postdoctoral Studies for acceptance, the dissertation entitled:

Structural insights into the modulation of bacterial peptidoglycan synthase activity

submitted by Nathanael A. Caveney in partial fulfillment of the requirements for

the degree of Doctor of Philosophy

in Biochemistry and Molecular Biology

Examining Committee:

Natalie C. J. Strynadka, Professor, Biochemistry and Molecular Biology, UBC
Supervisor

Rachel C. Fernandez, Professor, Microbiology and Immunology, UBC
Supervisory Committee Member

Calvin K. Yip, Associate Professor, Biochemistry and Molecular Biology, UBC
Supervisory Committee Member

Nobuhiko Tokuriki, Associate Professor, Biochemistry and Molecular Biology, UBC
University Examiner

Martin Tanner, Professor, Chemistry, UBC
University Examiner

Alessandra Polissi, Professor, Pharmacological Sciences, University of Milan
External Examiner

Abstract

The bacterial cell wall plays a crucial role in cellular viability and is an important drug target. The bacterial cell wall is constructed using a complex biosynthetic pathway, which ultimately terminates in the activity of peptidoglycan synthases. These synthases act to polymerize the lipid-linked cell wall precursors and crosslink these strands into the existing sacculus. The activity of these synthases can be modulated in two key ways. First, there are proteins which modulate the type of synthase activity. In most bacteria, the peptidoglycan synthase crosslinking reaction uses D,D-transpeptidase activity. However, an alternate crosslinking mechanism involving the formation of a complex between peptidoglycan synthases and the L,D-transpeptidase YcbB can lead to bypass of D,D-transpeptidation, β-lactam resistance, typhoid toxin release, and stress linked cell wall crosslinking. Second, there are proteins which associate with peptidoglycan synthases to stimulate or inhibit the canonical synthase activity. In *E. coli*, there are the positive regulators LpoA and LpoB, and the negative regulator CpoB. These proteins seen in *E. coli* are conserved across a large number of Gram-negative organisms, though the human pathogen *P. aeruginosa* is seen to have an alternative to LpoB, known as LpoP. Here, we provide insight into the structure and function of YcbB and LpoP. We show that the crystallographic structure of YcbB from *E. coli*, *S*. Typhi, and *C. rodentium* consists of a conserved L,D-transpeptidase catalytic domain, substrate capping loop subdomain, peptidoglycan-binding domain and scaffolding domain. Meropenem and ertapenem acylation of YcbB gives insight into inhibition by carbapenems, the singular antibiotic class with significant activity against L,D- transpeptidases. Additionally, we probe the interaction network of this pathway, assay β-lactam resistance *in vivo*, and provide insight into the role of YcbB in acute bacterial infection. Second, we show that the

crystallographic structure of LpoP consists of tandem tetratricopeptide repeats, distinct from the structure of the canonical LpoB. Using *in vitro* glycosyltransferase and transpeptidase assays, we compare and contrast the structure of LpoP- and LpoB-PBP1b systems. As a whole, this thesis provides insight into both forms of modulation of peptidoglycan synthase activity and lays the groundwork for further understanding of this complex biosynthetic pathway.

Lay Summary

Bacteria have a wall around their cells, which is important to the maintenance of bacterial life. This cellular wall is made through the use of a complex set of stepwise enzymatic reactions. This set of reactions, or pathway, terminates with enzymes called peptidoglycan synthases. These enzymes perform the last two steps in the pathway. Due to the complexity of bacterial life, these enzymes are tightly controlled, and their activity can be modulated by other proteins. Two such proteins which can modulate the activity of these peptidoglycan synthases are YcbB and LpoP. YcbB acts to change the way in which the synthase performs its final step, while LpoP acts to stimulate both of the normal activities of the synthase. In this work, we show the structure of both YcbB and LpoP and provide crucial insight into their modulation of the synthases. This work can assist in the development of better antibiotics.

Preface

Many aspects of **Chapter 1** (**Introduction**) are influenced by and adapted from a published review. Caveney, N.A., Li, F.K.K., and Strynadka, N.C.J. (2018) Enzyme structures of the bacterial peptidoglycan and wall teichoic acid biogenesis pathways. Curr. Opin. Struct. Biol. 53:45-58. I was responsible for writing the peptidoglycan portion of this review article.

A version of **Chapter 2** has been published. Caveney, N.A. *et al*. (2019) Structural insight into YcbB-mediated beta-lactam resistance in *Escherichia coli*. Nat. Commun. 10:1849. I designed and conducted the crystallography, microscale thermophoresis, and molecular dynamics experiments, performed a majority of the analysis, and wrote the manuscript. Initial protein preps and crystals were developed by my undergraduate student Caballero, G. and microbiological assays (as in Figure 2.7) were largely performed by Voedts, H.

Chapter 3 contains the work of a collaboration between the Strynadka and Finlay laboratories at UBC. I designed, conducted, and analyzed the structural work. I was involved in the development of the bacterial strains for the mouse studies, and Deng, W., Palacios, A.S., Woodward, S., and Bozorgmehr, T. from the Finlay lab conducted the mouse experiments (as seen in Figures 3.1 and 3.2). This work is in preparation for publication.

Chapter 4 contains the work of a collaboration between the Strynadka, Simorre, and Vollmer laboratories. I designed, conducted, and analyzed the crystallographic portions of this work. As well, I was responsible for writing the majority of the manuscript. Simorre, J-P. was responsible for performing the NMR portions of the research (Figures 4.1, 4.2, and 4.7), and Egan, A. was responsible for performing the *in vitro* assays for PG synthase activity (Figures 4.5 and 4.6). This work is published, Caveney, N.A., Egan, A., *et al*. (2020) Structure of the peptidoglycan synthase activator LpoP in *Pseudomonas aeruginosa.* Structure. 28(6):643-650.

The reuse and reprint of all published work is with permission from all journals referenced.

Table of Contents

List of Tables

List of Figures

List of Symbols

α	alpha
β	beta
Δ	delta
δ	delta
γ	gamma
Å	angstrom
%	percent
°	degree
μ	micron

List of Abbreviations

β-lac^R	β-lactam resistance
β-lac^S	β-lactam sensitivity
Δδ	chemical shift perturbation
BLI	biolayer interferometry
C_{55}-P	undecaprenyl phosphate
cryoEM	cryogenic electron microscopy
DAP	diaminopimelic acid
DDM	N-dodecyl-D-maltopyranoside
DMEM	Dulbecco's modified Eagle's medium
EDC	N-(3-dimethylaminopropyl)-N′-ethylcarbodiimide
EPEC	enteropathogenic *E. coli*
EHEC	enterohemorrhagic *E. coli*
GlcNAc	*N*-acetylglucosamine
GT	glycosyltransferase
GTase	glycosyltransferase
hGPT	GlcNAc-1-P-transferase
HRV	human rhinovirus
IPTG	isopropyl β-d-1-thiogalactopyranoside
K_D	equilibrium dissociation constant
Ldt	L,D-transpeptidase
MIC	minimum inhibitory concentration

min	minute
MME	monomethyl ether
Moe A	moenomycin A
MOP	multidrug/oligosaccharidyl-lipid/polysaccharide
MST	microscale thermophoresis
MurNAc	*N*-acetylmuramic acid
MVF	mouse virulence factor
NMR	nuclear magnetic resonance
PBPs	penicillin-binding proteins
PBS	phosphate-buffered saline
PEG	polyethylene glycol
PEP	phosphoenolpyruvate
PG	peptidoglycan
PIC	protease inhibitor cocktail
PMSF	phenylmethylsulphonylfluoride
PNPT	polyisoprenyl-phosphate *N*-acetylglucosaminosugar-1-phosphate-transferase
ppGpp	alarmone
RMSD	root-mean-square deviation
SEC	size exclusion chromatography
SEDS	shape, elongation, division and sporulation
SIR	single isomorphous replacement
SPR	surface plasmon resonance
T3SS	type three secretion system

TCA	trichloroacetic acid
TM	transmembrane
TP	transpeptidase
TPase	transpeptidase
TPR	tetratricopeptide repeat
UDP	uridine diphosphate

Acknowledgements

"Am I allowed to plagiarize this part?" – Nathanael A. Caveney, as he read Dr. Craig H. Kerr's emotional and heartfelt thesis acknowledgements section in a desperate attempt for inspiration.

All joking aside, I have never been the best at these heartfelt thank-you's or much in the way of any emotional writing – perhaps an influencing factor on my desire to become a scientist. Regardless, there are so many people that have made this journey to get a PhD possible, even enjoyable, and at times fantastic, so I will try and lay out just how thankful I truly am to have you all in my life below:

First and foremost, I want to say thank you to my amazing supervisor Dr. Natalie Strynadka. It has been such an honour to work in your lab over the past five years and it truly would not have been possible without you and your mentorship. I am not completely certain what made you take a chance on me five years ago when I walked into your office for that interview. Despite my complete lack of scientific confidence in myself at the time, you took the gamble and welcomed me into the Strynadka lab family. Over the last few years you have really allowed me to develop as a scientist in my own right, all the while providing some of the most thoughtful (and downright genius) suggestions. It truly has been a great pleasure to work with you and learn from you, and I will be forever grateful.

I also want to send a heartfelt thanks to my committee members Rachel and Calvin. I am so thankful for your support over the last five years and for believing in me over the course of this PhD.

Next, I must thank my fellow members of the Strynadka lab. I won't go into a big long speech about every single one of you – as that would probably end up longer than the rest of my

thesis – but I do want to thank each and every one of you for the friendship, compassion, mentorship, and comradery you have shown me over the past five years.

In particular, I want to give the biggest shout-out to my dear friend Dr. Sean D. Workman. Honestly, I didn't know what I was getting to that one faithful day that you invited me to join the dodgeball team, but what ensued has been one of the most rewarding friendships of my life. Beyond all the shenanigans – and there were many – I have enjoyed beyond words the impact that you have had on my abilities as a scientist. You have taught me how meticulous it is possible to be as a structural biologist, and if I have picked up on even 2% of that, I think my science will be far better for it. As well, I could always rely on you to light a candle under my…rear (can I swear in this?) when I was being lazy or demotivated in the lab. I was able to be there for so many beautiful milestones in your life; your bachelor party, your wedding, your comps, your defense, etc. and I am looking forward to your future milestones (BABIES), which might even bring me to go visit Regina. I look forward to having you around for some key milestones in my life (whenever they may come – Mom, don't read into this), despite the thousands of miles of separation. Anyway, I love you bud, thanks for being you.

Ok, next I want to give the biggest shout-out to Dr. Liam J. Worrall. I don't know how you put up with my insistent questions but thank goodness you did. I have really enjoyed your mentorship in the lab over the last five years and, more recently (once I grew up a bit), your friendship. You have taught me so many things about crystallography, electron microscopy, and just how to be a good scientist. I really cannot thank you enough.

I also want to thank my (and really everyone in the lab's) "lab mom", Marija Vuckovic. Honestly, from a practical standpoint, one of the people that I could not have done this PhD without. Thanks for "helping" me with all my cloning issues over the last five years. I would

probably still be cloning genes to this day without you. Beyond the help that you provided in the lab, I cannot thank you enough for the kind friendship and support you have shown over these years. You truly are like a family member to me, helped kick my but into gear to get a girlfriend, and other motherly things.

One final lab member I need to give a huge shout-out to is my former undergrad (now turned PhD candidate extraordinaire), Guillermo Caballero. I really lucked out when Solmaz hired you and subsequently went away on maternity leave. That lovely circumstance not only lead to some of the most productive work of my PhD, but also to a beautiful friendship. I have had such a blast seeing you transform from an amazing undergraduate to an amazing PhD candidate, and I am excited to see what the future holds for you, as I believe you can do anything you put your mind to.

I want to give a big thanks to my numerous collaborators that I have had over the past five years. It has been such a pleasure to work with so many brilliant scientists from both UBC, Canada, and across the world. In particular, I want to thank Dr. Jean-Pierre Simorre for his mentorship, both locally during sabbatical, and from all the way in Grenoble. You have really taught me so much about science, but also about how to foster a collaborative environment and work as a team to perform the best science possible.

Next I want to thank all of my numerous friends at UBC for their friendship and support over the last five years. I truly consider everyone in both the BMB and M&I departments such dear friends, but I have to highlight a few of the special people that made this PhD such a magical time. The biggest thanks of all needs to go to my dodgeball/karaoke team family. I honestly cannot even imagine this PhD without you all. You guys were always there to support me in any and everything, always ready to chat our faces and thumbs off, and definitely always ready to grab a

beer during times of good or bad. Sean, Guillermo, Craig, Udit, Dan 1.0, Dan 2.0, Bill, Brown, Keith, Blair, Red, Jan, Jeff, Sam, Zach, and Sarah – you are all such amazing wonderful people.

I especially want to thank a few of the "old guard" for letting a young punk like me be your friend. Brown, Craig, Jan, Keith – you have all become such successful scientists now, and you truly have been such an inspiration to me and have shown me that I can try to achieve on that level as well. Craig, in particular, I have watched you as you absolutely crushed your PhD, obtained a sweet postdoc position, and have done amazing science. All of that, on top of being the greatest bud and always down to grab a beer and talk science. I am looking forward to the many more beers we will consume down at Stanford.

Finally, I need to thank my family. Without the unending support for you all during this, it would never have happened. I honestly cannot thank you enough. Dad – you aren't the only Dr. Caveney on the block anymore, sorry, not sorry. Thanks for showing me it was possible to get those letters before my name. Mom, I need to thank you so much for your support in particular. I know you never really understood much of anything related to my research, but you were always there to listen to me prattle on about it and show your love and support. Last but not least, I want to thank my beautiful girlfriend, Iris. I know we have only known each other for a fraction of this PhD, but it feels like I have known you my whole life. I cannot wait to see what the future has in store for us both.

For my family.

Chapter 1: Introduction

1.1 Introduction to peptidoglycan biosynthesis

The bacterial cell wall, and the unique enzymes and chemistries responsible for its biogenesis remain as attractive targets for the development of novel antibiotics. The effectiveness of disrupting peptidoglycan (PG) synthesis for treating bacterial infections is long proven and best exemplified by β-lactam antibiotics, which inhibit penicillin-binding proteins (PBPs) from catalyzing the crosslinking transpeptidation of PG (King, Sobhanifar, and Strynadka 2016). PG is composed of polymerized glycan strands of alternating β-1-4 linked *N*-acetylglucosamine (GlcNAc) and *N*-acetylmuramic acid (MurNAc), with the latter covalently bound via the D-lactoyl moiety to characteristic pentapeptide "stems" (commonly L-Ala-γ-D-Glu-*meso*-DAP (or L-Lys)-D-Ala-D-Ala where DAP is diaminopimelic acid). Crosslinking of adjacent glycan strands generally occurs between the carboxyl group of the penultimate D-Ala at position 4 and the amino group of the diamino acid at position 3, either directly or through a short peptide bridge, with the terminal D-Ala lost during the reaction. PG crosslinking is essential for the strength and viability of a bacterium and disruption of any step of PG biosynthesis, up to and including the late stage transpeptidation, typically results in cell death of bacteria in their physiological environs (Fleming 1929; Liu and Tomasz 1985; Tomasz 1986). Despite several decades of successful efforts to effectively target PG biosynthesis by the pharmaceutical industry, specifically PBP mediated transpeptidation, bacteria have inevitably developed a variety of mechanisms of resistance to these antibiotics. Examples include expression of β-lactam hydrolyzing enzymes known as β-lactamases, production of PBPs with low affinity for β-lactams, and particularly in Gram-negative

bacteria, utilization of drug efflux pumps (Sobhanifar, King, and Strynadka 2013). Another resistance mechanism of particular relevance to this is thesis is that of the L,D-transpeptidase YcbB, which has been shown to provide resistance to β-lactams through the formation of an alternate PG synthase complex with canonical PG synthase machinery (Hugonnet et al. 2016; Caveney et al. 2019). While research into developing novel β-lactams, new classes of transpeptidase inhibitors and combinatorial strategies for combating the resistance crisis are ongoing, this represents only a molecular tip of the potential multi-enzyme PG pathway to be capitalized on therapeutically. A major hurdle in this regard has been the lack of atomic level detail on many of the critical enzymes in the pathway, particularly those spanning or associated with the cytosolic membrane. Several recent structures however have now helped pave the way for future drug discovery efforts. Notably, peptidoglycan is initially synthesized in the cytoplasm on a lipid carrier, commonly undecaprenyl phosphate (C_{55}-P), with lipid-bound precursors then necessarily flipped across the membrane for covalent attachment of the polar "head" groups onto the existing cell wall in the periplasm. Subsequent recycling of the released lipid carrier back to the cytoplasmic leaflet for PG biogenesis to continue efficiently is also an essential and catalyzed end point of the process. The lipid carrier is an energetically costly molecule to synthesize and potentially membrane perturbing at high concentrations. Here, I will provide a structural overview (Figure 1.1) of recently characterized enzymes with key roles in PG biogenesis and provide additional insight into the role of two proteins, YcbB and LpoP, in the modulation of PG synthase activity.

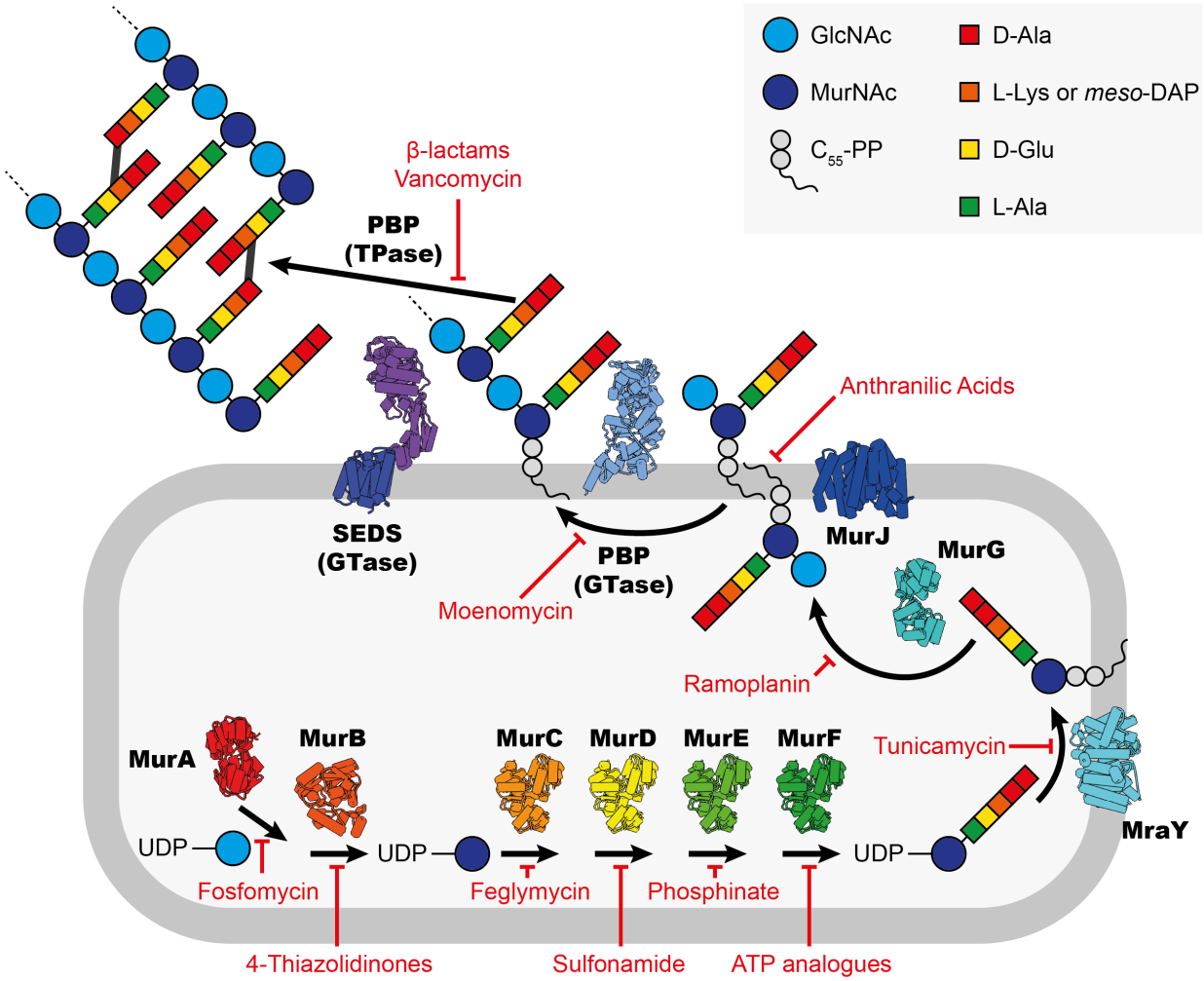

Figure 1.1 The peptidoglycan biosynthetic pathway.
Overview of the core peptidoglycan biosynthesis pathway. MurNAc-pentapeptide synthesis in the cytosol by the Mur enzymes (A-F), lipid II assembly by MraY and MurG, lipid II flipping by MurJ, and peptidoglycan synthase activity by class A PBPs or SEDS-class B PBP pairs. Enzymes are labelled in black and bold, key inhibitors of the various steps of the pathway are labelled in red, and substrates and products are coloured and described in the legend (upper right of figure). PDB IDs for the various models used are as follows: MurA – 3SPB, MurB – 4JB1, MurC-F – 1UAG, MraY – 4J72, MurG – 1NLM, MurJ – 5T77, class A PBP (PBP1b) – 5HLD, SEDS (RodA) – 6BAR, class B PBP (FtsI) – 4WEK.

1.2 The peptidoglycan biosynthetic pathway

1.2.1 Peptidoglycan pentapeptide synthesis

The first steps of PG biosynthesis occur in the bacterial cytoplasm catalyzed by several well characterized enzymes (the Mur pathway) which act successively to form a uridine diphosphate (UDP)-MurNAc pentapeptide. The first of these, MurA, transfers enolpyruvate from a phosphoenolpyruvate (PEP) acceptor substrate to donor UDP-GlcNAc (Figure 1.2 A). MurA structures have been determined from several species, in both the apo-enzyme form and in complex with a variety of ligands (Skarzynski et al. 1996; Schönbrunn et al. 1996; Zhu et al. 2012; Eschenburg et al. 2003). The bi-lobal domain architecture, each consisting of a threefold repeat of a four-stranded β-sheet, two helix subdomain, is seen to rearrange into a more compact form upon substrate binding, bringing the active site residues into position to act on the substrates. A covalent adduct of PEP is initially formed through nucleophilic attack of PEP C2 by a cysteine sulfanion. Enolpyruval UDP-GlcNAc is formed, via a tetrahedral reaction intermediate, and subsequently acted upon by the second enzyme in the cascade, the acetylenolpyruvylglucosamine reductase MurB (Figure 1.2 B). This results in conversion to UDP-MurNAc in an NADPH dependent manner. Several structures of MurB have been solved in the apo-enzyme form and in complex with substrate, revealing NADPH and enolpyruval UDP-GlcNAc bind successively to the same site, with two distinct hydride transfer reductions via a FAD cofactor occurring for each (Benson, Walsh, and Hogle 1996; Lees et al. 1996; Benson, Walsh, and Hogle 1997; Chen et al. 2013).

Subsequently, the product UDP-MurNAc undergoes a series of stepwise amino acid additions initiating at the carboxylate of the C3 D-lactoyl moiety and catalyzed by the amino acid ligases MurC-F (Figure 1.2 C). The ligases act in an ATP dependent manner and are known to have structural commonalities, despite low sequence homology. These include an N-terminal Rossmann fold, here involved in coordination of the growing substrate, a central ATPase domain and a second C-terminally disposed Rossmann fold which serves to bind the amino acid to be ligated (Spraggon et al. 2004; Yan et al. 2000; Gordon et al. 2001; Bertrand et al. 1997). MurC and MurD catalyze the addition of L-Ala and D-Glu respectively, followed by addition of mesodiaminopimelic (*meso*-DAP) acid in *E. coli* or L-Lys in *S. aureus* by MurE and finally the addition of a D-Ala-D-Ala dipeptide to form the completed UDP-MurNAc pentapeptide by MurF. The catalytic mechanism of these Mur ligases is conserved. The first step in the ligation mechanism is the activation of the nucleotide substrate by ATP through magnesium ion facilitated phosphorylation. The phosphate of the formed acyl-phosphate intermediate is then displaced by the condensing amino acid substrate via a nucleophilic attack to form the elongated peptide product (Kouidmi, Levesque, and Paradis-Bleau 2014). It has been speculated that the cytosolic Mur pathway enzymes form a complex with facilitated passage of successive products, but this remains to be demonstrated.

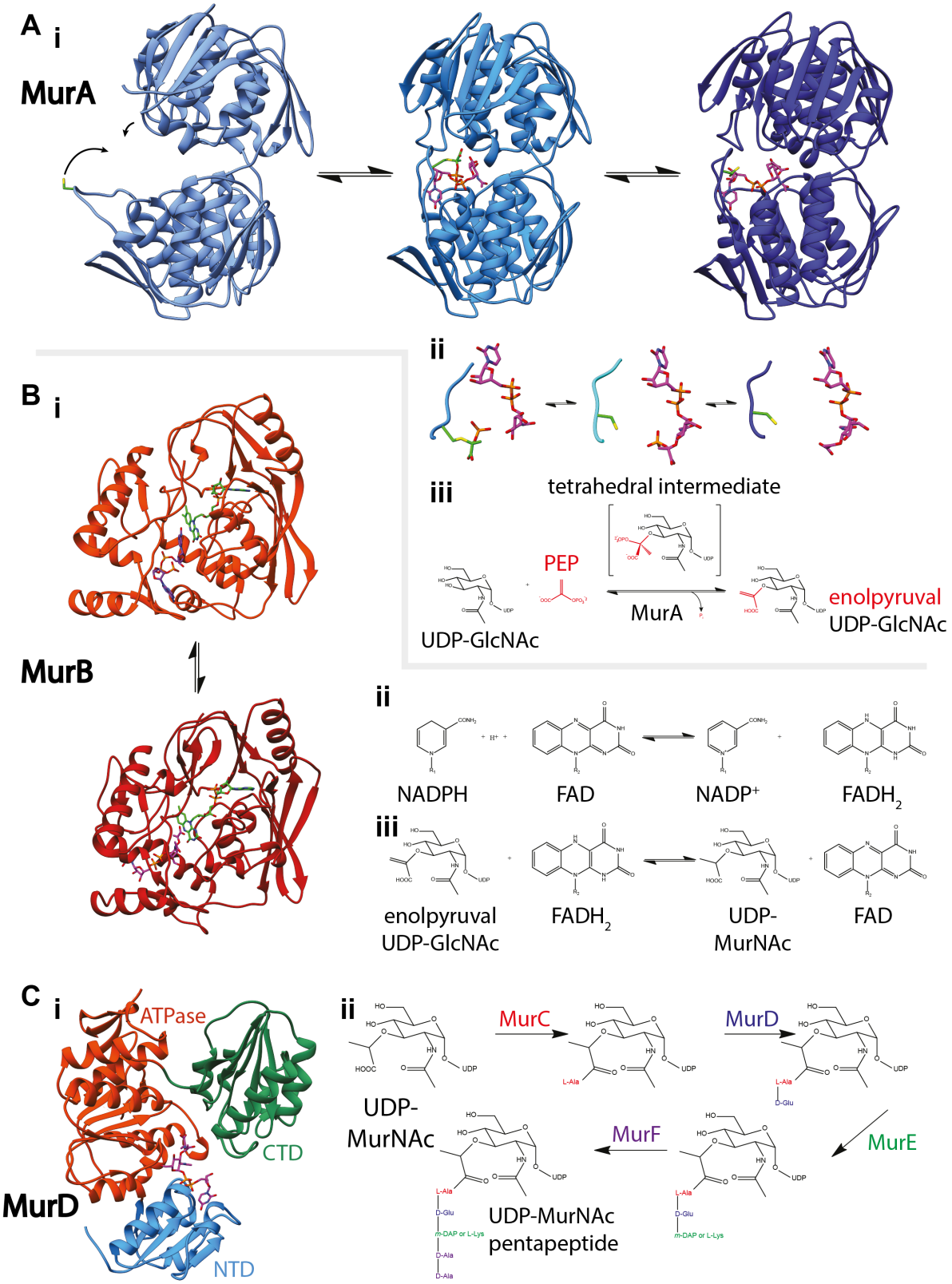
A
i
MurA
ii
tetrahedral intermediate
iii
PEP
UDP-GlcNAc
MurA
enolpyruval
UDP-GlcNAc
B
i
MurB
ii
NADPH
FAD
NADP+
FADH2
iii
enolpyruval
UDP-GlcNAc
FADH2
UDP-
MurNAc
FAD
C
i
ATPase
CTD
MurD
NTD
ii
MurC
MurD
MurE
MurF
UDP-
MurNAc
UDP-MurNAc
pentapeptide

Figure 1.2 First steps in pentapeptide synthesis catalyzed by MurA through MurF.
(**A i**) Large conformational changes are seen as the substrates, UDP-GlcNAc (magenta) and PEP (green in covalent complex with C115), bind **MurA** (blue) (*E. cloacae*, 3SPB – unliganded, 3SWA – UDP-GlcNAc and PEP, 3SWQ – enolpyruval UDP-GlcNAc). The two domains close in on the active site and the loop containing the catalytic C115 (green) swings inward to form a covalent linkage to PEP. (**A ii, iii**) After substrate binding, the conversion of UDP-GlcNAc to enolpyruval UDP-GlcNAc proceeds via a tetrahedral intermediate (*E. Cloacae*, 1Q3G), which resolves to the product with a release of inorganic phosphate. (**Bi**) **MurB** (red-orange) performs two successive reactions, the first involving the binding of FAD and NADPH and resulting in $FADH_2$ (green) and release of $NADP^+$ (purple) (*P. aeruginosa*, 4JB1). Upon $NADP^+$ release, enolpyruval UDP-GlcNAc (magenta) (*E. coli*, 2MBR) binds and is reduced to UDP-MurNAc. (**B ii**) The first reduction-oxidation reaction, involving NADPH and FAD, and (**B iii**) the second, involving enolpyruval UDP-GlcNAc and $FADH_2$. (**C i**) Tri-domain architecture of MurD (*E. coli*, 1UAG), characteristic of **MurC-F**, showing the N-terminal substrate binding domain (blue), ATPase domain (orange) and C-terminal amino acid binding domain (green). The MurC product and MurD substrate, UDP-MurNAc-L-Ala, is seen bound to the substrate binding domain. (**C ii**) An outline of the various enzymatic amino acid additions to UDP-MurNAc, which form UDP-MurNAc pentapeptide. Adapted from (Caveney, Li, and Strynadka 2018).

1.2.2 Assembly of the lipid II building block of peptidoglycan

In the first membrane-associated step of PG synthesis, this product is transferred to a C_{55}-P lipid carrier. *De novo* synthesis of C_{55}-P occurs through successive condensation catalyzed by the synthase UppS to form C_{55}-PP (Fujihashi et al. 2001). This product is then dephosphorylated by the polytopic membrane spanning phosphatase UppP to form the membrane localized C_{55}-P lipid carrier (Manat et al. 2014) (Figure 1.3 A). The structure of *E. coli* UppP has recently been solved, providing the first structural insight into lipid carrier recycling (Workman, Worrall, and Strynadka 2018; El Ghachi et al. 2018). UppP is largely composed of ten transmembrane (TM) α-helices, six of which are full-span TM helices and four which, unexpectedly, form two antiparallel re-entrant helix-loop-helix regions. UppP is a dimer both in solution and in the crystal packing with a twofold axis of symmetry bisecting the membrane. The UppP active site is a membrane

embedded hydrophobic cleft, as opposed to the surface localized active sites of other characterized phosphatases. A monoolein lipid used in the lipidic cubic phase crystallization lies within the active site, acting as a substrate mimic of C_{55}-PP and allowing for insight into the phosphatase mechanism (Workman, Worrall, and Strynadka 2018). The catalytic serine carries out nucleophilic attack on the terminal phosphate of the C_{55}-P, with the pentavalent transition state stabilized by a coordinated metal ion and arginine. The resultant phosphoenzyme intermediate is then hydrolyzed by a glutamate-activated water, resulting in the release of C_{55}-P and inorganic phosphate. Interestingly, UppP has structural similarities to various proteins involved in cross-membrane transport suggesting the possibility for a phosphatase activated transport mechanism of C_{55}-P back to the cytoplasmic leaflet, a recycling process that ostensibly plays an important role in the generation of dephosphorylated lipid carrier for ongoing biosynthesis of PG.

The subsequent phospho-MurNAc pentapeptide transfer to C_{55}-P and membrane is catalyzed by a second polytopic membrane protein MraY, a member of the polyisoprenyl-phosphate *N*-acetylglucosaminosugar-1-phosphate-transferase (PNPT) superfamily of prokaryotic and eukaryotic prenyl sugar transferases (Figure 1.3 B). Recent structures of MraY from both *Aquifex aeolicus* and *Clostridium bolteae* in the apo and inhibitor bound forms have provided important first insights into this critical step of PG biosynthesis (Chung et al. 2013, 2016; Hakulinen et al. 2017). MraY is comprised of 10 TM α-helices per monomer. A homodimeric form is observed in all structures with 2 monomers arranged in a parallel fashion relative to the membrane axis and the predicted active site regions of both monomers lying at the cytosolic face. Although structures with donor (UDP-MurNAc pentapeptide) or acceptor (C_{55}-P) substrates were not captured in these studies, an observed extended hydrophobic groove is proposed to

accommodate the acyl lipid tail of the substrate. In structures of MraY in complex with the natural product inhibitors muraymycin D2 and tunicamycin there is seen to be rearrangement of TM helices 1, 5 and cytosolic loops 5, 7 and 9 to accommodate the compounds and allowed for prediction of potential nucleotide binding and active site candidates near the cytoplasmic face of the enzyme (Chung et al. 2016; Hakulinen et al. 2017). The conformational plasticity of MraY observed in comparisons of the apo form and these complexes may be important for enzyme catalysis, as well as presumably enable the accommodation of the wide array of diverse natural product inhibitors identified for this enzyme class. The natural product inhibitor tunicamycin is of note, as it is seen to effectively inhibit both PG and WTA biosynthesis through inhibition of MraY and paralog TarO respectively, and indeed is commonly used as an inhibitor in other members of the PNPT family including those involved in N-linked glycosylation (Yoo et al. 2018). The structure of one such N-linked glycosylase, human GlcNAc-1-P-transferase (hGPT), was recently solved in complex with tunicamycin (Yoo et al. 2018). Modification of the GlcNAc portion of tunicamycin is seen to reduce the inhibition of hGPT while maintaining inhibition of MraY (Yoo et al. 2018) and gives promise that downstream structure-guided drug design can lead to the development of further novel and specific MraY inhibitors. The chemical mechanism of MraY has been debated with latest evidence lending support to a one-step, single-displacement over a two-step variant (Al-Dabbagh et al. 2016; Stickgold and Neuhaus 1967; Al-Dabbagh et al. 2008). Regardless of whether a covalent intermediate is formed, the mechanism is proposed to involve deprotonation of the phosphate moiety of C_{55}-P by a catalytic aspartate. Also of note is an essential magnesium which presumably coordinates the phosphate groups of the nucleotide substrate. Transfer of phospho-MurNAc pentapeptide to C_{55}-P results in the first lipid precursor of PG biosynthesis, termed lipid I.

Lipid I is subsequently converted into lipid II with the transfer of a GlcNAc from a UDP-GlcNAc donor by the membrane-tethered glycosyltransferase (GT) MurG (Figure 1.3 C). This conversion is presumably closely coupled to MraY activity, as little lipid I is observed to exist in the bilayer (van Heijenoort et al. 1992; Bouhss et al. 2004). Structures of MurG have a common GT-B fold comprised of two α/β domains with an extended active site cleft at their interface (Hu et al. 2003). MurG catalysis occurs via a sequential Bi Bi ordered mechanism, whereby the UDP-GlcNAc donor binds first, inducing the requisite rearrangements in a loop containing a conserved GGS motif to facilitate subsequent lipid I acceptor binding and conversion to lipid II product (Hu et al. 2003).

1.2.3 Lipid II transfer across the cytoplasmic membrane

For PG assembly to proceed, the large, electronegative head group of lipid II must be efficiently flipped to the outer leaflet to be acted upon by PBPs in the final stages of the biosynthetic pathway. It has long been proposed that the necessary flipping would be specifically catalyzed by a component of the biosynthetic machinery, as transfer of lipid II across the bilayer is non-spontaneous (van Dam et al. 2007). Two candidates for the lipid II flippase role have been previously suggested, MurJ and FtsW/RodA.

Bioinformatic approaches first identified MurJ as a potential flippase of lipid II, and recent structural studies have supported this claim (Ruiz 2008; Kuk, Mashalidis, and Lee 2017) (Figure 1.3 D). MurJ belongs to the mouse virulence factor (MVF) subfamily of the

multidrug/oligosaccharidyl-lipid/polysaccharide (MOP) superfamily. Of note in MurJ are two α-helices in addition to the 12 core TM helices common to most members of the MOP superfamily. The structure of MurJ from *Thermosipho africanus* recently solved was observed to be in an inward facing "N-shaped" conformation, distinct from the outward facing "V-shaped" conformations of all other MOP superfamily structures solved to date. At the intramembranal interface of the bi-lobed structure lies an internalized polar cavity, a commonly localized binding site for cargo in the MOP superfamily. In the inward facing conformation of MurJ, a hydrophobic groove, formed by the additional two helices, extends toward the central portal suggesting a unique modification that can accommodate the hydrophobic tail of lipid II with the negatively charged head group occupying a cationic portion of the central portal. It is likely that MurJ acts to flip lipid II in an alternating-access transport mechanism (Kuk, Mashalidis, and Lee 2017), with MurJ transitioning between inward and outward facing conformations to export lipid II to the outer leaflet.

Despite the evidence for MurJ as a lipid II flippase, there is a compelling argument that FtsW also has potential to play a role in this critical step of PG synthesis. FtsW, a member of the SEDS protein family (shape, elongation, division and sporulation), has been shown to directly translocate 7-nitro-2,1,3-benzoxadiazol-4-yl lipid II across membranes (Mohammadi et al. 2011). In the same work, no appreciable activity from MurJ could be detected by the assay. As well, it is known that FtsW and other closely related SEDS proteins, RodA and SpoVE, interact with PBPs (Fraipont et al. 2011; Leclercq et al. 2017). This aligns with the notion that lipid transfer is coupled to the GT/TP activities of PBPs (van Dam et al. 2007). Remarkably, SEDS proteins have recently been proposed to have in of themselves inherent lipid II polymerizing GT activity (Meeske et al.

2016; Emami et al. 2017), albeit with as yet little clarity toward their ability to also or instead act as lipid II flippases. One appealing proposal is that these SEDS proteins act as coupled lipid II flippase-glycosyltransferases, perhaps the latter driving the flipping energetically. Using evolutionary guided *de novo* structural prediction, a model of FtsW was developed which supports this dual-functionality hypothesis (Ovchinnikov et al. 2015). In 2018, the structure of RodA from the thermophile *Thermus thermophilus* was solved via lipid cubic phase crystallography (Sjodt et al. 2018). The structure loosely supports the notion that these SEDS proteins are indeed glycosyltransferases, while not strictly precluding the possibility they may be involved in transmembrane transport. Further structural studies are required to further inform the role of these proteins in either glycosyltransferase or flippase activity.

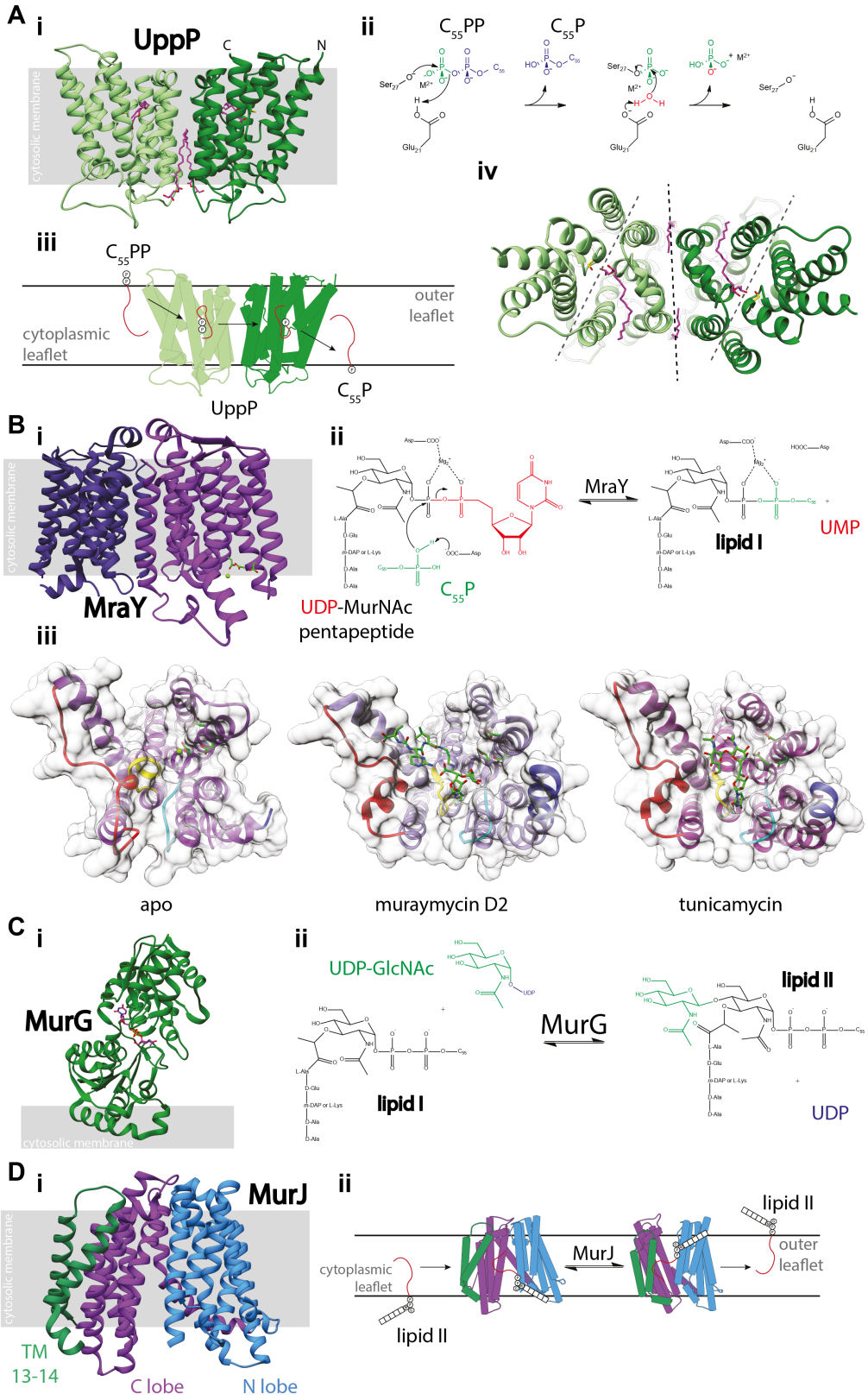
A
i
UppP
C
N
cytosolic membrane
ii
C55PP
C55P
iii
C55PP
cytoplasmic leaflet
outer leaflet
UppP
C55P
iv
B
i
MraY
cytosolic membrane
ii
MraY
UDP-MurNAc pentapeptide
C55P
lipid I
UMP
iii
apo
muraymycin D2
tunicamycin
C
i
MurG
cytosolic membrane
ii
UDP-GlcNAc
lipid I
MurG
lipid II
UDP
D
i
MurJ
cytosolic membrane
TM 13-14
C lobe
N lobe
ii
lipid II
cytoplasmic leaflet
MurJ
outer leaflet
lipid II

Figure 1.3 Initial membrane associated steps of peptidoglycan biosynthesis.
Lipid carrier synthesis and recycling, membrane associated Lipid II synthesis, and transfer to the outer leaflet of the cytosolic membrane. (**A i**) Structure of **UppP** (green) in complex with structural lipid and substrate mimic, monoolein (pink) (*E. coli*, 6CB2). (**A ii**) Proposed reaction mechanism for UppP mediated dephosphorylation of $C_{55}PP$. (**A iii**) Schematic representation of UppP's proposed UPP phosphatase-coupled lipid flippase activity. (**A iv**) Twofold symmetry axis of the UppP dimer (black) and twofold pseudosymmetry axes of each monomer (grey). (**B i**) Apo **MraY** dimer (purple) (*Aquifex aeolicus*, 4J72) with placement in the cytosolic membrane (grey). The catalytically important aspartate residues and magnesium ion are shown in green. (**B ii**) The proposed one-step mechanism for MraY. (**B iii**) Conformational changes seen upon binding of either muraymycin D2 (*Aquifex aeolicus*, 5CKR) or tunicamycin (*Clostridium bolteae*, 5JNQ) inhibitors. Catalytic aspartate residues and the two inhibitors are shown in green. Changes are seen to the end of TM helix 1 (blue), the end of TM helix 5 and loop 5 (yellow), loop 7 (cyan) and loop 9 (red). It is proposed that the conformational flexibility seen could play a role in MraY binding and function with its natural substrate. (**C i**) The bi-domain architecture of **MurG** (green) in complex with UDP-GlcNAc substrate (magenta) (*E. coli*, 1NLM), shown in relation to the cytosolic membrane. MurG is seen to associate with the cytosolic membrane and thought to receive lipid I substrate directly from MraY. (**C ii**) Chemical structures of the MurG catalyzed transition from lipid I to lipid II with the addition of GlcNAc. (**D i**) Structure of inward facing **MurJ** (*Thermosipho africanus*, 5T77). With the N lobe (blue), C lobe (purple) and TMs 13-14 (green) forming a unique N-shaped architecture. (**D ii**) The proposed alternating-access mechanism for lipid II flipping by MurJ. Upon lipid II binding, the inward N-shaped conformation (*Thermosipho africanus*, 5T77) switching to a proposed V-shaped conformation, as modelled previously (Kuk, Mashalidis, and Lee 2017), allowing transfer of the lipid II to the outer leaflet of the cytosolic membrane. Adapted from (Caveney, Li, and Strynadka 2018).

1.2.4 Glycopolymerization and transpeptidation by penicillin binding proteins

The final steps in the biosynthesis of PG involve catalysis by membrane anchored PBPs on the outer leaflet of the cytoplasmic membrane. These PBPs first act to polymerize lipid II disaccharide units into PG strands, followed by (regulated) transpeptidase-mediated crosslinking to the existing sacculus to form mature PG (Sobhanifar, King, and Strynadka 2013) (Figure 1.4).

In most bacterial species the bulk of the GT activity has historically been proposed to involve specific PBPs, with various species having several acting in different capacities during

growth, division, environmental stress and antibiotic resistance. These PBPs exist within complex regulatory networks, involving numerous protein-protein interactions, to ensure proper spatial and temporal regulation of PBP activity (reviewed in (Egan et al. 2015)). Of note are the crystallographic and nuclear magnetic resonance (NMR) structures of two regulatory outer-membrane anchored lipoproteins LpoA (Sathiyamoorthy et al. 2017) and LpoB (Egan et al. 2014; King, Lameignere, and Strynadka 2014), which have been observed to interact with selected PBP partners to stimulate late stage PG synthesis (Egan et al. 2015). The high molecular weight Class A PBPs, bifunctional enzymes which encapsulate both GT and transpeptidase (TP) activities in distinct active sites, as well as monofunctional GT variants, act to catalyze the attachment of the lipid II disaccharide to the C4' OH of the donor PG strand via a β1,4-glycosidic linkage (Sobhanifar, King, and Strynadka 2013). The first structures of full-length class A PBPs revealed an unprecedented GT domain with an active site cleft at the interface between a solvent exposed α-helical 'head' subdomain somewhat reminiscent of the PG hydrolase lysozyme and a distinct membrane embedded 'jaw' subdomain common only to these lipid activated family of PG glycosyltransferases (Lovering et al. 2007). As with lysozyme, the structure indicated six sugar moieties occupy the active site cleft and orient the growing PG donor strand away from the identified catalytic glutamate. A hydrophobic channel in the 'jaw' subdomain acts as a binding site for the extended acyl chain of the donor lipid II. Co-crystallization with a natural product inhibitor, Moenomycin A (Moe A) (Lovering et al. 2007; King et al. 2017), and lipid II analogs (Huang et al. 2012) validated these predictions and has provided further insight into PG polymerization. The Moe A complex structures indicate this potent, sub nM inhibitor acts as a substrate mimic of the tetrasaccharide-C_{55}PP product of the first round of polymerization, lipid IV (Lovering et al. 2007; Huang et al. 2012; King et al. 2017). The GT mechanism is initiated with action of the catalytic

glutamate acting as a Brønsted base in deprotonation of the acceptor C4 hydroxyl of the lipid II, followed by a nucleophilic attack on the donor MurNAc anomeric C1 of the glycosylphosphate in an S_N2 like reaction with inversion of stereochemistry to form the β1,4-glycosidic linkage (Huang et al. 2012; Lovering et al. 2007).

The final step in PG biosynthesis is the periodic crosslinking (transpeptidation) of glycan strands into the existing PG sacculus. TP activity provides rigidity and structure to the PG layer necessary for its protective function (Sobhanifar, King, and Strynadka 2013) and occurs through a two-step mechanism that begins with a serine-mediated acylation of the penultimate residue, D-alanine, of the pentapeptide on the growing PG strand. The covalent acyl-enzyme intermediate is subsequently deacylated via a nucleophilic attack of a side chain or terminal amino group of the third residue, *meso*-DAP, L-lysine, or L-lysine-pentaglycine, on an adjacent PG strand. This reaction is famously inhibited by β-lactam antibiotics, such as penicillin, which act as a substrate mimic of donor peptide and inhibit through long lived acylation of the catalytic serine. Alternate PBPs, such as PBP2a in MRSA, which are poorly acylated by β-lactam antibiotics, can be upregulated in the presence of β-lactam stress to provide resistance (Lim and Strynadka 2002). Further, structural and computational analysis of PBP2a indicates the potential for allosteric effects of bound PG fragments in its resistance phenotype (Otero et al. 2013; Mahasenan et al. 2017). For class A bifunctional PBPs, TP activity is thought to be coupled to intramolecular GT activity, with the glycan strand snaking from the membrane embedded GT catalytic domain directly to the extracellular TP domain (Sung et al. 2009). For class B monofunctional PBPs such as the aforementioned PBP2a, TP activity is likely coupled to the GT activity of a class A PBP or a monofunctional glycosyltransferase (including the recently proposed SEDS family). Indeed, the

major class A and B PBPs of cell division in *E. coli* are thought to exist only in tight complex with FtsW at the divisome (Leclercq et al. 2017). It is clear that these final stages of PG synthesis are far more complex than previously thought, with recent work suggesting that many of the enzymes involved interact as a highly regulated macromolecular machine (Egan et al. 2015).

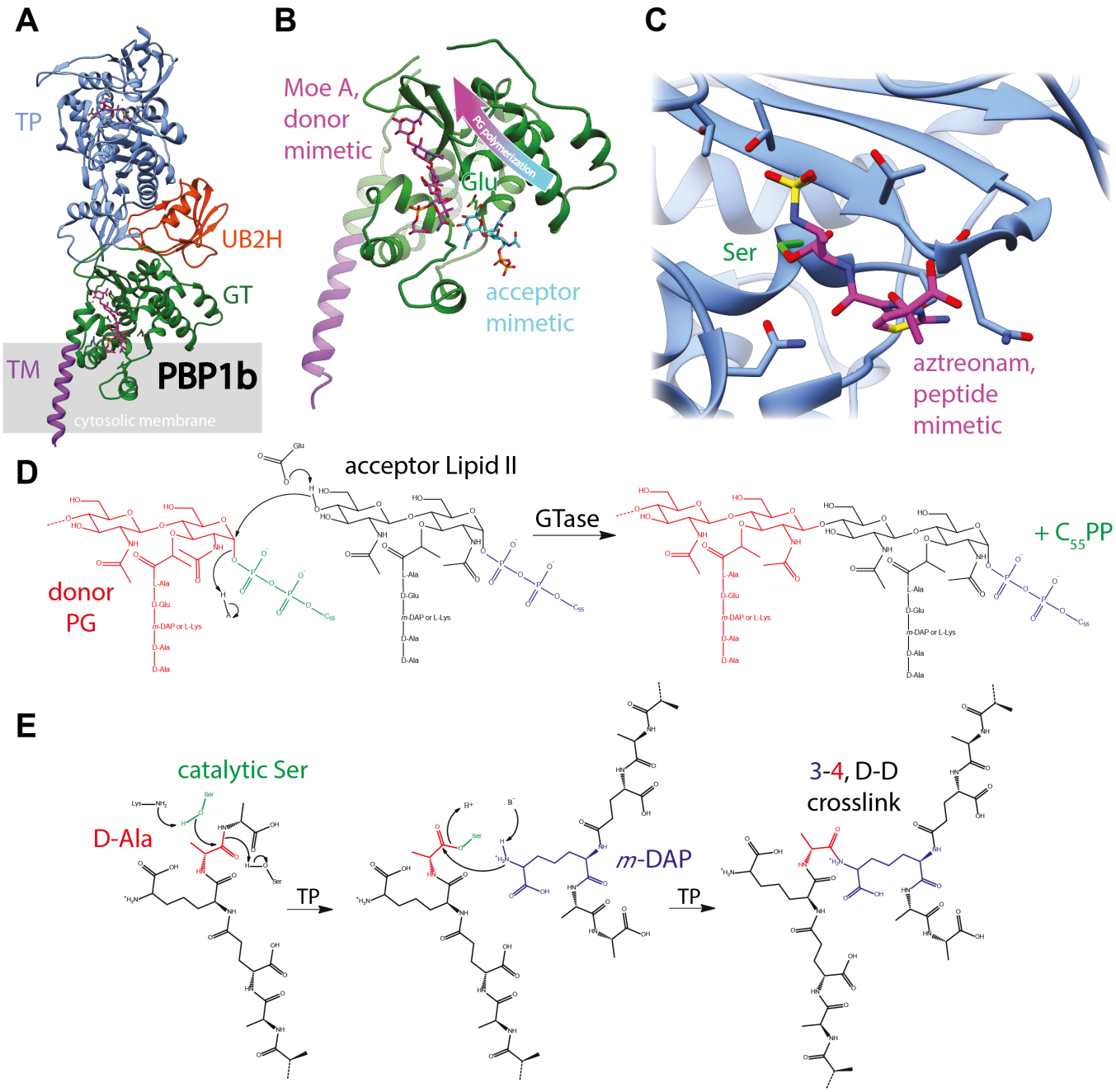

Figure 1.4 Final stages of PG biosynthesis by PBPs.
(**A**) Acyl-aztreonam and moenomycin A (Moe A) inhibited PBP1b, a bi-functional PBP (*E. coli*, 5HLB). GT domain seen in green, TP domain in blue, TM helix in purple and UB2H interaction domain in orange. (**B**) GT domain of PBP1b inhibited by Moe A (magenta) (*E. coli*, 5HLB), which acts as a donor PG strand mimetic to inhibit the GT activity of PBPs. Lipid II acceptor mimetic (cyan) from a monofunctional GTase co-structure (*S. aureus*, 3VMT) is shown aligned with its potential position in the GT domain of PBP1b. The catalytic glutamate is shown (green) in its position between the donor and acceptor. (**C**) Active site of PBP1b with acyl-aztreonam (*E. coli*, 5HLB). Aztreonam (magenta) is a monobactam which acts as a peptide mimetic and suicide inhibitor of the TP activity of PBPs. (**D**) The catalytic mechanism of PBP GT activity, showing the polymerization of an acceptor lipid II into the donor, growing strand. (**E**) The catalytic mechanism of the 3-4, D-D, transpeptidase activity of PBPs. Adapted from (Caveney, Li, and Strynadka 2018).

1.3 The role of YcbB in modulation of the peptidoglycan biosynthetic pathway

The continued use and misuse of β-lactam antibiotics in the clinic has led to the increasing development of bacterial resistance to whole classes of β-lactams. This has necessitated the targeting of alternate or tangential pathways of bacterial biogenesis to combat infections effectively. One such potential avenue for inhibition is the targeting of L,D-transpeptidases (Ldts), which, unlike PBPs, catalyse the formation of DAP^3_{donor} - $DAP^3_{acceptor}$ crosslinks (Magnet et al. 2008; Hugonnet et al. 2016) and are largely uninhibited by β-lactam antibiotics. At the moment, only carbapenems (e.g., meropenem and imipenem) exert any inhibition of Ldt activity. It is reasonable to assume, therefore, that continued reliance on this subclass of antibiotics will eventually lead to the further emergence of bacterial resistance.

One Ldt in particular, YcbB (alternately named LdtD), has come into the spotlight recently due to its role in a number of stress-related situations including outer envelope stress (Morè et al. 2019), β-lactam stress (Hugonnet et al. 2016), and a role in secretion of typhoid toxin under stress

of host infection (Geiger et al. 2018). In addition, copper has recently been found to inhibit Ldts, resulting in suppression of β-lactam resistance due to Ldt-mediated bypass of PBPs (Peters et al. 2018) and YcbB was discovered to play a role in crosslinking of stalk PG in *Caulobacter crescentus* (Stankeviciute et al. 2019). Due to the increasing relevance of YcbB as a potential drug target, the X-ray crystallographic structure of *E. coli* YcbB was recently determined (Caveney et al. 2019) to provide structural insight into these aforementioned mechanisms and allow for structure guided design of novel and specific YcbB inhibitors. Here, we will discuss the *in vivo* observations regarding the role of YcbB under stress conditions to provide comprehensive insight into the role of YcbB at a cellular level.

YcbB was originally linked to its role in cell wall crosslinking (Magnet et al. 2008) without a clear understanding of the physiological activation and role of these enzymes. It was only with the fortuitous identification of *ycbB* in a microarray screen of genes modulated by the Cpx envelope stress response (Raivio, Leblanc, and Price 2013) that the understanding of the physiological role of YcbB began to grow. This was subsequently followed up by *in vitro* and *in vivo* studies (Bernal-Cabas, Ayala, and Raivio 2015; Delhaye, Collet, and Laloux 2016) definitively linking *ycbB* expression to the Cpx stress response and the Cpx promoter (CpxR).

The importance of YcbB was then noted through its role in a β-lactam resistance mechanism found in *E. coli* (Hugonnet et al. 2016). Here, it was discovered that the PBP1b-PBP5-YcbB pathway can equip the bacterium with resistance to β-lactam antibiotics upon upregulation of alarmone (ppGpp) synthesis. This phenomenon was unraveled using combinatorial techniques involving the generation of a variety of mutant *E. coli* strains that constitutively resist β-lactam

antibiotics, as well as validation of YcbB activity using mass spectrometry. This pivotal study laid the foundation for further study of YcbB and the role of Ldts in a clinically relevant context.

Next, it was discovered that YcbB and a variety of other Ldts tested are susceptible to inhibition by $CuCl_2$ (Peters et al. 2018). This effect was shown by analysis of PG from *E. coli* cultured in the presence of $CuCl_2$ at 0.5 × minimum inhibitory concentration (MIC), revealing a lack of L,D-crosslinking. Also, it was observed that purified *E. coli* YcbB could be inhibited with low micromolar concentrations of $CuCl_2$ in an *in vitro* assay, while sub-MIC levels of $CuCl_2$ were found to resensitize YcbB-mediated β-lactam resistant strains.

Shortly thereafter, YcbB was implicated in the release of typhoid toxin in pathogenic *S.* Typhi (Geiger et al. 2018). Using combinatorial bacterial knockout strains and validation with both secretion assays and *in vitro* TtsA muramidase activity assays, typhoid toxin release was shown to depend on the effect of a muramidase, TtsA, which in turn depends on YcbB. The L,D-transpeptidation of YcbB acts to guide and presumably regulate the activity of TtsA, with TtsA activity only seen on PG with L,D-crosslinks. Interestingly, the authors show that low levels of both detergents and antimicrobial peptides, which both destabilize the outer membrane, could be used to trigger the process of typhoid toxin release.

In a more recent publication (Morè et al. 2019), it was discovered that YcbB mediates survival in bacteria with severe outer envelope deficiency. It was observed that an increase in L,D-crosslinking takes place in bacteria with defective lipopolysaccharide export. Through deletion of individual *ldt* genes, Morè *et al*. concluded that YcbB is the Ldt responsible. The authors also performed experiments to show that, similar to the initial steps of the YcbB-mediated β-lactam resistance pathway, a likely transient complex of PBP1b-PBP6-YcbB is involved in this stress condition. In this study the authors probed the conditions under which the *ycbB* promoter is activated. Using *promoter-lacZ* fusion plasmids, it was determined that *pycbB*, rather than the promoter of other Ldts, is activated under envelope stress conditions. The other Ldts were shown to be regulated by known housekeeping pathways, while the stress induced *pycbB* activation presumably ties into the Cpx stress response pathway under these conditions.

As a collective body of work, we begin to appreciate the intricacies of YcbB activity in the context of its important role in bacterial cell wall biogenesis. One underlying theme behind these rather distinct situations of YcbB-mediated survival is stress. In the case of β-lactam antibiotic-induced and outer envelope stress there is an activation and mobilization of these alternative PG synthase complexes that compensate for the compromised activities of conventional PG synthesis enzymes. This would then play a role in the structural interplay between the outer membrane and PG sacculus (Rojas et al. 2018), allowing for continued resistance to environmental stress. Given the activation of typhoid toxin release by detergents and antimicrobial peptides, it would be logical that the general outer envelope stress during infection triggers activation of *pycbB* in *S*. Typhi through the analogue of the *E. coli* Cpx response. This system could then act as a rudimentary signaling pathway to transduce the notion of infection, through L,D-transpeptidation and

subsequently TtsA muramidase activity, to the final release of typhoid toxin. Clearly, the specifics of this gene activation under these stressful conditions are an area of interest for future investigation as not only inhibition of YcbB itself but also inhibition of its upregulation, could represent susceptible nodes for pharmaceutical intervention in both pathogenic *E. coli* and *S.* Typhi.

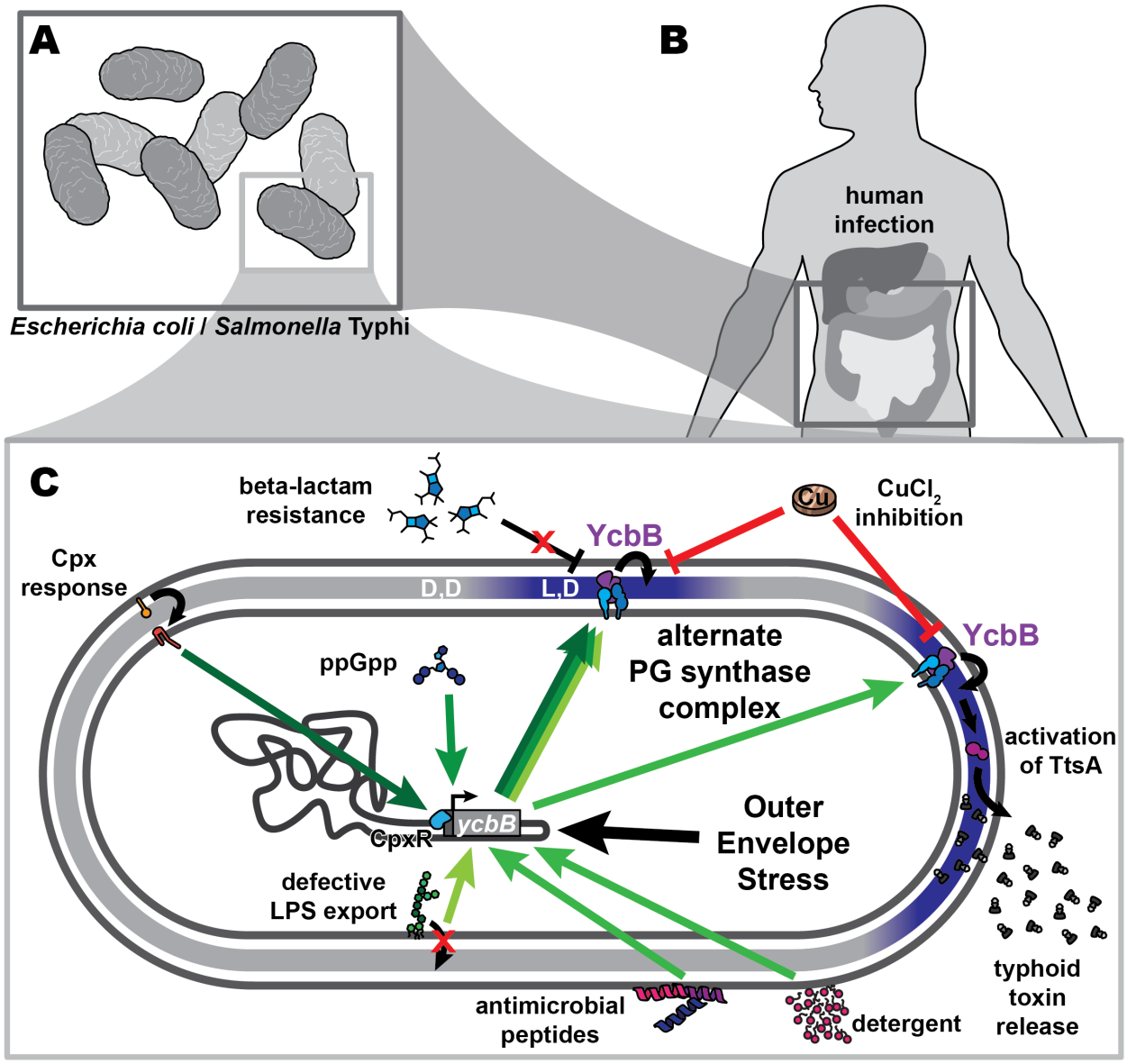

Figure 1.5 Cellular mechanisms of YcbB L,D-transpeptidation.
(**A**) The cellular roles of YcbB have been explored in both *E. coli* and *S.* Typhi. (**B**) Due to the nature of these mechanisms, it is likely that some or all of the YcbB-related cellular mechanisms occur in either enteropathogenic *E. coli* or *S.* Typhi infection of a human host. (**C**) Graphical summary of cellular processes that influence YcbB levels and recognized cellular effects on the cell. The Cpx response related activation of *ycbB*, YcbB-mediated β-lactam resistance, YcbB in mediating typhoid toxin release, and YcbB in surviving an outer membrane transport deficiency are represented with green arrows (from darkest to lightest). Susceptibility of Ldts to $CuCl_2$ is represented in red. D,D-crosslinked PG/cell wall is represented in grey, while L,D-crosslinked PG is represented in dark blue. The gene *ycbB* and its promoter *pycbB* are represented grey and dark grey respectively.

1.4 The role of LpoP in modulation of the peptidoglycan biosynthetic pathway

Over the last years, it became evident that the activities of some class A PBPs are regulated by cognate outer membrane-anchored lipoprotein activators, LpoA and LpoB (Typas et al. 2010; Paradis-Bleau et al. 2010). Moreover, *E. coli* subjects the LpoB-mediated stimulation of PBP1B to regulation by CpoB, which functions together with members of the Tol system to coordinate outer membrane constriction with septal PG synthesis (Gray et al. 2015). These regulators were all identified in *Escherichia coli* and recent work provided insights into their structures, interface with the PBP and mechanisms of PBP activation (Egan et al. 2014; King, Lameignere, and Strynadka 2014; Jean et al. 2014; Egan et al. 2018; Kelley, Vijayalakshmi, and Saper 2019). These studies suggest that activators bind to a non-catalytic docking domain causing conformational changes in the PBP that ultimately affect active site residues. *Pseudomonas aeruginosa* has a lipoprotein activator of PBP1B, termed LpoP, which likely functions in a similar way as LpoB in *E. coli* (Greene, Fumeaux, and Bernhardt 2018). However, while LpoP was shown to be essential for PBP1B function in the cell, the structure of LpoP is not known and the previous work did not demonstrate the direct mechanism of activation for PBP1B by LpoP (Greene, Fumeaux, and Bernhardt 2018).

1.5 Treatment and resistance of bacterial infections

As a large component of this thesis centres around potential antibiotic targets for inhibition during bacterial infection, it is of interest to provide a brief comment on current strategies to treat bacterial infections and the resistance mechanisms currently being faced in the clinic. The targets

in this thesis broadly relate to three species; *E. coli, S. enterica, and P. aeruginosa*, all of which are prevalent human pathogens.

1.5.1 *Escherichia coli* infection treatment and resistance

Escherichia coli, one of the most widespread model organisms in microbiology, is an increasingly prevalent human pathogen, causing diarrheagenic infections which can be broadly classified into six major categories: enteropathogenic *E. coli* (EPEC), enterohemorrhagic *E. coli* (EHEC), enterotoxigenic *E. coli* (ETEC), enteroaggregative *E. coli* (EAEC), enteroinvasive *E. coli* (EIEC), and diffusely adhering *E. coli* (DAEC) (Torres, Zhou, and Kaper 2005). In addition, *E. coli* is a main component of urinary tract infections (UTIs), with such strains known as uropathogenic *Escherichia coli* (UPEC). Regardless of the mode or region of infection, treatment of cases warranting clinical intervention largely falls in the hands of antibiotics. Due to increased cases of resistance, antibiotic selection is typically tailored to the site, severity, and antibiotic susceptibility of the particular infection (Bush and Perez 2018a). Strains are often resistant to ampicillin (a β-lactam, TPase inhibitor) and tetracycline (a ribosomal translation inhibitor). Treatment often includes β-lactam antibiotics such as cefazolin and piperacillin (Vancouver Coastal Health 2016), though there is an increasing presence of *E. coli* encoding extended-spectrum β-lactamases, resulting in resistance to penicillins, cephalosporins, and monobactams (TPase inhibitors) (Bush and Perez 2018a). Treatment in these cases is often through the use of carbapenem antibiotics (a TPase inhibitor), though carbapenemase producing isolates (CP-*Ec*) have begun to emerge and are now labelled as a “critical” level pathogen for the development of new antibiotics (WHO 2017).

1.5.2 *Salmonella enterica* infection treatment and resistance

In addition to *E. coli, Salmonella enterica* is an increasingly troublesome human pathogen, with both carbapenemase producing *Salmonella* and fluoroquinolone resistant Salmonella ranking on the WHO priority pathogens list, as "critical" and "high" priority respectively (WHO 2017). In humans, Salmonella infection can broadly be classified into typhoidal and non-typhoidal infections (Gibani, Britto, and Pollard 2018), with treatments largely centering around β-lactam antibiotics in typhoidal and severe non-typhoidal infections (Vancouver Coastal Health 2016). Carbapenem and fluoroquinolone antibiotics are currently in use of resistant infections as "last resort" antibiotics, though new antibiotics are direly needed as we begin to enter into a post carbapenem and fluoroquinolone era.

1.5.3 *Pseudomonas aeruginosa* infection treatment and resistance

Finally, the third human pathogen of relevance to this thesis work is *Pseudomonas aeruginosa*. *P. aeruginosa* infection is often hospital acquired, particularly among immunocompromised patients (Bush and Perez 2018b). Among the most common *P. aeruginosa* infections are hospital-acquired pneumonia (HAP) and ventilator-associated pneumonia (VAP) (Bush and Perez 2018b), which are commonly treated with β-lactam antibiotics, and in severe cases carbapenem antibiotics (Vancouver Coastal Health 2016). As in both *E. coli* and *S. enterica* infections, β-lactam resistance is increasingly common, resulting in increased usage of carbapenem antibiotics. This in turn has led to the emergence of carbapemase producing *P.*

aeruginosa, which tops the WHO priority pathogens list with a “critical” priority ranking (WHO 2017).

1.6 Research questions and thesis goals

In this work, we provide insight into the structural and functional features of various forms of modulation of peptidoglycan synthase activity. We will focus on the structural and functional features of the L,D-transpeptidase YcbB and the aPBP activator LpoP. With these insights, we allow for the further understanding of the complex nature of peptidoglycan biosynthesis and promote the pursuit of novel antibacterial therapies that target the key proteins studied herein.

Chapter 2: Structural insight into YcbB mediated β-lactam resistance in *Escherichia coli*

2.1 Introduction

The bacterial cell wall plays a critical role in the strength and viability of bacteria within their natural environs. Underscored by the development of β-lactam antibiotics such as penicillins and cephalosporins, biosynthesis of the major structural component of the bacterial cell wall, peptidoglycan (PG), has been long recognized as an important drug target. PG is composed of extended polymerized glycan strands of alternating β-1,4 linked *N*-acetyl-glucosamine-*N*-acetyl-muramic acid which crosslink into a net-like mesh via short peptide segments covalently attached at the C3-OH position of the latter sugar (Sobhanifar, King, and Strynadka 2013). The precursor subunits of PG are synthesised in the cytosol and transferred to an undecaprenyl phosphate lipid carrier (Lovering, Safadi, and Strynadka 2012). This moiety is then flipped to the periplasmic face of the membrane, where polymerisation into glycan strands, release from lipid carrier and peptide crosslinking to the existing PG sacculus occur in concert (Lovering, Safadi, and Strynadka 2012; Caveney, Li, and Strynadka 2018).

In *Escherichia coli*, this peptide crosslinking reaction is primarily carried out by class A and B penicillin-binding proteins (PBPs). These proteins have D,D-transpeptidase activity and catalyse the cleavage of a D-Ala^4-D-Ala^5 peptide bond of the acyl donor and subsequent crosslinking of the D-Ala^4 carbonyl to the primary amine of a diaminopimelic acid (DAP) residue

on the acceptor. This results in a D-Ala$^{4}_{donor}$-DAP$^{3}_{acceptor}$ crosslink (Sobhanifar, King, and Strynadka 2013). This D,D-transpeptidase activity can be blocked by β-lactam antibiotics, which act as a substrate mimetic of the donor strand peptide bond. Inhibition of this final and crucial step in PG biosynthesis results in destabilisation of the cell wall and ultimately cell death (King, Sobhanifar, and Strynadka 2016).

Despite the success of β-lactam antibiotics in the clinic, it has recently been shown that an alternate crosslinking mechanism can lead to the bypass of PBP mediated D,D-transpeptidation. The L,D-transpeptidase YcbB (alternately named LdtD), with remarkably few additional accessory factors, is able to undertake this recovery of PG crosslinking function, even in the presence of many clinically used β-lactam antibiotics. The factors required include the upregulation of alarmone (ppGpp) synthesis, the class C monofunctional PBP5, and an associated glycosyltransferase (GTase) activity attributed to the class A bifunctional PBP1b (Hugonnet et al. 2016) which harbours both GTase and TPase activities in distinct active sites. As with D,D-crosslinked PG, the bypass pathway initiates with GTase catalyzed polymerisation of PG; the resultant growing product strand is subsequently acted upon by PBP5 which catalyses a carboxypeptidase reaction targeting removal of the terminal D-Ala^{5} resulting in a donor glycan-tetrapeptide for YcbB to act upon. In the last step of the bypass pathway, YcbB catalyses the L,D-transpeptidation using a tetrapeptide-containing donor to form a DAP$^{3}_{donor}$-DAP$^{3}_{acceptor}$ crosslink (Hugonnet et al. 2016). L,D-transpeptidases, including YcbB, are not efficaciously inactivated by β-lactams except by the carbapenems (Hugonnet et al. 2016). The formation of thioester-containing L,D-transpeptidase-β-lactam adduct is slow for penicillins and cephalosporins (Triboulet et al. 2013). This is in large part due to the mM K_D values for Ldts and most β-lactam

antibiotics (Triboulet et al. 2013). The acylation in the case of non-carbapenem β-lactam antibiotics is followed by fragmentation of the acylated antibiotic and swift hydrolysis, thereby preventing inactivation of the enzyme and rendering the antibiotic useless for further inhibition. (Triboulet et al. 2013). The D,D-carboxypeptidase PBP5, required for production of the tetrapeptide donor of the L,D-transpeptidation reaction, is inhibited only at high concentrations of β-lactam (Curtis et al. 1979).

Despite YcbB's resistance to most β-lactam antibiotics, it is susceptible to inhibition by carbapenem antibiotics such as meropenem and imipenem (Hugonnet et al. 2016). Carbapenem antibiotics are a subset of β-lactam antibiotics which have previously been shown to inhibit other L,D-transpeptidases (Kumar et al. 2017). This class of antibiotic is of interest, not only due to its ability to inhibit YcbB, but as well the carboxypeptidase activity of PBP5 and the D,D-transpeptidase activity of PBP1b. Further insight into the inhibition of the enzymes in the D,D-transpeptidase bypass pathway could lead to the development of novel inhibitors to better address the current β-lactam resistance crisis. Additionally, it was recently shown that copper can inhibit L,D-transpeptidation of bacterial cell walls and specifically inhibit YcbB (Peters et al. 2018). This plays an important role in the inherent antimicrobial activity of copper.

In this work, we report the structure of *E. coli* YcbB acylated with meropenem. YcbB is seen to consist of a conserved L,D-transpeptidase catalytic domain, with the notable additions of a subdomain on the substrate capping loop, a PG binding domain, and a large scaffolding domain potentially important in mediating partner interactions. This complex domain architecture is unique in comparison to that of well characterised Gram positive and *Mycobacterium* L,D-

transpeptidases. In addition, we report in parallel, the structure of a PBP5-meropenem acyl enzyme complex in order to completely describe the molecular interactions which facilitate meropenem inhibition of the YcbB and PBP5 partners. Our results provide structural insight into D,D-transpeptidase bypass in *E. coli* and structural insight into the role of L,D-transpeptidation of PG in Gram negative bacteria. Additionally, we probe the protein interaction network and affinities for the D,D-transpeptidase bypass pathway and assay YcbB mediated β-lactam resistance in an *in vivo* setting allowing further mechanistic insight into this drug resistance pathway and generated phenotype.

2.2 Results and discussion

2.2.1 *E. coli* YcbB X-ray crystallographic structure

To investigate the role of YcbB in β-lactam resistance at the atomic level and provide insight into L,D-transpeptidase activity in Gram negative bacteria, the x-ray crystallographic structure of *E. coli* YcbB was pursued. Cocrystals, generated in the presence of 1 mM meropenem at pH 7.5, displayed $P4_32_12$ symmetry with unit cell dimensions of a = 126.5 Å, b = 126.5 Å, c = 88.8 Å and a diffraction resolution of 2.76 Å. There is one molecule of YcbB in the asymmetric unit. The structure solution was phased using a distinct SIR dataset of a heavy atom (ethyl mercury) soaked crystal with final refinement statistics presented in Table 2.1. The resulting maps showed well resolved electron density for the majority of the enzyme chain, allowing near complete tracing of the YcbB model (see methods). As in solution, the structure indicates a monomeric form of the enzyme with no obvious crystallographic formation of larger oligomers. The overall dimensions

of the enzyme are 74 x 73 x 40 Å with a total surface area of ~24,400 $Å^2$, and with a largely positive electrostatic distribution across the catalytic domain and largely apolar distribution across the PG and scaffolding domains. An extended electropositive active site demarcated by bound meropenem antibiotic lies across the catalytic domain with appropriate clefts for both donor and acceptor substrates adjacent and continuous (Figure 2.1). The observed overall architecture of YcbB (Figure 2.1) has several distinct features from all currently deposited L,D-transpeptidase structures, as suggested from the unique insertions and substitutions in sequence alignments with previously characterized Gram positive and mycobacterial species (7.1-14.3% sequence identity). The well ordered central catalytic domain, comprised of residues 375-576, forms a canonical L,D-transpeptidase fold harbouring an extended active site cleft with the expected conserved active site motif (Bianchet et al. 2017) (HX_{15-18}[S/T]XGC*h*[R/N], where X represents any residue, and *h* is any hydrophobic residue), but with the notable insertion of a unique substrate capping sub-domain (residues 422-495), unprecedented in size and observed secondary structural elements and lying adjacent to the meropenem-acylated catalytic site. On the opposite face of the central catalytic domain, an also unprecedented N-terminal region, central helix, and C-terminal helical tail (residues 37-233, 352-374, and 605-615 respectively) are proximal and form a collective helical bundle we term the scaffold domain, and predict to play a potential role in protein-protein interactions in YcbB-mediated resistance (Hugonnet et al. 2016). Residues 234-351 form a small antiparallel three helical bundle, with features reminiscent of previously observed peptidoglycan binding regions – and thus we term here the PG domain (Maciejewska et al. 2017). The residues (577-604) form a β-hairpin linker between the catalytic domain and the C-terminal recursion.

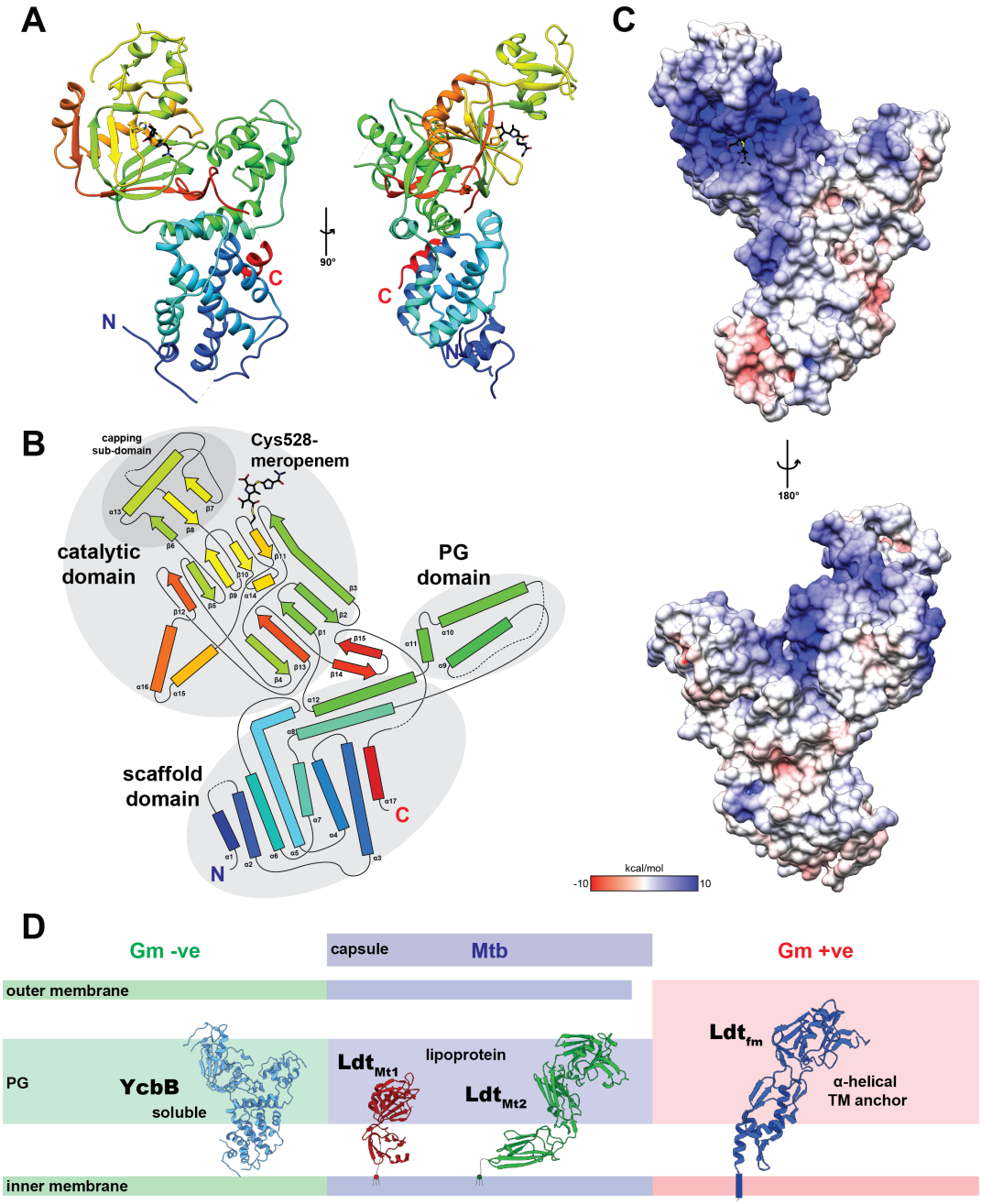

Figure 2.1 Overall architecture and activity of *E. coli* YcbB.
(**A**) The crystal structure of YcbB-meropenem acyl-enzyme complex in ribbon representation, coloured in rainbow from N-terminus (blue) to C-terminus (red). Meropenem stick representation is coloured in black and by heteroatom. Two views related by a 90° rotation along the y-axis. (**B**) Topology diagram of YcbB-meropenem acyl-enzyme complex, coloured as in **A**. The catalytic, PG and scaffolding domains are annotated and circled in grey. (**C**) Electrostatic surface representation of YcbB in two views related by a 180° rotation around the y-axis. (**D**) Diversity of structurally characterised L,D-transpeptidases. Gram negative (green background), soluble YcbB

in sky blue; Mycobacterial (blue background), lipoprotein Ldt_{Mt1} (PDBID 5E5L (Kumar et al. 2017)) and Ldt_{Mt2} (PDBID 5DU7(Kumar et al. 2017)) in red and green; Gram positive (red background), TM anchored Ldt_{fm} (1ZAT (Biarrotte-Sorin et al. 2006)) in dark blue. Adapted from (Caveney et al. 2019).

Table 2.1 *E. coli* YcbB and PBP5 data collection, phasing and refinement statistics.

	YcbB Refined	YcbB Native	YcbB Hg	PBP5
Data collection				
Space group	P 4_3 2_1 2	P 4_3 2_1 2	P 4_3 2_1 2	C 2
Cell dimensions				
a, *b*, *c* (Å)	126.499, 126.499, 88.8011	126.824, 126.824, 87.903	127.689, 127.689, 87.5560	124.81, 50.8, 80.22
a, b, g (°)	90, 90, 90	90, 90, 90	90, 90, 90	90, 118.688, 90
Resolution (Å)	72.68 - 2.76 (2.859 - 2.76)*	47.92 - 2.19 (up to 3.10 used by SHARP)	47.83 - 2.10	46.08 - 2.2 (2.279 - 2.2)
R_{merge}	0.168 (2.723)	0.075	0.169	0.1767 (1.558)
I / sI	9.96 (1.05)	9.2	5	4.86 (0.78)
Completeness (%)	99 (100)	71 (96% up to 2.7A)	89 (100% up to 2.6A)	100 (99)
Redundancy	12.5 (12.8)	6.4	10.7	3.3 (3.2)
R_{cullis}			0.773	
Refinement				
Resolution (Å)	2.76			2.2
No. reflections	18942 (1826)			22576 (2204)
R_{work} / R_{free}	25.61 (42.21) / 29.85 (41.93)			21.03 (39.82) / 25.65 (44.21)
No. atoms				
Protein	4066			2942
Ligand/ion	51			26
Water	21			78
B-factors (Å^2)				
Protein	76.8			53.6
Ligand/ion	85.0			70.7
Water	55.7			53.8
R.m.s deviations				
Bond lengths (Å)	0.016			0.006
Bond angles (°)	1.88			0.99

*Values in parentheses are for highest-resolution shell.
Adapted from (Caveney et al. 2019).

2.2.2 YcbB scaffold domain structure

The scaffold domain of YcbB is comprised of ten helices packed into a helical bundle. The seven core α-helices are contributed by residues 100-213, with the eighth α-helix contributed from the C-terminal recursion involving residues 600-615 (Figure 2.1). Two additional helices (residues 214-233 and 352-374) cap the domain and structurally link the catalytic and PG binding domains. Residues downstream (31-99) form a generally less ordered region with interspersed α-helical segments which sit distal to the other domains of YcbB. The scaffold domain is unique to the YcbB sub-family of L,D-transpeptidases, suggesting a specific functional and/or regulatory role we predict to involve interaction with the known YcbB unique protein partners PBP5 and PBP1b (Hugonnet et al. 2016). These interactions are likely crucial for localization of YcbB to the site of late stage PG synthesis, as, unlike L,D-transpeptidases from Gram positive bacteria or *Mycobacterium*, YcbB does not have a α-helical transmembrane tether or N-terminal lipidation (Figure 2.1 D). Rather, YcbB is predicted to be targeted to the periplasmic space using a characteristic sec-dependent signalling sequence (residues 1-30 – SignalP 4.1 (Petersen et al. 2011)), which is subsequently processed through proteolytic cleavage with release of soluble YcbB.

2.2.3 YcbB peptidoglycan binding domain

Many characterized L,D-transpeptidases have been shown to contain PG binding motifs/domains, often a LysM domain consisting of a βααβ fold with the two α-helices located on the same side of an antiparallel β-sheet (Bielnicki et al. 2006). In YcbB, residues 234-351 form a

small antiparallel three helical bundle which, based on these prior observations, is suggestive of a putative PG binding domain (Figure 2.2) albeit a PG binding domain more characteristic of lytic phage enzymes and a Zn-dependent bacterial amidase than PG binding motifs observed in other structurally characterized L,D-transpeptidases. Structural homology analysis, via the DALI protein structure comparison server (Holm and Rosenström 2010), finds close structural homologues – gp144, a *Pseudomonas aeruginosa* phage phiKZ endolysin (PDB ID 3BKH (Fokine et al. 2008), Z-score 9.7, root-mean-square deviation (RMSD) 1.9), a *Clostridium acetobutylicum* zinc-dependent amidase (PDB ID 4XXT, Z-score 9.6, RMSD 1.9), a *Clostridioides difficile* PBP (PDB ID 5TV7, Z-score 9.4, RMSD 2.0), and gp15, a *Burkholderia* AP3 phage endolysin (PDB ID 5NM7 (Maciejewska et al. 2017), Z-score 9.4, RMSD 2.0). The three antiparallel helices are common to all five PG binding domains, though in YcbB the loop region between the first and second helices contains a dynamic and relatively conserved extension (residues 262-318 with the central region therein highly disordered). Due to the lack of this loop extension in the above identified structural homologues, it is possible that these residues become more stabilised upon PG binding, increasing the effective interaction interface or specificity with PG substrates in this family. The PG domain of YcbB contains many conserved residues with other YcbB family members primarily in the hydrophobic core of the motif (Val252, Leu259, Ala324, Val325, Phe328, Gln329, Leu334, Thr344, Leu348) as well as in two surface exposed residues, Arg244 and Asp337, which have been implicated previously as essential in peptidoglycan binding (Maciejewska et al. 2017).

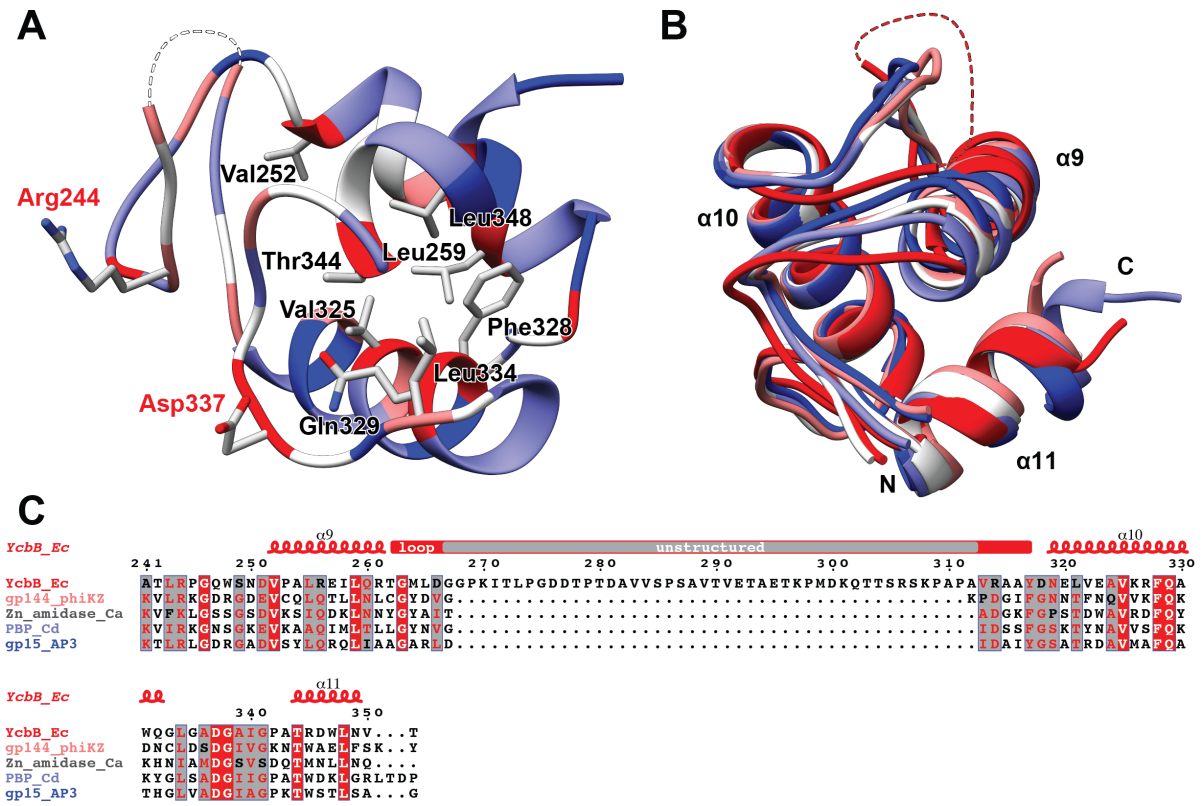

Figure 2.2 Structure of the *E. coli* YcbB peptidoglycan binding domain.
(**A**) The structure of the *E. coli* YcbB peptidoglycan binding domain, residues 241-351, with residue conservation mapped to backbone colour from red to blue in decreasing conservation. Conserved core packing residues labelled in black and key, surface exposed, peptidoglycan binding residues labelled in red. (**B**) Overlay of YcbB peptidoglycan binding domain and high scoring peptidoglycan binding domains from a structural homology search on the Dali server (Holm and Rosenström 2010). YcbB in red, gp144, a *Pseudomonas aeruginosa* phage phiKZ endolysin in salmon (PDB ID 3BKH (Fokine et al. 2008)), a *Clostridium acetobutylicum* zinc-dependent amidase in white (PDB ID 4XXT), a *Clostridium difficile* PBP in pale blue (PDB ID 5TV7), and gp15, a *Burkholderia* AP3 phage endolysin in dark blue (PDB ID 5NM7 (Maciejewska et al. 2017)). Peptidoglycan binding domain structures are coloured from red to blue based on decreasing structural homology. (**C**) The sequence of *E. coli* YcbB (YcbB_Ec) aligned with peptidoglycan binding domains from phiKZ gp144 (gp144_phiKZ), *C. acetobutylicum* zinc-dependent amidase (Zn_amidase_Ca), *C. difficile* PBP (PBP_Cd), and AP3 gp15 (gp15_AP3). Secondary structure of *E. coli* YcbB is displayed atop the sequence alignment, with the extended loop shown in red and the unstructured region in grey. Adapted from (Caveney et al. 2019).

2.2.4 YcbB catalytic domain

The central YcbB catalytic domain adopts a characteristic L,D-transpeptidase fold (Figure 2.3) constructed of two (five and six stranded) curved, mixed β-sheets disposed in a clam-shell like manner with α-helices 15 and 16 situated in the cleft between. Acting as a hinge, β-strand 3 participates in both β-sheets of the domain. Situated just downstream of β-strand 11, the active site is demarcated by the meropenem acylated catalytic cysteine nucleophile (Cys528) with the conserved histidine base (His509) protruding from β-strand 10. The oxyanion hole, presumed to stabilize the developing tetrahedral oxyanion transition state during acylation and deacylation is comprised of the main chain nitrogen atoms of Cys528 and Tyr507.

One notable feature of the catalytic domain of YcbB is the large substrate capping sub-domain (residues inserted between β-strands 5 and 9). This region has been seen to be variant in currently solved structures of L,D-transpeptidases, ranging from small turns (YkuD (Bielnicki et al. 2006)) to larger loops of up to 19 residues which extend over the active site (Ldt_{fm} (Biarrotte-Sorin et al. 2006; Lecoq et al. 2013)) (Figure 2.3 B). However, YcbB is the first structure characterized which contains significant secondary structural elements and consequent folded sub-domain in this region (residues 423-487). In YcbB this putative substrate capping sub-domain is comprised of a small three stranded β-sheet (β6,8,7) and α-helix 13, which sits perpendicular to the β-sheet at one end. Between β-strand 7 and 8 there is a large loop region from residue 453 to 481. β-strand 6 and α-helix 13 are seen to hinge towards the active site in the meropenem acyl-enzyme complex structure. It has been proposed previously that the substrate capping loop in earlier structures serves to provide inherent flexibility during roles in substrate entrance, capping,

and release (Gokulan et al. 2018). Despite the more structured and significant nature of the YcbB sub-domain, the density, although traceable, was less well resolved and displayed generally higher temperature factors, all in keeping with an analogous inherent flexible nature and potential similar role(s) in catalysis. Further, crystallographic structures and molecular dynamics simulations of Ldt_{Mt2} from *Mycobacterium tuberculosis* have recently shown that the substrate capping loop can have variable flexibility dependent on the presence of differing inhibitors with obvious implications for drug discovery efforts against this family (Gokulan et al. 2018; Fakhar et al. 2017). To probe further the potential analogy with the more structured sub-domain in YcbB, we performed 10 ns molecular dynamics simulations (Figure 2.4) using a CHARMM36 forcefield (see methods) which additionally supported the propensity for its highly mobile nature. Interestingly, simulations with meropenem showed increased RMSD spread in the capping loop region but an overall stabilisation of the remainder of the catalytic domain, while in apoenzyme simulations there was increased motion not only in the capping sub-domain but as well over the entirety of the catalytic domain. It is likely that in the action of YcbB on extended native PG substrates, this motion would provide for additional interactions to facilitate binding and product release. In the YcbB-meropenem acyl-enzyme complex structure, the capping subdomain is seen to be stabilised in a position adjacent to the active site, creating a distinct cap over the two substrate binding clefts (Figure 2.3 C). Meropenem occupies, as expected of a β-lactam antibiotic, the donor site, further demarcating the adjacent and unoccupied acceptor site. The corresponding volume under the cap in the closed conformation observed is approximately 810 $Å^3$, as calculated by the 3V server (Voss and Gerstein 2010).

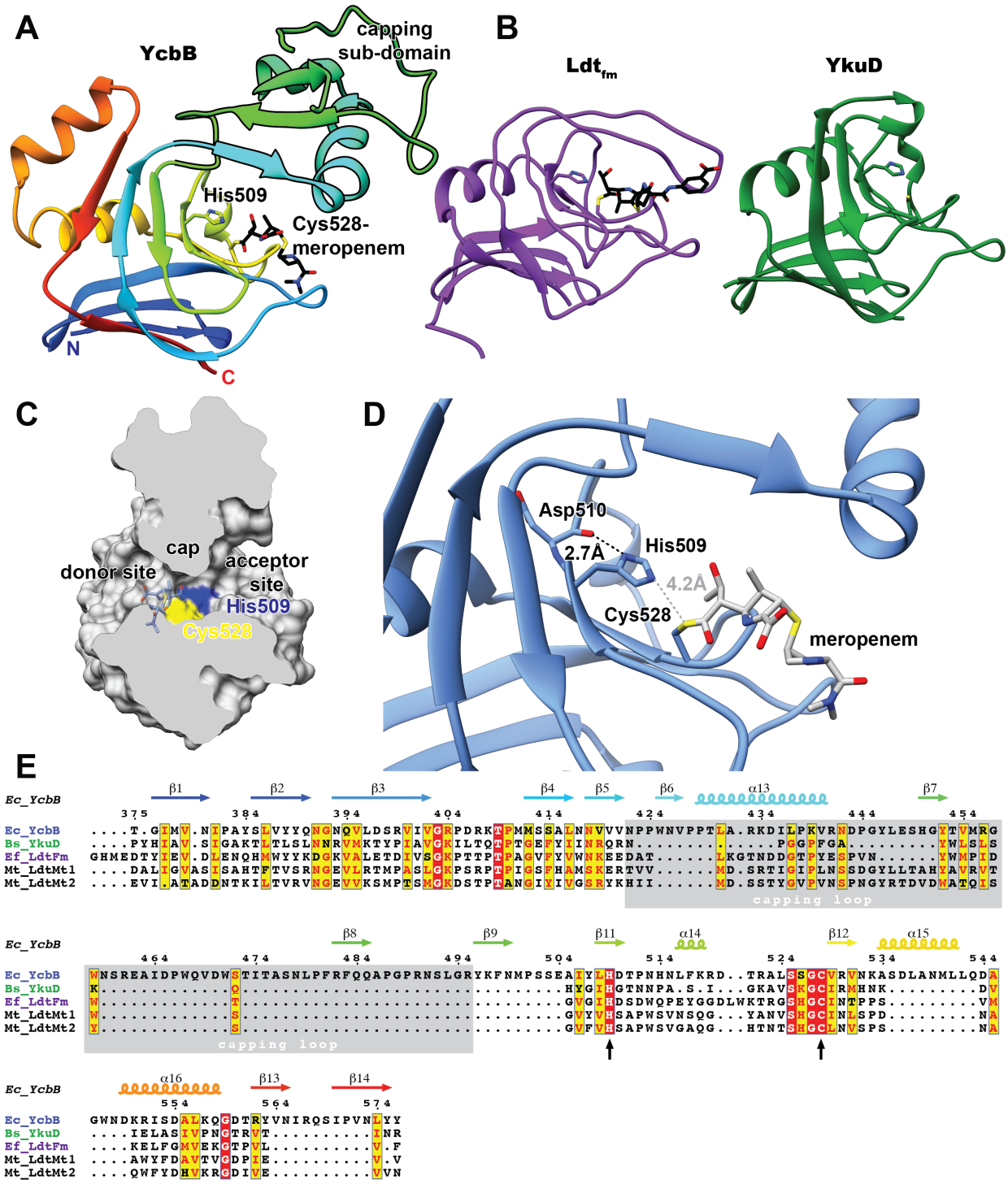

Figure 2.3 Structure of the *E. coli* YcbB catalytic domain.
(**A**) A ribbon representation of the YcbB catalytic domain, residues 375-576, coloured in rainbow from red (N-terminus) to blue (C-terminus). Meropenem is represented in black and coloured by heteroatom. The unique capping sub-domain is highlighted in a bold silhouette. (**B**) The catalytic domain architecture of *Enterococcus faecium* Ldt$_{Fm}$ (PDB ID 3ZGP (Lecoq et al. 2013)) and

Bacillus subtilis YkuD (PDB ID 1Y7M (Bielnicki et al. 2006)) highlighting the differences seen among L,D-transpeptidase catalytic domains in the capping loop region. (**C**) Cut surface representation of the YcbB catalytic domain, showing the capped cleft formed between the donor and acceptor sites by the capping loop sub-domain. The catalytic Cys528 and His509 are coloured in yellow and blue respectively. Meropenem (blue) is overlaid in its position in the donor site, acylating the catalytic cysteine. (**D**) The active site architecture of *E. coli* YcbB. The catalytic Cys528 is acylated by meropenem and the sulphide is rotated away from the N^{τ} of His509 (4.2 Å) which activated the cystine prior to acylation. The N^{π} of His509 is seen to be in close proximity with the backbone carbonyl of the adjacent Asp510 (2.7 Å), stabilising and promoting formation of the histidine cation. (**E**) The sequence of *E. coli* YcbB (Ec_YcbB) aligned with the aforementioned catalytic domains from *E. faecium* and *B. subtilis* (Ef_Ldtfm and Bs_Yku, respectively) as well as Ldt_{Mt1} and Ldt_{Mt2} from *Mycobacterium tuberculosis* (Mt_LdtMt1 and Mt_LdtMt2, respectively). Adapted from (Caveney et al. 2019).

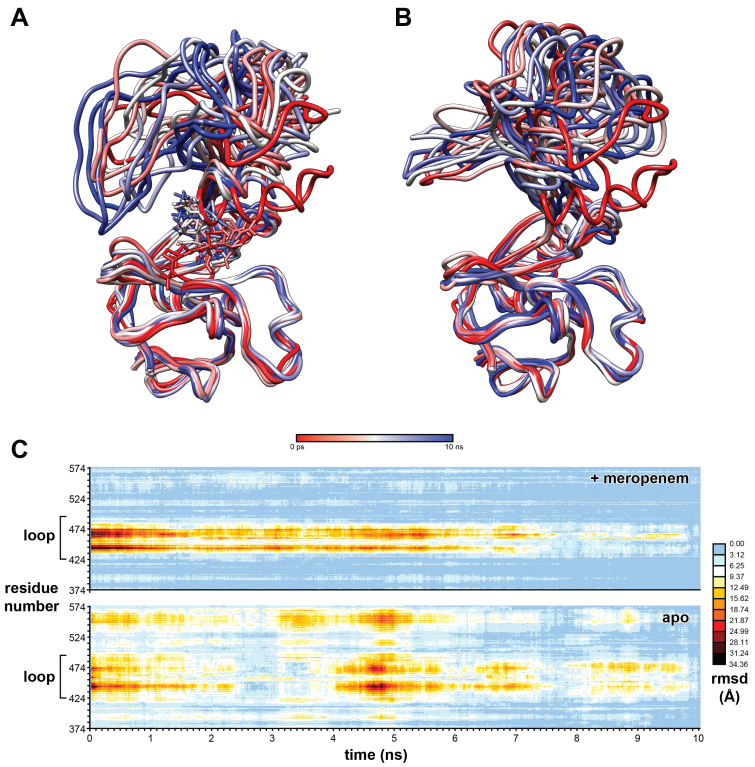

Figure 2.4 Molecular dynamics of *E. coli* YcbB.
(**A**) 10 ns simulation of YcbB and meropenem at 1ns increments, catalytic domain show, coloured from red to blue. (**B**) 10 ns simulation of YcbB at 1ns increments, catalytic domain show, coloured from red to blue. (**C**) RMSD of catalytic domain backbone carbons, in angstrom, of YcbB in complex with meropenem (top) and as apoenzyme (bottom). Adapted from (Caveney et al. 2019).

2.2.5 YcbB L,D-transpeptidase mechanism

From the structure of meropenem acylated YcbB, we propose a catalytic mechanism of the L,D-transpeptidase activity of YcbB, which despite the architectural differences is in keeping to what has been proposed for other L,D-transpeptidases previously (Erdemli et al. 2012) (Figure 2.5). In the proposed mechanism, the conserved Cys528 carries out a nucleophilic attack on the penultimate residue, *meso*-DAP, of a tetrapeptide on the donor PG strand, resulting in the release of the terminal D-Ala. This acyl-enzyme intermediate is subsequently deacylated via nucleophilic attack of a side chain amino on the *meso*-DAP on an adjacent acceptor PG strand. Conserved His509 of the catalytic dyad is seen to be located in close proximity to the catalytic Cys528 (distance Nτ to acylated Cys S of 4.2 Å); we suggest the hydrogen bond distance and angle between base and nucleophile are presumably optimized only in the apo form of the enzyme due to steric restraints induced by the covalently bound substrate in the subsequent acyl intermediate as captured here. Indeed several structures of acylated and apo forms of PBPs support this with high resolution structures showing the hydroxyl group of the catalytic serine nucleophile swings away from the conjugate base upon acylation (King et al. 2017). As well, we observe this in our apo molecular dynamics simulations, where the serine swings toward His509 within 10 ns of simulation to a final distance of 3.1 Å between the His Nτ to apo Cys S. The backbone carbonyl of the adjacent Asp510 is seen to be located near the Nπ of His509 (2.7 Å), forming a stabilising hydrogen bond and potentially modulating the pK_a of the His509 to improve its role as a general base. His509 is seen to be positioned both proximal to not only the catalytic cysteine, but as well the acceptor site of the catalytic cleft (Figure 2.3 C, D). This supports the notion that His509, stabilised by Asp510, acts as the general base for the activation of both the acylation and

deacylation steps of the L,D-transpeptidase reaction. It has been proposed previously for other L,D-transpeptidases that the catalytic histidine may act as both the general base, as well as to protonate the leaving groups (Erdemli et al. 2012), but from our YcbB-meropenem complex structure we propose that Tyr507 is a more likely candidate for this protonation in the case of YcbB. Tyr507 is more appropriately positioned, in angle and at 4.2 Å from the leaving group nitrogen, than the catalytic histidine, which is positioned 7.2 Å away and appears unlikely to donate this proton. As well, the nearby electropositive Lys497 (4.5 Å away) and potential hydrogen bond partner Trp425 (3.6 Å away) could serve to reduce the pK_a of the Tyr507 and allow for its role in protonation of the leaving group. The role of the Tyr507 at this position would be analogous to the role of the SXN motif serine (Ser139 in PBP5) in PBPs (Alexander et al. 2018), a role which has been very well characterized. We note that while a tyrosine residue exists at this position in L,D-transpeptidases from a variety of other species, it is not completely conserved at this position in the L,D-transpeptidase motif. The specific nature of these protonation events can perhaps be unravelled in future Michaelis complex structures of L,D-transpeptidases.

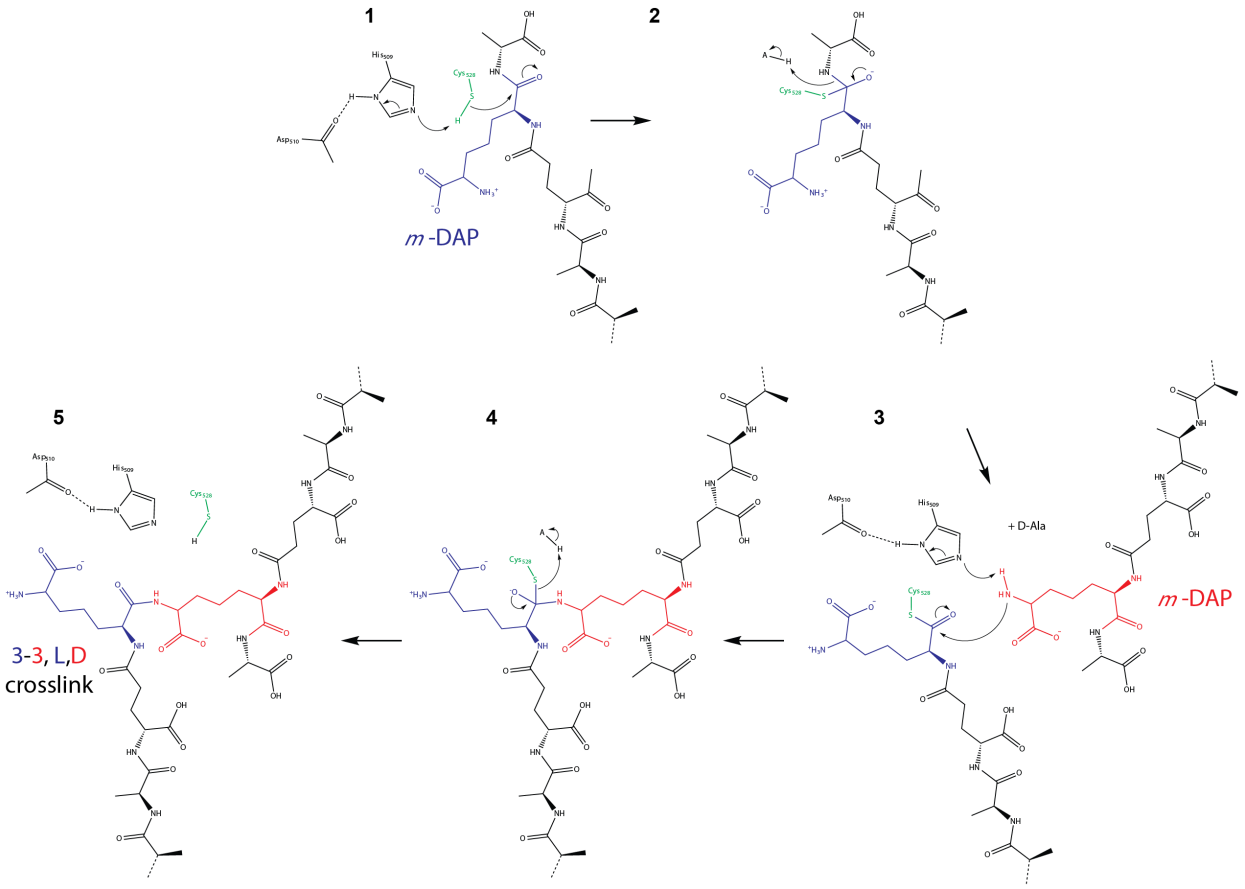

Figure 2.5 Catalytic mechanism of *E. coli* YcbB L,D-transpeptidase activity.
(**1,2**) Activation of Cys528 by His509 and subsequent cysteine mediated acylation of the penultimate residue, *meso*-DAP, of the tetrapeptide on the growing donor PG strand. This results in the release of the terminal D-Ala residue of the tetrapeptide. (**3,4**) Deacylation of the covalent acyl-enzyme via nucleophilic attack of a side chain *meso*-DAP on an adjacent acceptor PG strand. (**5**) The resultant 3-3, L,D crosslink is formed and the enzyme is returned to its starting state. Adapted from (Caveney et al. 2019).

2.2.6 Inhibition of the L,D-transpeptidase mediated resistance pathway

In order to probe the inhibition of the YcbB-mediated β-lactam resistance pathway to the fullest extent, meropenem acylation of both the L,D-transpeptidase and D,D-carboxypeptidase activities required was investigated (Figure 2.6). The YcbB-meropenem complex map had ordered density defining the active site residues including the thiol ester covalent link of Cys528 and acylated meropenem (Figure 2.6 B). A 2.2 Å resolution structure of PBP5 acylated with meropenem was also solved with very well ordered density for the covalently bound meropenem (Figure 2.6 C). Relative to previously published PBP5 structures, we were able to trace additional residues at the C-terminus of PBP5 (387-397; likely afforded by the differential packing with a neighboring molecule in our unique crystal lattice). Regardless, the conserved binding mode of the ligands between the PBP5-meropenem structure and the PBP5-imipenem structure (PDB ID 3MZF (Nicola et al. 2010)) indicates similar modes of enzyme acylation and binding. On the other hand, despite the similarity in the PG substrates for the YcbB L,D-transpeptidase and PBP5 D,D-carboxypeptidase, we observe the binding and stabilisation of meropenem between the two enzymes is quite distinct.

Meropenem binds PBP5 in a typical PBP fashion using the conserved SXXK, SXN, and KTG active site sequence motifs common to this broad class of activated serine carboxypeptidases. The meropenem is acylated at C7 by the Ser73 side chain hydroxyl of the SXXK motif (the proximal Lys76 of the motif playing the general base role) and stabilised through an extensive hydrogen bond and electrostatic network (Figure 2.6 C, G). The carbonyl oxygen on C7 of meropenem occupies the enzyme oxyanion hole comprised of main chain nitrogens at position 73

and 245, forming strong hydrogen bonds that polarize and stabilize the carbonyl during acylation and formation of oxycarbanion intermediates (Figure 2.6 D). The side chain hydroxyl of Ser 139 of the SXN motif resides adjacent to the leaving group nitrogen of meropenem, the likely source for protonation of that moiety to promote acylation. The Asn141 side chain amide of the SXN motif hydrogen bonds with the 1-hydroxyethyl group on C6 of meropenem, while the Thr243 side chain hydroxyl of the KTG motif forms bidentate hydrogen bonds to the carboxylic acid group of meropenem (C3). The latter is further stabilized by longer range electrostatic interactions with the side chain amido of Lys242 of the motif as well as the guanidinium group of Arg277. As well there are typical hydrogen bonds formed, backbone amide of His245 and water-mediated interactions with the backbone amide of Arg227 and the backbone carbonyl of Leu137.

In contrast, meropenem binding of YcbB is void of this extensive network of hydrogen bonds, instead consisting of acylation at C7 by the catalytic Cys528 and a few key hydrogen bonds (Figure 2.6 B, F). The carbonyl oxygen on C7 of acylated meropenem protrudes into an oxyanion hole consisting of, analogous to the PBPs, the amide nitrogen of the nucleophile, here Cy528. However, the second commonly observed main chain nitrogen amide of the PBPs is replaced in YcbB by a close interaction to the carbonyl oxygen at Ala 505 which has an interaction with the substrate. A further markedly distinct feature in the meropenem complex is the minimal non-covalent interactions of the C3 carboxylate of meropenem with enzyme. One hydrogen bond to the backbone carbonyl of Ala505 is the primary interaction, replacing the typical electrostatic interactions observed for this ubiquitous functional group of β-lactam antibiotics. Despite the relative proximity of electropositive groups such as Arg407, Arg433, Lys434, and Lys497 the proline rich insertion centered at Pro428 appears to provide a structural ridge that prevent

meaningful interaction. At the same time hydrophobic interactions between enzyme and substrate appear more prominent, with, for example, Trp425, Pro428 and Leu431 forming an explicit apolar pocket for binding of the C1 methyl of meropenem. The general lack of complex hydrogen bonding and increased hydrophobic interactions is characteristic of L,D-transpeptidase acyl-enzyme complexes with carbapenem inhibitors and is seen in meropenem acylation of Ldt_{Mt2} (PDB ID 4QR7 (Gokulan et al. 2018)). Pre-acylation, there could be additional stabilisation of meropenem from residues of both the active site and the capping loop that allow for proper positioning of the drug for acylation by the catalytic cysteine.

Despite the similarities in the activities of PBP5 and YcbB and therefore some of the common attributes to the inhibition of these enzymes by meropenem, there are vast differences in the overall stabilization of these drugs post-acylation. It is likely that PBPs were the target of the evolution of this class of antibiotics, originally in *Streptomyces cattleya* and in subsequent drug development (Birnbaum et al. 1985). This is exemplified by structural properties of the inhibition of these enzymes, with the generally more stabilized meropenem of the acylated PBP5 proving a better inhibitor. As we continue to unravel the importance of L,D-transpeptidase mediated β-lactam resistance, it will become increasingly relevant to revisit this important class of antibiotic and, using structure guided design, improve upon the binding and inhibition of L,D-transpeptidases by carbapenems.

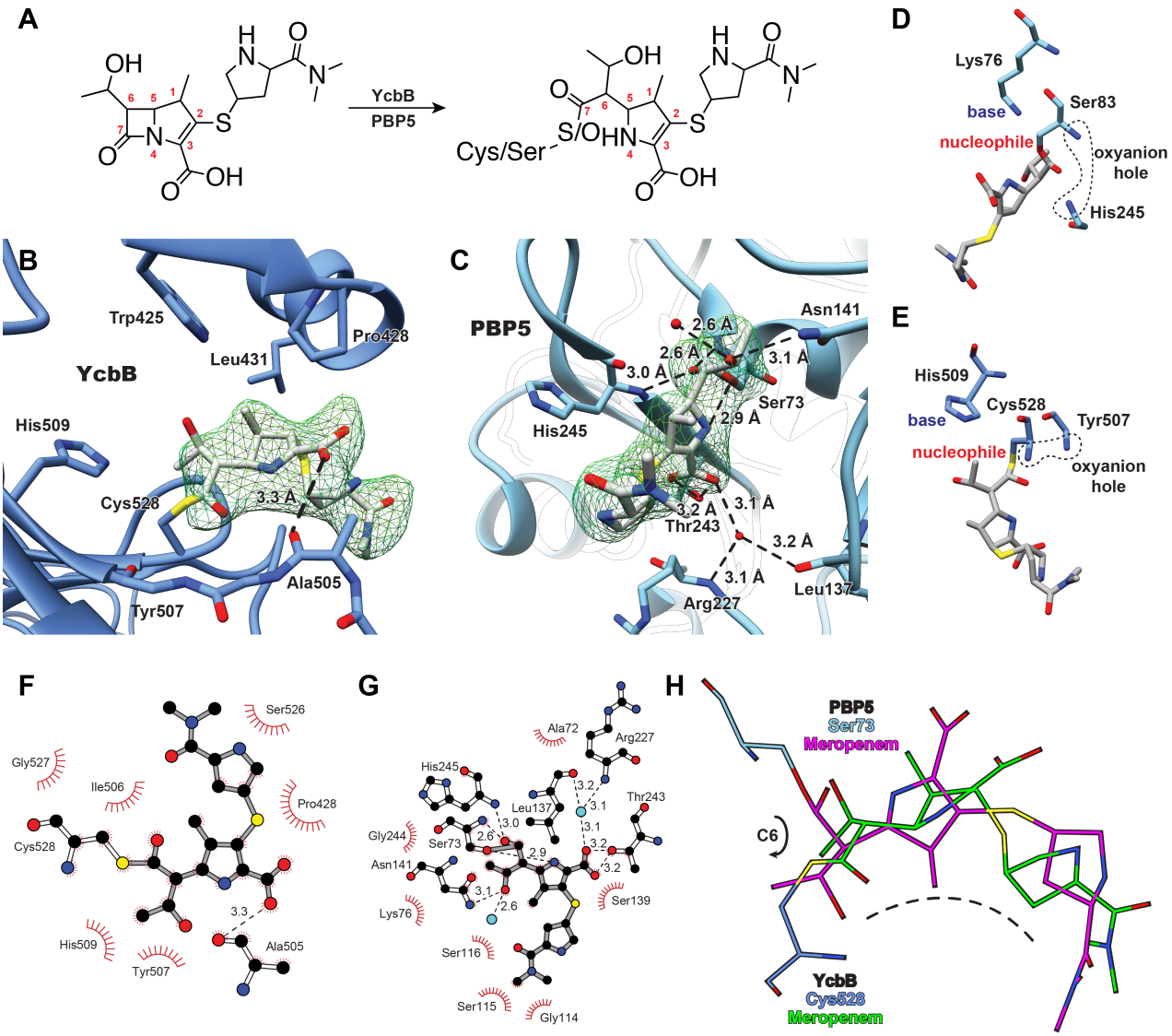

Figure 2.6 Meropenem inhibition of *E. coli* YcbB and PBP5.
(**A**) Chemical diagram of meropenem pre- and post-acylation by YcbB and PBP5. (**B**) mF_o-DF_c simulated annealing omit map for the acylated meropenem on Cys528 of YcbB, contoured at 2σ. YcbB is in blue and meropenem in grey. The catalytic diad (Cys528 and His509), relevant residues, and meropenem are coloured by heteroatom. Hydrogen bonding between meropenem and the backbone carbonyl of Ala505 is represented with dashed lines. (**C**) mF_o-DF_c simulated annealing omit map for the acylated meropenem on Ser73 of PBP5, contoured at 2σ. PBP5 is in blue and meropenem in grey. PBP5 residues involved in the stabilization of meropenem, relevant water molecules, and meropenem are coloured by heteroatom. Hydrogen bonding between meropenem, relevant residues, and water is represented with dashed lines. Relative arrangement of nucleophile, general base and oxyanion hole (backbone atoms shown) for PBP5 (**D**) and YcbB (**E**). (**F,G**) LigPlot diagrams of meropenem acyl-enzyme complexes. (**F**) YcbB-meropenem complex with meropenem in grey and protein residues in white, with atoms coloured by heteroatom. (**G**) PBP5-

meropenem complex coloured as in **F**. (**H**) Overlay of meropenem-acylated catalytic residues of YcbB (darker blue and green) and PBP5 (lighter blue and pink) showing a similar general curvature of both meropenem molecules, with the notable exception of an approximate 180° rotation about meropenem C6 due to the differing active site architectures of YcbB and PBP5. Adapted from (Caveney et al. 2019).

2.2.7 *In vivo* assay of YcbB mediated β-lactam resistance

In order to correlate the sequence and structural aspects of *E. coli* YcbB to its role in antibiotic resistance, antibiograms using a β-lactam disk diffusion assay were performed (Figure 2.7). The antibiotics ampicillin and ceftriaxone were chosen for use in these assays, as they are well characterized, non-carbapenem, β-lactam antibiotics that provide insight into the general trends in β-lactam resistance apart from carbapenems. Unsurprisingly, replacements of both the catalytic cysteine and histidine resulted in a complete loss of the β-lactam resistance (β-lac^{R}) phenotype seen in the assay with wild type YcbB.

Of greater interest was the contribution of the capping loop to antibiotic resistance. To this end, the assay was performed with a truncated YcbB containing a YkuD-like capping stub (*ycbB* Δ426-491), as well as with a Trp425Ala replacement designed to interfere with the significant hydrophobic interactions the indole side chain was observed to mediate with meropenem in our complex structure. Both of these replacements resulted in an β-lactam sensitivity (β-lac^{S}) phenotype. This further validates the proposition that the capping loop, despite its inherent flexibility, plays a crucial role in facilitating YcbB mediated L,D-transpeptidation.

Replacements of the catalytic domain and capping sub-domain provide insight into the requirement for functional L,D-transpeptidase activity in antibacterial resistance, yet an understanding of the role of the PG domain in this resistance and the activity of L,D-transpeptidases in general was poorly understood. While many L,D-transpeptidase enzymes have PG domains of one type or another, these domains have yet to be specifically linked to their role LD-transpeptidation *in vivo*. Replacements of both the presumed PG binding residues of the YcbB PG domain (Asp337 and Arg244), as well as a truncation to the extended loop (ycbB Δ268-312) unique to the YcbB PG domain in comparison to homologous PG domains in other enzymes, were tested in the *in vivo* β-lactam resistance assay. Interestingly enough, only the Asp337Ala replacement and Δ268-312 deletion resulted in β-lactam sensitivity. The Arg244Ala replacement resulted in a continued β-lactam resistance phenotype. We propose that this is likely due to a greater contributing role of the Asp337 in the binding of PG in comparison to Arg244. Asp337 is positioned more closely to the cleft between the catalytic and PG domains (Figure 2.7 A), where the acceptor PG strand would likely lie in order to have access to the acceptor site of the catalytic domain. In contrast, Arg244 is positioned further away from the cleft and less likely to be forming as strong an interaction with the acceptor PG strand (Figure 2.7 A). Regardless of the contribution of Arg244 in PG binding, this is the first evidence of how an accessory PG binding domain can have implications on L,D-transpeptidase function in an *in vivo* setting. As the extended loop on the PG domain is on the opposite side of the domain from the proposed residues that are involved in binding the acceptor PG strand, it is possible that it is mediating additional interactions with the existing PG sacculus that are important in the context of the greater YcbB mediated resistance pathway. Overall, this clearly shows the importance of the accessory PG binding domains in L,D-transpeptidase function *in vivo*.

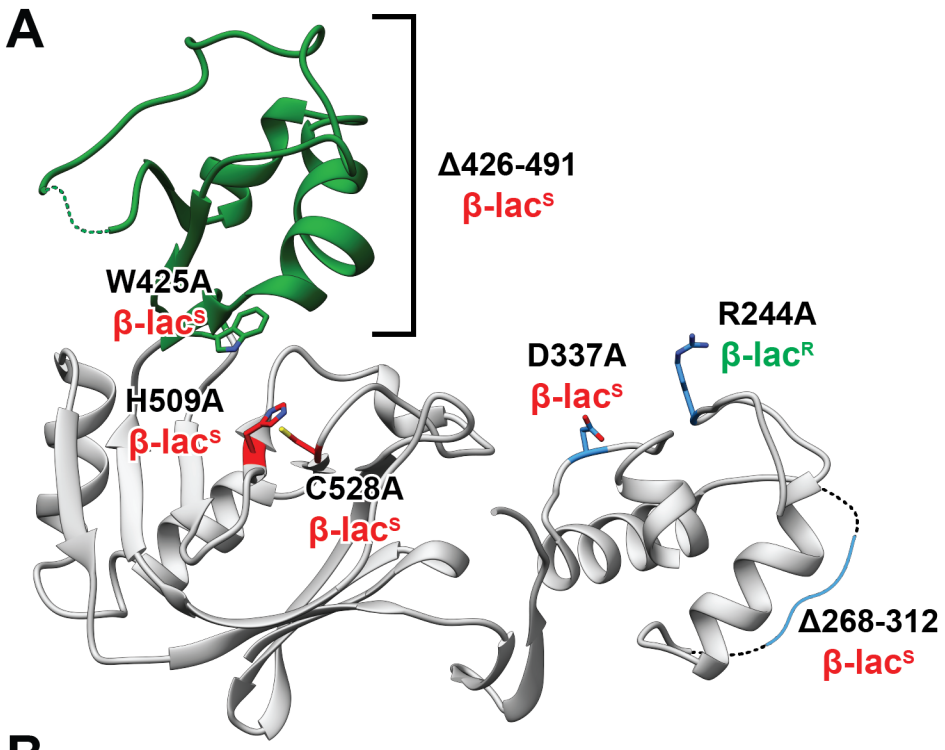

B

	mutant	mutant group	phenotype
i	Cys528Ala	catalytic	β-lac^S
ii	His509Ala		β-lac^S
iii	Δ426-491	capping loop	β-lac^S
iv	Trp425Ala		β-lac^S
v	Arg244Ala	PG binding	β-lac^R
vi	Asp337Ala		β-lac^S
vii	Δ268-312		β-lac^S
viii	wt	-	β-lac^R

Figure 2.7 *In vivo* assay of YcbB mediated β-lactam resistance.
(**A**) Various replacements and deletions of the catalytic residues (in red), capping loop region (in green) and PG binding domain (in blue), mapped onto the catalytic and PG domains of YcbB. Replacements retaining YcbB mediated β-lactam (ampicillin and ceftriaxone) resistance are denoted as β-lac^R, while replacements and deletions resulting in β-lactam (ampicillin and ceftriaxone) susceptibility are denoted as β-lac^S. (**B**) Replacements and deletions of pTK2(*ycbB*) (**i-viii**) are listed with their resulting phenotype. Adapted from (Caveney et al. 2019).

2.2.8 Interaction of YcbB with PBP1b and PBP5

Ycbb, PBP5 and PBP1b are known to contribute sequentially in a D,D-transpeptidase bypass pathway in *E. coli* (Hugonnet et al. 2016). It was of interest, therefore, to determine whether YcbB interacts directly with these PBPs that provide substrate. To do this assessment, YcbB-PBP1b and YcbB-PBP5 interactions were assayed using microscale thermophoresis (MST). Styrene-maleic acid co-polymer solubilised PBP1b was used to mitigate protein aggregation issues in the capillary that were encountered with detergent-solubilised PBP1b. The YcbB-PBP1b interaction was seen to have a K_d of 250 ± 30 nM (Figure 2.8 A). The YcbB-PBP5 interaction was seen to be somewhat weaker, with the MST data suggesting at most a K_d in the low micromolar range (~2 μM) (Figure 2.8 B). These affinities are consistent with the generally-accepted understanding regarding the dynamic nature of PG biosynthetic complexes in response to environmental challenges or the particular stage in the life cycle of the bacterium (Pazos, Peters, and Vollmer 2017). Due to the relatively apolar nature of the scaffolding domain of YcbB (Figure 2.1) we postulate that these interactions with PBP1b and PBP5 primarily occur through interactions with apolar regions of PBP1b and PBP5. Both PBP1b and PBP5 are seen to exhibit similar electrostatic surface charge characteristics to YcbB, with localized electropositive surface regions about their active sites and more apolarity to their other surface regions (Figure 2.9). The association of YcbB to the apolar hinge region of PBP5 and the apolar regions of PBP1b's glycosyltransferase domain would localise YcbB to receive the proper substrates from PBP1b and PBP5 to successfully mediate β-lactam resistance.

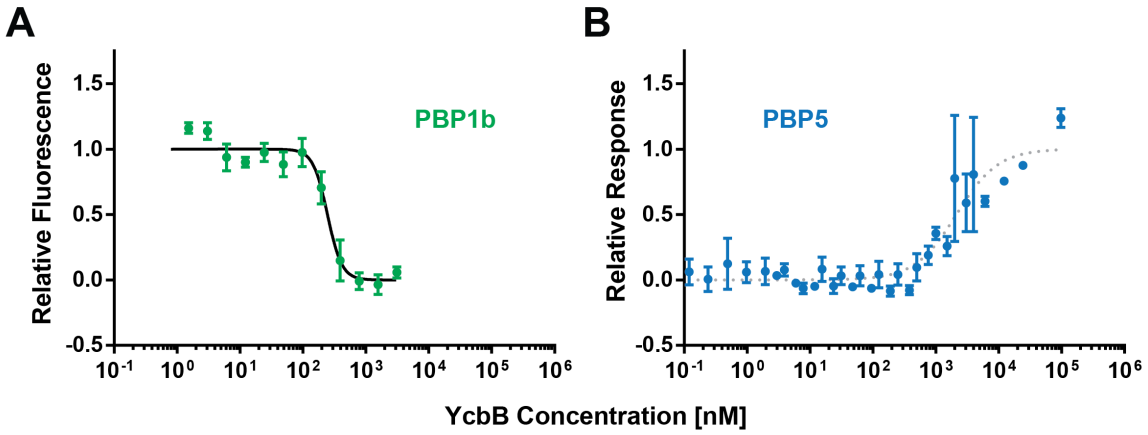

Figure 2.8 *E. coli* YcbB interaction with PBP1b and PBP5.
Microscale thermophoresis analysis of PBP1b (**A**) and PBP5 (**B**) interaction with YcbB. (**A**) YcbB-PBP1b interaction was evaluated using relative fluorescence and the data was best fit by a binding isotherm with a K_d of 250 ± 30 nM and a Hill coefficient of 3.8. (**B**) YcbB-PBP5 interaction was evaluated using relative MST response. While it was not possible to work with PBP5 concentrations sufficiently high to observe saturation of all binding sites on YcbB, fitting the data to a binding isotherm yielded K_d and Hill coefficient values of 2.1 ± 0.5 μM and 1.3, respectively. The affinity between YcbB and PBP5 is the estimated maximum affinity for the complex. Measurements for the YcbB-PBP1b interaction were performed in triplicate with two technical replicates of each. Measurements for the YcbB-PBP5 interaction were performed in triplicate. Error bars represent the standard deviation of the measurements in both cases. Adapted from (Caveney et al. 2019).

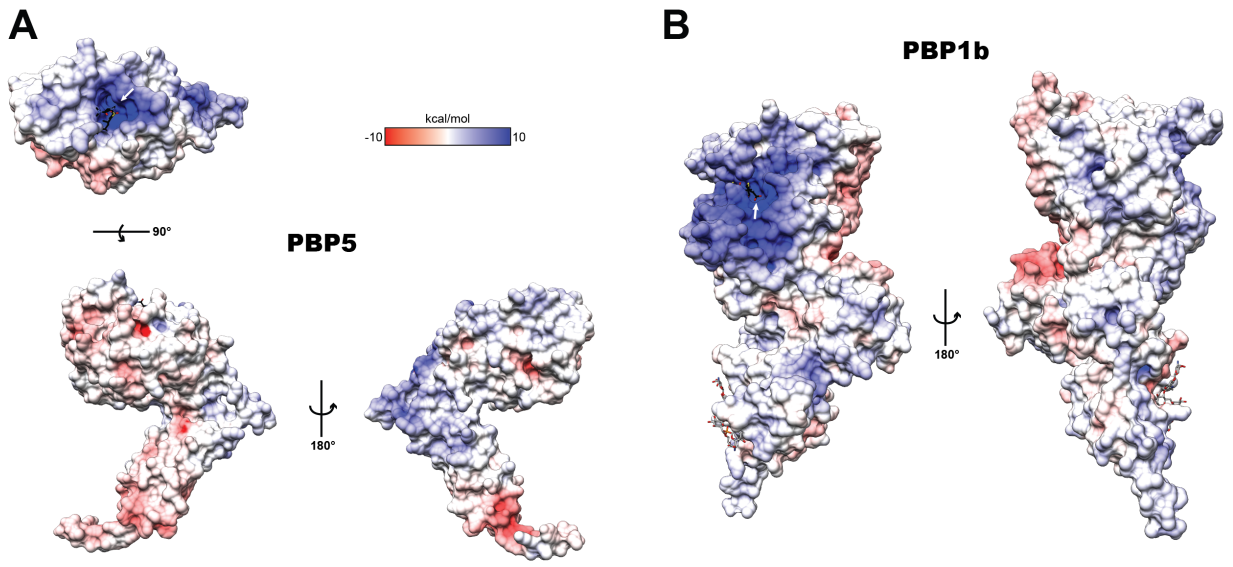

Figure 2.9 Electrostatic surface potential of *E. coli* PBP5 and PBP1b.
(**A**) Electrostatic surface representation of PBP5-meropenem acyl-enzyme complex in three views related by a 90° rotation around the x-axis and a 180° rotation around the y-axis. (**B**) Electrostatic surface representation of PBP1b-CENTA acyl-enzyme complex (PDBID 5HLD (King et al. 2017)) in two views related by a 180° rotation around the y-axis. Electro positive transpeptidase active sites marked with white arrows in both **A** and **B**. Adapted from (Caveney et al. 2019).

2.2.9 Implications on YcbB mediated β-lactam resistance

The structures reported here further develop our understanding of YcbB mediated β-lactam resistance and allow us to expand upon the previously proposed model of the resistance pathway (Hugonnet et al. 2016) (Figure 2.10). Under conditions of increased alarmone production, YcbB and PBP5 are likely able to form a transient complex with PBP1b. The soluble protein YcbB is likely able to couple to the two monotopic membrane proteins, PBP1b and PBP5, to interact directly through its putative interaction/helical domain. As well, YcbB is likely assisted in this localisation and oriented in position to crosslink a polymerising PG strand by its PG binding domain mediated interaction with the existing sacculus. This is distinct from the role of the LysM-like PG binding domain of YkuD (Schanda et al. 2014) and other Ldt enzymes, in which the PG binding domain is oriented adjacent to the donor site of the catalytic domain, as opposed to the acceptor site seen in YcbB. Once the complex has been formed, PBP1b could act to polymerise periplasmicaly oriented lipid II into a growing PG strand. As β-lactam drugs inhibit the transpeptidase domain of PBP1b, PBP5 could then assist in rescue of PG formation by removing the terminal D-Alanine, thereby providing the substrate for YcbB. This growing strand would orient itself adjacent to the donor site of YcbB, with the tetrapeptide stem entering into the catalytic cleft. In parallel, the PG domain associated acceptor PG strand would enter the acceptor site of the catalytic cleft. YcbB mediated L,D-transpeptidase activity and substrate release would occur involving rearrangement of the substrate capping loop/sub-domain and resulting in the capped substrate cleft (seen in the acyl-enzyme complex structure) to re-orient into an open cleft. This proposed mechanism for this resistance pathway is consistent with the growing understanding in the field that PG biosynthesis depends on a number of dynamic and variable multi-protein

complexes (Pazos, Peters, and Vollmer 2017) that are regulated spatiotemporally and, as in the case of YcbB mediated β-lactam resistance, by external stimuli. As we enter into an era of increasing antibiotic resistance, unravelling the intricacies of these non-canonical PG biosynthetic complexes will be of increasing importance as bacteria deploy these flexible pathways to evade antibiotic assault.

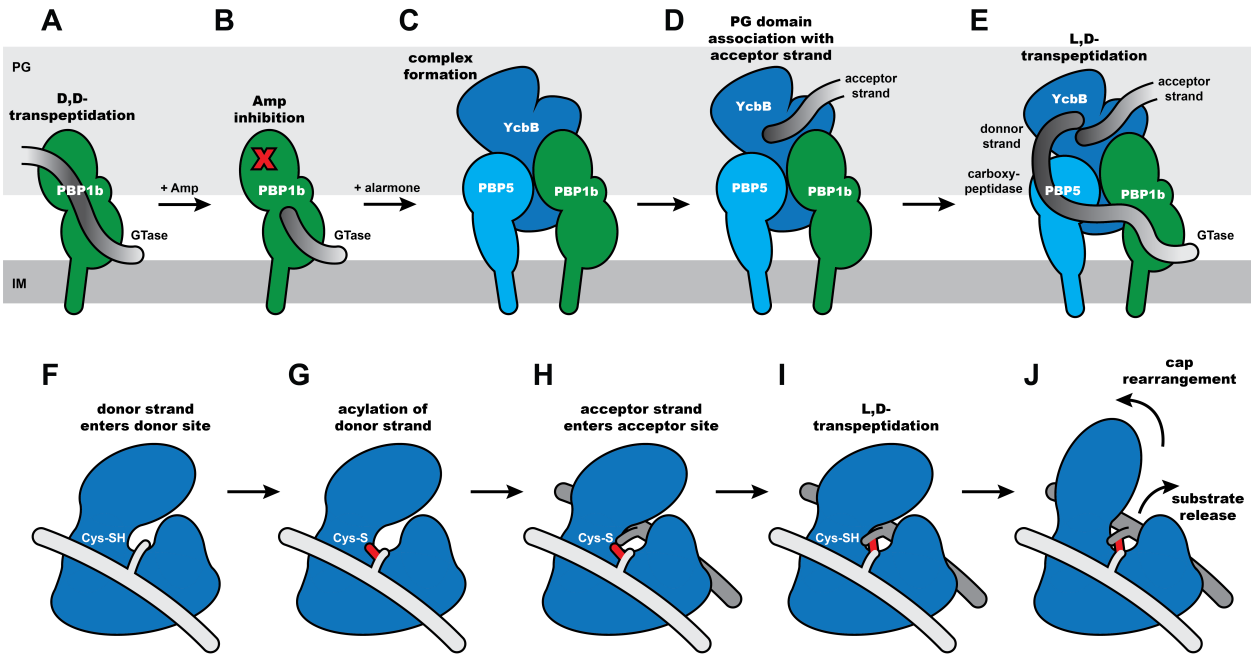

Figure 2.10 Schematic representation of YcbB mediated β-lactam resistance.
(**A-E**) Assembly and function of the YcbB mediated β-lactam resistance pathway. (**A**) PBP1b function in the absence of β-lactam antibiotics. PBP1b acts as both glycosyltransferase and D,D-transpeptidase. (**B**) PBP1b function in the presence of β-lactam antibiotics, such as ampicillin. PBP1b can maintain glycosyltransferase activity, but D,D-transpeptidation is inhibited. (**C**) β-lactam resistance complex formation upon production of alarmone. YcbB likely interacts with PBP1b and PBP5 through its putative interaction/helical domain. (**D**) YcbB is likely additionally associated and oriented through its PG binding domain interacting with the acceptor strand of the existing PG sacculus. (**E**) The resistance complex can successfully rescue crosslinking function. PBP1b polymerizes PG strands with glycosyltransferase activity, PBP5 removed a terminal D-alanine with its carboxypeptidase activity, and YcbB acts on the modified peptides with L,D-transpeptidase activity to crosslink the PG strand into the sacculus. (**F-J**) Function and mechanism of the YcbB catalytic domain during L,D-transpeptidation. (**F**) Tetrapeptide of the donor PG strand enters the donor site of the catalytic domain. (**G**) Donor tetrapeptide is acylated at its *meso*-DAP residue by the catalytic cysteine, resulting in the loss of the terminal D-alanine. (**H**) Adjacent acceptor PG peptide enters the acceptor site of the catalytic domain. (**I**) The covalent acyl-enzyme is deacylated via nucleophilic attack of the side chain *meso*-DAP on the adjacent acceptor PG strand, forming the L,D-crosslink. (**J**) Rearrangement of the capping loop/sub-domain from a capped conformation to an open cleft will occur, resulting in the release of the crosslinked substrate. Adapted from (Caveney et al. 2019).

2.3 Methods

2.3.1 Cloning and protein expression

Escherichia coli YcbB without its signal peptide (residue 31 onward) was cloned into the expression vector pET41b-GST with a thrombin cleavable, C-terminal 8x His-tag. *E. coli* PBP1b from residue 58 onward was cloned into the expression vector pET41b-GST with a thrombin cleavable, C-terminal 8x His-tag. *E. coli* PBP5 from residue 30 onward was cloned into the expression vector pET41b-GST with a human rhinovirus (HRV) 3C protease cleavable, C-terminal 8x His-tag. Expression constructs were transformed into *E. coli* BL21 (DE3) for expression of YcbB and PBP5. PBP1b expression construct was transformed into *E. coli* C41. Cells were cultured in ZYP-5052 autoinduction media for four hours at 37°C followed by overnight protein expression at 25°C. Cells were pelleted and stored at -80°C until required.

2.3.2 Protein purification

For purification of YcbB and PBP5, cell pellets were resuspended in lysis buffer (20 mM Hepes, pH 8.0, 300 mM NaCl, 10% glycerol) and lysed by processing twice with a homogenizer (15 kPa; Avestin). Cellular debris was pelleted by centrifugation at 125,000 x g for 1 hour. The resultant supernatant was loaded onto a 1/5 mL Ni2+-saturated HisTrap HP Sepharose cartridge (GE Lifesciences), washed with 75 mM imidazole in Buffer A (20 mM Hepes, pH 8.0, 300 mM NaCl), and the protein was eluted with 300 mM imidazole in Buffer A. 1 U of HRV 3C protease or thrombin was added per mg of protein to remove the N-terminal His-tag overnight at 4°C.

Samples were purified further by size exclusion chromatography (SEC) with a Superdex 200 column (GE Lifesciences) equilibrated in Buffer B (20 mM Hepes, pH 8.0, 150 mM NaCl). Fractions containing pure PBP5 or YcbB were pooled and concentrated to 10 to 40 mg/mL. Protein was frozen rapidly in liquid nitrogen and stored at -80°C until required. For purification of PBP1b, cell pellets were resuspended in lysis buffer (20 mM Hepes, pH 8.0, 300 mM NaCl, 10% glycerol) and lysed by processing twice with a homogenizer (15 kPa; Avestin). Cellular debris was pelleted by centrifugation at 10,000 x g for 30 minutes. The resultant supernatant was centrifuged at 125,000 x g for 1 hour to pellet membranes. The membranes were solubilised in Buffer A with 1% (w/v) N-dodecyl-D-maltopyranoside (DDM) overnight at 4°C and loaded onto a 1/5 mL Ni^{2+}-saturated HisTrap HP Sepharose cartridge (GE Lifesciences), washed with 75 mM imidazole in Buffer A with 0.016% DDM, and the protein was eluted with 300 mM imidazole. 1 U of thrombin was added per mg of protein to remove the N-terminal His-tag overnight at 4°C. Samples were purified further by SEC with a Superdex 200 column (GE Lifesciences) equilibrated in Buffer B with 0.2% DM. Fractions containing pure PBP1b were pooled and concentrated to 10 to 40 mg/mL. Protein was frozen rapidly in liquid nitrogen and stored at -80°C until required. SMA-solubilised PBP1b was prepared as above, with the extraction occurring in 2% activated SMA and subsequent buffers having no detergent present.

2.3.3 Microscale thermophoresis

Microscale thermophoresis (MST) assays were conducted using a Monolith NT.115Pico (NanoTemper). YcbB, PBP5 and PBP1b were fluorescently labelled using Alexa Fluor 647 NHS Ester (Thermo Fisher Scientific). To evaluate the binding of PBP1b to YcbB, increasing

concentrations of unlabelled YcbB (1.5 nM – 3.1 μM) were used to titrate fluorescently labelled SMA-solubilised PBP1b at a constant concentration (100 nM). To evaluate the binding of PBP5 to YcbB, increasing concentrations of unlabelled PBP5 (120 pM – 98 μM) were used to titrate fluorescently labelled YcbB at a constant concentration (15 nM). Experiments were carried out in a Buffer C. Data was analysed using the NanoTemper MO Affinity Analysis software. The PBP1b-YcbB interaction data was analysed using fluorescence values, while the PBP5-YcbB data was analysed using microscale thermophoresis. The data was fit to the equation for a binding isotherm with adjustable Hill coefficient.

2.3.4 X-ray crystallography and structure determination

E. coli YcbB protein was crystallized at 20°C by sitting drop vapour diffusion using 0.2 μL protein solution (30 mg/mL purified protein in Buffer A) and 1 μL of mother liquor (1.44 M lithium sulfate, 0.08 M HEPES pH 7.5, 0.02 M sodium acetate pH 4.6, 0.015 M ammonium sulfate, 4% (w/v) polyethylene glycol (PEG) 2000 monomethyl ether (MME)) with the addition of 1 mM meropenem. The best diffracting YcbB crystal had the addition of a tetrapeptide (L-Ala-D-Glu-*m*DAP-D-Ala) at 1 mM, though no density could be found for this ligand. *E. coli* PBP5 protein was crystallized at 20°C by sitting drop vapour diffusion using 0.2 μL protein solution (5 mg/mL purified protein in Buffer A) and 1 μL of mother liquor (0.1 M tris pH 7, 7% PEG 400) with the addition of 1 mM meropenem. X-ray diffraction data of YcbB-meropenem-ethylmercury and PBP5 was collected on Canadian Light Source beamline 08B1-1 using crystals flash-frozen in liquid nitrogen with the addition of 20% glycerol to the mother liquor. Data for native YcbB-meropenem was collected on Advanced Light Source beamline 501. For phasing of YcbB, a YcbB-

meropenem crystal was soaked in mother liquor supplemented with 1 mM ethylmercury phosphate for 30 seconds. A single isomorphous replacement (SIR) experiment was carried out using the ethylmercury phosphate soaked crystal. All datasets were processed with XDS (Kabsch 2010), run manually or through Autoprocess (Fodje et al. 2014). For the SIR dataset, SHARP (Bricogne et al. 2003) was used for phasing, model building was performed by AutoBuild (Terwilliger et al. 2007) and refined using Phenix (Adams et al. 2010) and Coot (Emsley and Cowtan 2004). For the native YcbB dataset and the PBP5 dataset, the structures were solved by molecular replacement using Phaser (McCoy et al. 2007). The SIR YcbB preliminary structure was used as the template for the YcbB structure and PDBID 3MZF was used to phase the PBP5 crystal. These structures were then refined using Phenix (Adams et al. 2010) and Coot (Emsley and Cowtan 2004). The capping loop region of YcbB was refined using density-guided iterative local refinement as implemented in Rosetta (DiMaio et al. 2015). See Table 2.1 for data collection and refinement statistics.

2.3.5 Molecular dynamics simulations

A complete model for the meropenem acyl and apoenzyme forms of YcbB for molecular dynamics simulations was built from our structure of YcbB-meropenem acyl-enzyme complex with missing disordered loop regions built in using ModLoop (Fiser and Sali 2003). This was then solvated and simulation input files were generated using Quick MD Simulator of the online CHARMM-GUI web service (Jo et al. 2008; Lee et al. 2016). Equilibration and production simulations were performed with GROMACS 5.1 (Abraham et al. 2015), using the CHARMM36 all-atom force field (Best et al. 2012) to represent all protein, solvent and ions. Production

simulations were run for 10 ns. RMSD calculations were performed using the RMSD Visualizer Tool and HeatMapper of VMD (Humphrey, Dalke, and Schulten 1996).

2.3.6 Impact of substitutions in YcbB on β-lactam resistance

β-lactam resistance mediated by bypass the PBPs requires high-level production of the alarmone (p)ppGpp and of YcbB (Hugonnet et al. 2016). In this study, we used strain BW25113Δ*relA*::Km^R pKT8(*relA'*), which allows the arabinose-inducible production of (p)ppGpp. The strain was transformed with the derivatives of pKT2(*ycbB*) for isopropyl β-d-1-thiogalactopyranoside (IPTG)-inducible expression of YcbB and pf derivatives with amino acid substitutions. The phenotype was analyzed using the disk diffusion assay in BHI agar supplemented with 50 µM IPTG, 1% arabinose, or both inducers, as previously described (Hugonnet et al. 2016). Disks were loaded with 10 µg of mecillinam, 10 µg of ampicillin, 30 µg of ceftriaxone, 30 µg of tetracycline, 30 µg of chloramphenicol, or 30 µg of kanamycin. Incubation was performed at 37°C overnight. Resistance to β-lactams [β-lac^R] was defined as growth at the contact of disk containing ampicillin and a diameter <17mm for the inhibition zone around the disk containing ceftriaxone, as previously described (Hugonnet et al. 2016). Susceptibility [β-lac^S] was defined as diameters >20mm and >35mm for the inhibition zones around the disks containing ampicillin and ceftriaxone, respectively. We checked that resistance to ampicillin and ceftriaxone was dependent upon the presence of both inducers.

2.4 Data availability

Atomic coordinates for the YcbB-meropenem and PBP5-meropenem models have been deposited in the protein data bank with accession codes 6NTW and 6NTZ respectively.

Chapter 3: Structural and cellular insights into the L,D-transpeptidase YcbB as a therapeutic target in bacterial infections

3.1 Introduction

The synthesis of the bacterial cell wall has long been a target of antibacterial strategies from both competing species (Aoki et al. 1976) as well as in drug development (Sabe et al. 2019; Decuyper et al. 2018). This is exemplified by the widespread use of β-lactam antibiotics, which target the final stages of this pathway. The targeting of cell wall biosynthesis is an excellent strategy due to the importance of the bacterial cell wall in bacterial viability. The bacterial cell wall consists of peptidoglycan (PG) – extended glycan strands of alternating β-1,4 linked *N*-acetyl-glucosamine-*N*-acetyl-muramic acid which are crosslinked into a net-like mesh via short peptide segments covalently attached at the C3-OH position of the muramic acid moiety (Caveney, Li, and Strynadka 2018).

This PG is synthesised through a multistage pathway transitioning from the bacterial cytosol with the formation of soluble precursors, to the inner leaflet of the cytoplasmic membrane where these precursors are assembled onto lipid carriers, to the outer leaflet of the cytoplasmic membrane where the polymerisation and crosslinking of the PG occurs through the activity of penicillin binding proteins (PBPs) (Caveney, Li, and Strynadka 2018; Sobhanifar, King, and Strynadka 2013).

PBPs are split into two major classes, class A and B (aPBP and bPBP, respectively). The aPBPs perform both a glycosyltransferase activity which polymerizes the recently flipped lipid II molecules into a growing PG strand and a D,D-transpeptidase activity which catalyses the cleavage of a D-Ala^4-D-Ala^5 peptide bond of the acyl donor and subsequently crosslinks the D-Ala^4 carbonyl to the primary amine of a diaminopimelic acid (DAP) residue on the acceptor. This results in a D-Ala$^4_{donor}$-DAP$^3_{acceptor}$ crosslink. The bPBPs perform only the latter D,D-transpeptidase activity (Sobhanifar, King, and Strynadka 2013; King et al. 2017). The D,D-transpeptidase activity of both aPBPs and bPBPs can be blocked by β-lactam antibiotics, which act as a substrate mimetic of the donor strand peptide bond. Inhibition of the crucial transpeptidation step in PG biosynthesis results in destabilisation of the cell wall and ultimately cell death (Fleming 1929; Liu and Tomasz 1985; Tomasz 1986).

Despite the success of β-lactam antibiotics in the clinic, the use and abuse of these potent antibiotics have led to the emergence of numerous bacterial resistance mechanisms. These include the well-known and characterized β-lactamases, drug efflux pumps, as well as many others. One more recently discovered mechanism was the ability for bypass of D,D-transpeptidation through the use of an alternate crosslinking mechanism – L,D-transpeptidation (Hugonnet et al. 2016).

It has been shown that, in *Escherichia coli*, an L,D-transpeptidase (Ldt) known as YcbB (and alternately LdtD) can compensate for inhibition of PBPs via β-lactam antibiotics with remarkably few other factors. Upon upregulation of alarmone ((p)ppGpp), YcbB, a carboxypeptidase (PBP5), and an aPBP (PBP1b) can form an alternate synthase complex and produce mature PG in a β-lactam resistant manner (Hugonnet et al. 2016; Caveney et al. 2019).

Ldts, such as YcbB, crosslink PG using an L,D-transpeptidation mechanism to form a DAP^3_{donor}-$DAP^3_{acceptor}$ crosslink between a tetrapeptide-containing donor and a tetra- or tripeptide acceptor (Hugonnet et al. 2016). L,D-transpeptidases, including YcbB, are not efficaciously inactivated by β-lactams with the exception of the carbapenem subclass. The thioester-containing L,D-transpeptidase-β-lactam adduct is slow to form for both penicillins and cephalosporins, while acylation of penicillins is followed by hydrolysis, thereby preventing full inactivation of the enzyme (Triboulet et al. 2013).

In addition to this, YcbB has been implicated in rescue of outer membrane defects (Morè et al. 2019), as well as the release of typhoid toxin in *Salmonella enterica* serovar Typhi (*S*. Typhi) (Geiger et al. 2018). A general trend in these scenarios is the presence of bacterial outer envelope stress, which can stimulate the well-known Cpx stress response. Indeed, in *E. coli*, the *ycbB* gene was shown to be under the control of the Cpx response transcription factor, CpxR (Bernal-Cabas, Ayala, and Raivio 2015; Delhaye, Collet, and Laloux 2016). Additionally, it has been proposed that L,D-transpeptidation may play a key role in PG maintenance in intercellular pathogens (García-del Portillo 2020). It is possible that due to the role of YcbB in outer envelope stress response, it is acting in equilibrium with the natural strength of D,D-crosslinked PG and the inherent strength of the outer membrane (Rojas et al. 2018) to mediate proper maintenance of outer envelope strength under stressful conditions. The role these enzymes may play during the stress-inducing conditions observed in bacterial infection of a host has yet to be observed.

Recently, we solved the structure of *E. coli* meropenem-YcbB acyl-enzyme complex via X-ray crystallography (Caveney et al. 2019). The structure was seen to consist of a novel tri-

domain architecture, which was quite distinct from L,D-transpeptidases solved at the time. There was also an interesting addition of a capping sub-domain on the otherwise canonical Ldt catalytic domain. We proposed that the capping sub-domain would hinge relative to the catalytic domain during the formation of L,D-crosslinks, in order to fully facilitate the crosslinking mechanism and release of crosslinked PG. Despite the insight gleaned from this structure, there are many more questions raised regarding the novel features observed.

Here we show that the general role of YcbB in PG reinforcement under bacterial outer envelope stress does not play a significant role in the infection of mice by *C. rodentium* and *S.* Typhimurium. This does not preclude the potential for anti-YcbB therapeutic agents in prevention of typhoid toxin release during treatment of *S.* Typhi infection. In tandem, we pursued the atomic level characterization of YcbB from both *Salmonella* Typhi and *Citrobacter rodentium* resulting in the crystallographic structures of both *S.* Typhi YcbB and *C. rodentium* YcbB acylated with ertapenem. From this data, we delineated the conserved structural characteristics and domain architecture of YcbB across a variety of Gram-negative pathogens and determined the breadth of conservation across their catalytic domains. In addition, we observe conformational reorientations in the capping sub-domain which provide further insights into the conformational space these sub-domains will sample in the greater mechanistic role of these enzymes. Cumulatively, in this work we provide a foundation for the development of novel YcbB specific antibacterial therapeutics to assist in treatment of increasingly drug resistant *S.* Typhi infections (Browne et al. 2020).

3.2 Results and discussion

3.2.1 Exploration of YcbB as a virulence factor

It has been postulated that anti-typhoid toxin immunization or therapeutics may benefit the treatment of *Salmonella* Typhi (Galán 2016), a host-restricted pathogen responsible for 10.9 million cases of typhoid fever (Stanaway et al. 2019) and ~200,000 deaths every year (Galán 2016). PG editing by YcbB has been linked to the release of this toxin (Geiger et al. 2018) and the inhibition of YcbB in *S*. Typhi may prove efficacious in reducing the severity of *S*. Typhi infection. Beyond this, it remains unknown whether these stress regulated proteins play a broader role in the virulence of bacterial pathogens in which they exist. YcbB is found in a handful of clinically relevant Gram-negative pathogens, such as enteropathogenic and enterohemorrhagic *E. coli* (EPEC, EHEC), and *Salmonella enterica* (including, but not limited to the serovar Typhi), so it was of interest to decipher the importance of its role in infection outside of the context of typhoid toxin release.

Fortunately, there are mouse models for both EPEC and *S*. Typhi infection, in *C. rodentium* and *S. enterica* serovar Typhimurium (*S*. Typhimurium) respectively. *S*. Typhimurium provokes typhoid-like symptoms in mice while not producing typhoid toxin, allowing one to probe the impact of YcbB in virulence outside of the context of typhoid toxin's role in *Salmonella* infection. Additionally, using an *S*. Typhimurium mouse infection model with streptomycin pre-treated mice, one can model *Salmonella* gastroenteritis.

These handful of relevant human pathogens and their respective models are known to depend on the proper functioning of a type three secretion system (T3SS) to persist within the host in a virulent state (Deng et al. 2017). The assembly of a functional T3SS in the bacterial membranes and cell wall requires PG remodeling. Therefore, it was of interest to first assay the role of YcbB in the ability of these bacteria to secrete effectors via the T3SS. YcbB knockout strains were generated for both *C. rodentium* (*Cr*Δ*ycbB*) and *S.* Typhimurium (*S*TmΔ*ycbB*) and tested for secretion activity. Neither YcbB knockout strain had any appreciable loss of T3SS secretion function in this established assay (Worrall et al. 2016) (Figure 3.1).

Once it was determined that the role of YcbB in a host environment was independent of the T3SS, various assays of cell fitness under envelope stress were performed *in vitro*. Upon challenge with bile salts, beta-lactams, and detergents, there was no appreciable difference in viability between a wild type and YcbB knockout strain in either *C. rodentium* (*Cr*Δ*ycbB*) and *S.* Typhimurium (*S*TmΔ*ycbB*). We postulated that the regulation of these effects may be more complex than could be assayed in simple growth assays, and mouse infection trials were conducted to see if the more fundamental role of YcbB in strengthening the cell wall under outer envelope stress conditions would be required in an *in vivo* infection setting. In the *C. rodentium* mouse infection model, fecal bacterial shedding post infection was monitored, as well as the survival of the infected C3H/HeJ mice. In both wild-type *C. rodentium* and Δ*ycbB* strain infected mice, similar levels of bacterial shedding were observed as the disease progressed (Figure 3.2 A). Survival curves between the two strains were likewise identical, with all mice reaching a humane endpoint within eight days post-infection (Figure 3.2 B).

In the *S*. Typhimurium model of typhoid infection, colonization of C57BL/6 mouse organs at three days post-infection was enumerated. In both wild-type *S.* Typhimurium and Δ*ycbB* strain infected mice, similar levels of *Salmonella* were found in all organs assayed (spleen, liver, cecum, colon, and ileum) (Figure 3.2 C). Likewise, in the *S*. Typhimurium model of gastroenteritis, colonization of C57BL/6 mouse organs from streptomycin pre-treated mice at three days post-infection was enumerated. In both wild-type *S.* Typhimurium and Δ*ycbB* strain infected mice, similar levels of *Salmonella* were found in all organs assayed (spleen, liver, cecum, colon, and ileum), with the increase in the colonization of the cecum, colon and ileum expected of the gastroenteritis model holding true for both strains (Figure 3.2 D).

From the results of these mouse models, we conclude that the general role of YcbB in maintenance of the PG layer under conditions of bacterial outer envelope stress is not a contributing factor in the ability of either *C. rodentium* or *S*. Typhimurium to establish acute infection in mice. Therefore, it is unlikely to play a significant role in the establishment of infection in either EPEC or *S. enterica* infections of humans. Amongst the small subset of relevant bacterial pathogens which contain the *ycbB* gene, we are left with the only pathogenesis-relevant roles for YcbB being its established role in *S*. Typhi (Geiger et al. 2018) and potential scenarios of β-lactam resistance (Hugonnet et al. 2016).

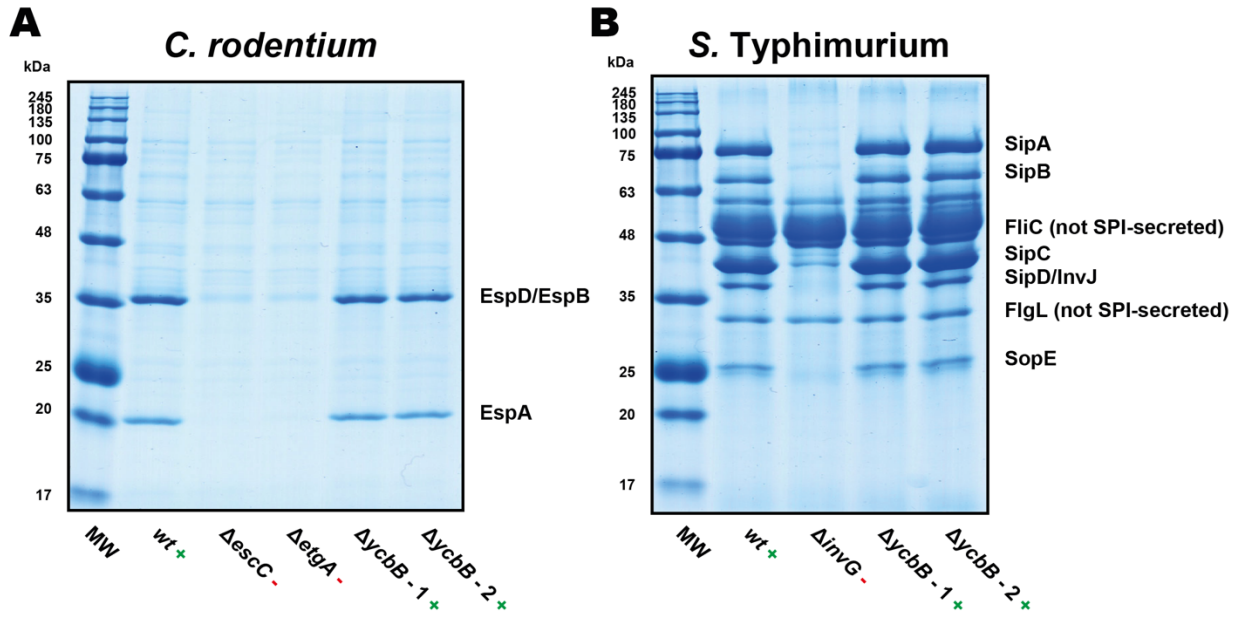

Figure 3.1 Secreted protein profiles from Δ*ycbB C. rodentium and S.* Typhimurium.
(**A**) Secreted protein profiles from *C. rodentium* strain DBS100, which utilises LEE-encoded T3SS. Wild type (*wt*) as a positive control and Δ*escC* and Δ*etgA* as negative controls. Δ*ycbB* is seen to retain LEE T3SS activity. (**B**) Secreted protein profiles from *S.* Typhimurium strain SL1344, which utilises SPI-1 T3SS. Wild type (*wt*) as a positive control and Δ*invG* as a negative control. Δ*ycbB* is seen to retain SPI-1 T3SS activity.

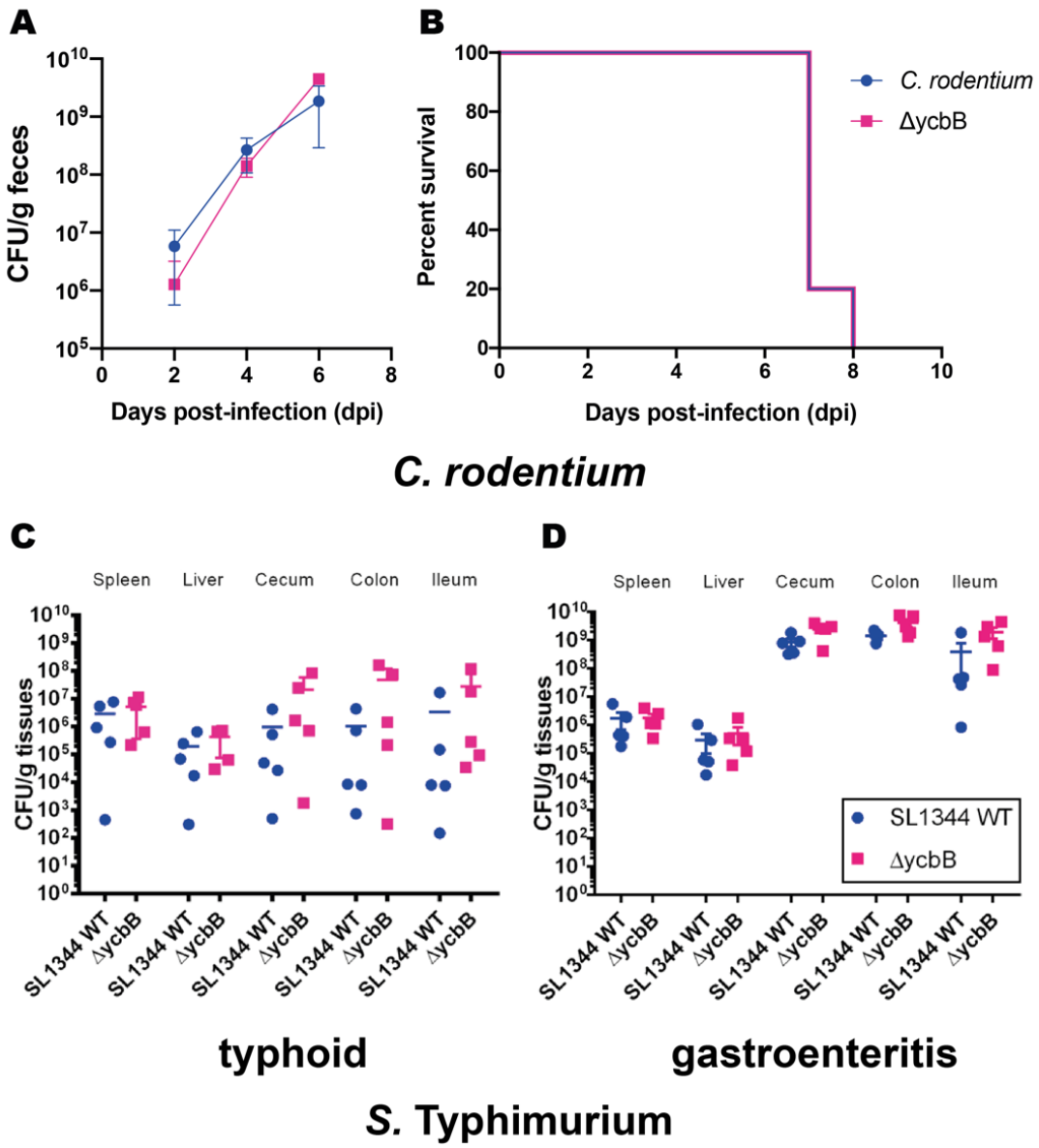

Figure 3.2 Infection and colonization of mice by *C. rodentium* and *S.* Typhimurium.
(**A**) Bacterial shedding in feces of C3H/HeJ mice (n=5) gavaged with ~3×10^8 CFU of *C. rodentium* wild-type (blue) and Δ*ycbB* (pink). (**B**) Survival curve of *C. rodentium* DBS100 infected mice, as in **A**. Mice were assessed daily for weight loss and clinical symptoms, and upon reaching the humane endpoint, mice were euthanized, and this time point was taken as time of death. (**C**) *S. enterica* serovar Typhimurium SL1344 wild-type (blue) and Δ*ycbB* (pink) colonization of C57BL/6 mouse organs (n=5) three days post infection with ~5×10^7 CFU of bacteria by oral gavage to generate typhoid symptoms. (**D**) *S. enterica* serovar Typhimurium SL1344 wild-type (blue) and Δ*ycbB* (pink) colonization of C57BL/6 mouse organs (n=5) three days post infection with ~5×10^7 CFU of bacteria by oral gavage. The mice were pretreated with 20 mg streptomycin one day before *S.* Typhimurium infection to generate gastroenteritis symptoms.

3.2.2 Structures of *Salmonella* Typhi and *Citrobacter rodentium* YcbB

Alongside these mouse trials, the structures of YcbB from both *C. rodentium* and *S.* Typhi/Typhimurium were pursued to provide insight into the structural conservation of the relevant Ldts. It should be noted that YcbB is 98-100% conserved amongst *Salmonella* Typhi and Typhimurium serovars. The *S. enterica* Typhi/Typhimurium YcbB studied herein is 98.5% identical in comparison to the clinically relevant multi-drug resistant CT18 strain, with no residues differing in the active site and only one differing within the catalytic domain (Figure 3.3 A). Amongst *Salmonella*, *Escherichia* and *Citrobacter* YcbBs, there is between 78 and 84% identity.

Ertapenem was chosen for co-crystallization after extensive screening with a small library of commercially available and clinically utilized carbapenem antibiotics. For both *S. Typhi* and *C. rodentium* YcbB, the co-crystals with ertapenem were the only crystals obtained. This is in contrast to *E. coli* YcbB, where crystals were obtained with a variety of carbapenem antibiotics and meropenem was selected due to preferential diffraction characteristic and resolution of these crystals (Caveney et al. 2019). Both ertapenem and meropenem are of current use in the treatment of bacterial infection, particularly β-lactam resistant cases. The two molecules are closely related, only differing at the periphery of the molecule (Figure 3.3 B). Crystals of *S.* Typhi YcbB, generated in the presence of 1 mM ertapenem (Figure 3.3 B) at pH 8.5, displayed $P3_12$ symmetry with unit cell dimensions of a = 75.3 Å, b = 75.3 Å, c = 194.4 Å and a diffraction resolution of 3.6 Å. Crystals of *C. rodentium* YcbB, generated in the presence of 1 mM ertapenem at pH 6.5, displayed $C222_1$ symmetry with unit cell dimensions of a = 90.0 Å, b = 117.7 Å, c = 125.2 Å and a diffraction resolution of 2.6 Å. There is one molecule of YcbB in the asymmetric unit of each crystal form.

The structure solution was phased by molecular replacement using *E. coli* YcbB (Caveney et al. 2019) split into two pieces and placed sequentially. The overall dimensions of both the *C. rodentium* and *S.* Typhi YcbB are as seen in the *E. coli* YcbB at approximately 75 x 75 x 40 Å. The overall architecture of the three currently characterized YcbB enzymes (Figure 3.3 C) features the same distinct tri-domain format. The well-ordered central catalytic domain, with the YcbB specific substrate capping sub-domain, proximal scaffold domain, and PG domain are conserved across all three YcbBs. The backbone RMSD between the three is 2.1 Å across the entirety of the modelled protein (452 residues), 1.6 Å when excluding the capping loop sub-domain region (across 396 residues – excluding residues 420-493 per *S.* Typhi numbering), and 1.0 Å across 372 common trimmed residues.

3.2.3 Conservation of YcbB active site architecture

The catalytic domains of both the *S.* Typhi and *C. rodentium* YcbB show both sequence (Figure 3.3 A, 3.4 Figure 3.4) and structural conservation (Figure 3.3 C, 3.5 A) with the canonical L,D-transpeptidase folds harbouring extended electropositive (Figure 3.5 B) active site clefts with the conserved active site motif (Bianchet et al. 2017) ($HX_{15\text{-}18}$[S/T]XGC*h*[R/N], where X represents any residue, and *h* is any hydrophobic residue) as seen in the *E. coli* YcbB (Caveney et al. 2019).

Despite the differences in acylation-state amongst the three YcbB homologues, there are remarkably few differences in either the peptide backbone or residue placement in the active site between the three (Figure 3.5 A). There is excellent structural conservation of both the nucleophilic

cysteine, the histidine general base which activates it, and the mainchain nitrogen atoms of the catalytic cysteine and adjacent tyrosine which form the oxyanion hole to stabilize the negatively charged transition state. In addition, many of the positively charged residues in and around the active site are well conserved, leading to a common positive electrostatic surface distribution amongst the three homologues (Figure 3.5 B).

From the conserved PG substrates and subsequent conserved structural elements of the catalytic domain, the broad ability of these YcbB homologues to be acylated by carbapenem ligands is understandable. It would therefore potentially pose a challenge to develop inhibitory molecules that are wholly specific to a single species' YcbB. Due to the presumed specificity of the role of YcbB in *S.* Typhi virulence, through its regulation of typhoid toxin release (Geiger et al. 2018), and the lack of a role in virulence observed in our *in vivo* mouse studies, the cross-reactivity of a developed anti-YcbB inhibitor would likely produce little off target effect within the mixed and complex bacterial population of the host gut. Inhibition of YcbB in other species which harbour this gene would not result in the death of the bacteria and therefore abate detrimental selective resistance pressures against these bacteria during treatment of *S*. Typhi infection. While not affecting these other bacteria, a successful anti-YcbB therapeutic would likely prevent the release of typhoid toxin (Geiger et al. 2018) and, in combination with standard antimicrobial agents, potentially reduce the severity of *S*. Typhi infection (Galán 2016). Such a therapeutic could be of interest in combination therapies with conventional β-lactam antibiotics for the thorough treatment of *S*. Typhi infection, particularly in a persistent or severe infection.

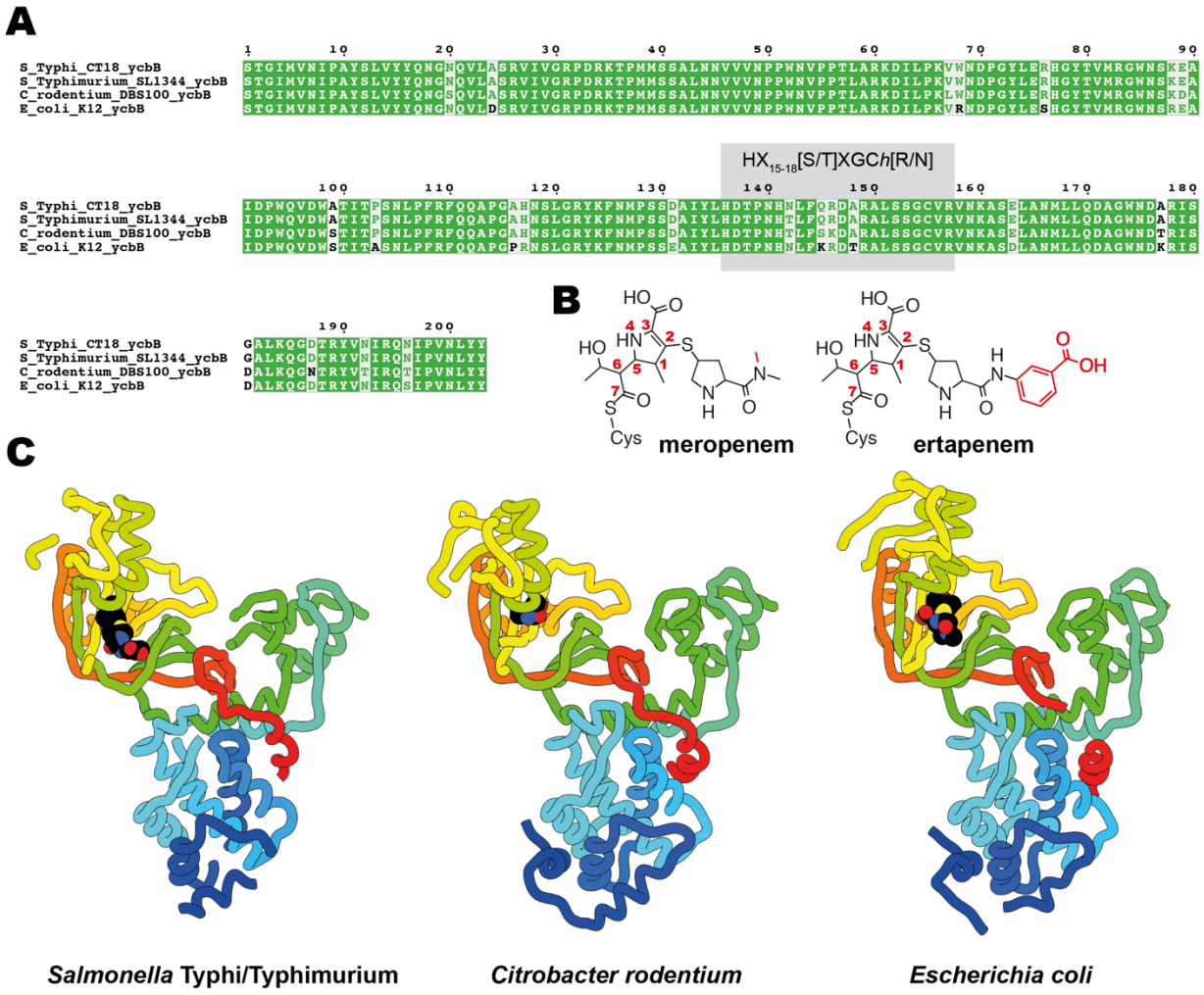

Figure 3.3 Multiple sequence alignment and structures of YcbB.
(**A**) Alignment of amino acid sequences from the catalytic domains of YcbB of YcbB from *Salmonella* Typhi CT18, *Salmonella* Typhimurium SL1344, *Citrobacter rodentium* DBS100, and *Escherichia coli* K12. $HX_{15\text{-}18}$[S/T]XGC*h*[R/N] (where X represents any residue, and *h* is any hydrophobic residue) is highlighted in grey. (**B**) Chemical diagrams of meropenem and ertapenem post-acylation by YcbB. Differences between meropenem and ertapenem are in red. (**C**) The structures of *S.* Typhi/Typhimurium and *C. rodentium* YcbB are shown in ribbon representation, coloured in rainbow from N- (blue) to C-terminus (red) in comparison to the previously solved *E. coli* YcbB (PDBID 6NTW (Caveney et al. 2019)) represented in the same scheme. Acylated drugs (ertapenem for *S.* Typhi/Typhimurium and meropenem for *E. coli*) are represented by spherical atoms, coloured in black and by heteroatom.

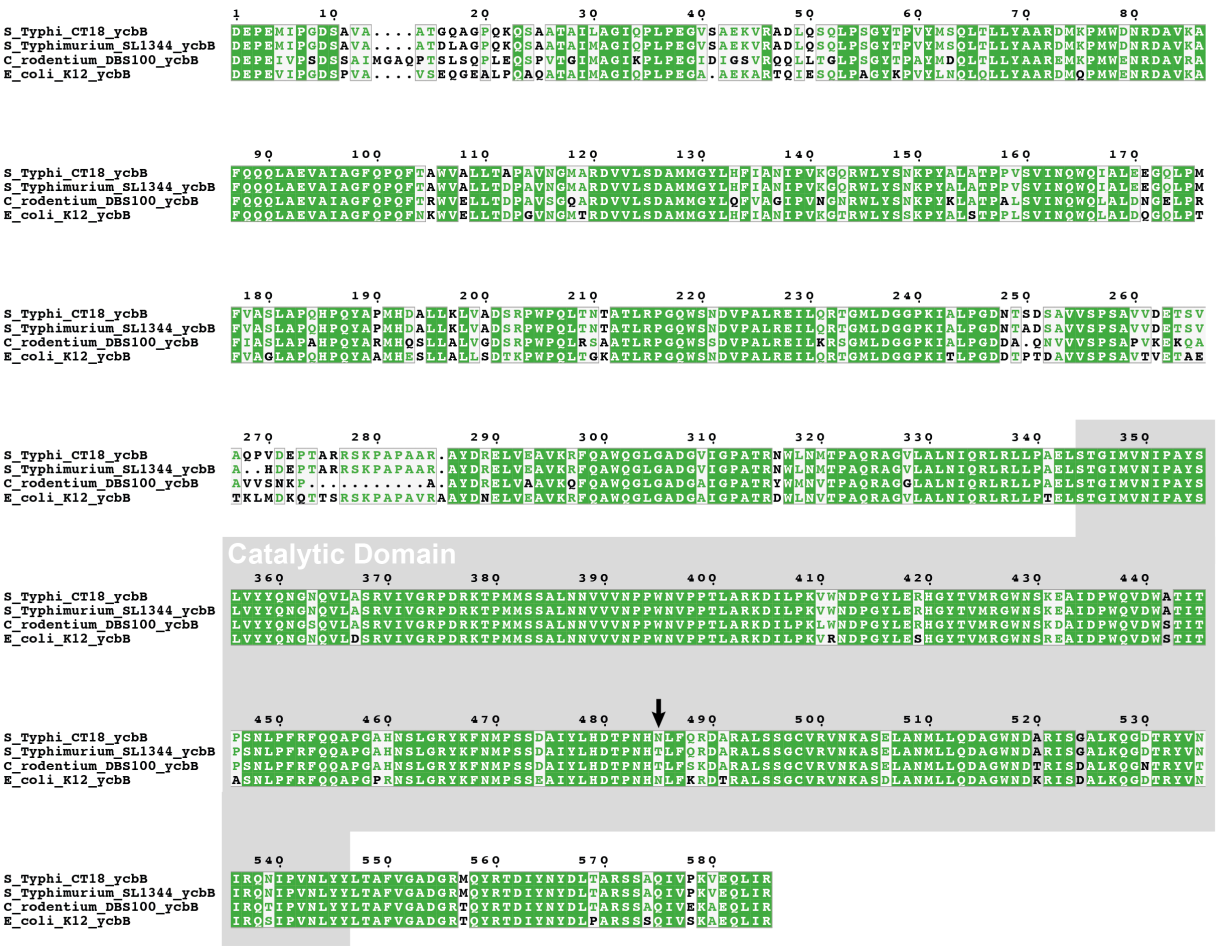

Figure 3.4 Multiple sequence alignment of YcbB.
Alignment of whole amino acid sequences (post signal peptide processing) of YcbB from *Salmonella* Typhi CT18, *Salmonella* Typhimurium SL1344, *Citrobacter rodentium* DBS100, and *Escherichia coli* K12. Catalytic domain (per Figure 3.3) is highlighted in grey. The lone catalytic domain difference between CT18 and DBS100 is denoted by an arrow.

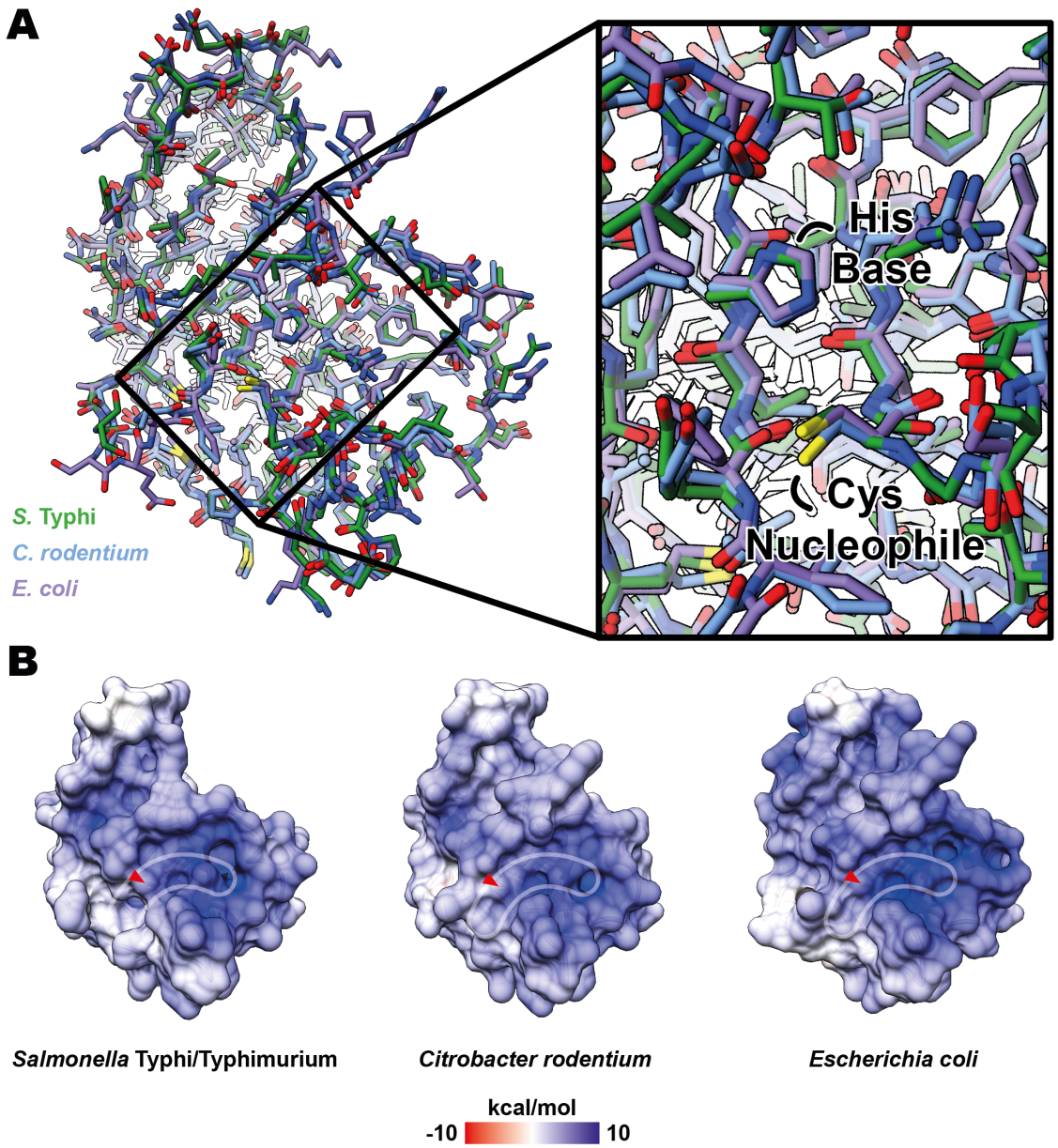

Figure 3.5 Molecular architecture and electrostatic surface potential of YcbB catalytic domain and active site.
(**A**) An overlay of the catalytic domain of various YcbB homologues (in their carbapenem acylated states, with carbapenem atoms removed for visualization), showing structural conservation of residues across the domain. *S.* Typhi/Typhimurium is represented in green, *C. rodentium* is represented in blue, and *E. coli* (PDBID 6NTW (Caveney et al. 2019)) is represented in purple. (**B**) The electrostatic surface potential of catalytic domains from various YcbB homologues, showing conservation of the extended electropositive active site (circled in white) across species. Placement of the catalytic cysteine is noted with red arrows.

3.2.4 Acylation of YcbB by ertapenem and meropenem

With the new structures of YcbB from *S.* Typhi and *C. rodentium* characterized here, we gain additional insights into the acylation of these YcbB proteins by carbapenem antibiotics. Amongst all three species' structures of YcbB, there is a lack of extensive hydrogen bonding networks seen between carbapenems and the various conserved motifs (SXXK, SXN, KTG) in PBPs (Figure 3.6 A, B).

In the case of the *S.* Typhi ertapenem-YcbB structure, we see well resolved density for the ligand as it acylates the catalytic Cys526 (Figure 3.6 A). The ertapenem is positioned similarly to the meropenem in the *E. coli* YcbB structure (Caveney et al. 2019), sitting in the donor side of the active site (Figure 3.6 C). The conserved core of carbapenem in particular, plays the same role in mediating the only hydrogen bonding present in between the drug and the active site, with the ethyl-alcohol group on C6 hydrogen bonding with both the Tyr505 of the active site Ldt motif as well as the conserved Trp423 of the capping loop (Figure 3.6 A). The proline rich insertion centered at Pro426 once again appears to provide a structural ridge that prevents significant interaction with nearby electrostatic residues, as seen in the *E. coli* YcbB structure. This observed lack of complex hydrogen bonding in favour of increased hydrophobic interactions is seen both in the *E. coli* YcbB structure, as well as many non-YcbB Ldts (Gokulan et al. 2018; Caveney et al. 2019).

One interesting feature of the ertapenem acylation of the *S.* Typhi YcbB is the presumed destabilization of the loop consisting of residues 502-504, which are not well resolved and could

not reliably be modelled in the density. We see a similar region of poor density on the same loop in the higher resolution *C. rodentium* ertapenem-YcbB structure, with poorly resolved density for residues 511-513, though only residue 512 could not be reliably modelled. In the case of the *S.* Typhi YcbB, the poorer density and presumed destabilization of this loop could in part be due to the crystal packing, as Tyr561 from an adjacent YcbB in the crystal lattice packs against resides 499 and 500 just prior to the region of poor density. No such packing is seen in the *C. rodentium* YcbB structure, leading one to postulate that some of this destabilization could indeed be due to the ertapenem acylation.

Beyond the conserved carbapenem core, the ertapenem extends out of the active site. In particular, the additional benzoic acid extension on ertapenem protrudes into a solvent channel and interacts with a neighbouring YcbB in the crystal lattice. This interaction stabilises the extended ertapenem molecule, which likely would not be well resolved to its terminus in the absence of these contacts. In the context of native YcbB in the periplasm, the acylation of YcbB by ertapenem would likely provide little additional contact in comparison to that of a shorter carbapenem such as meropenem (Figure 3.3 B).

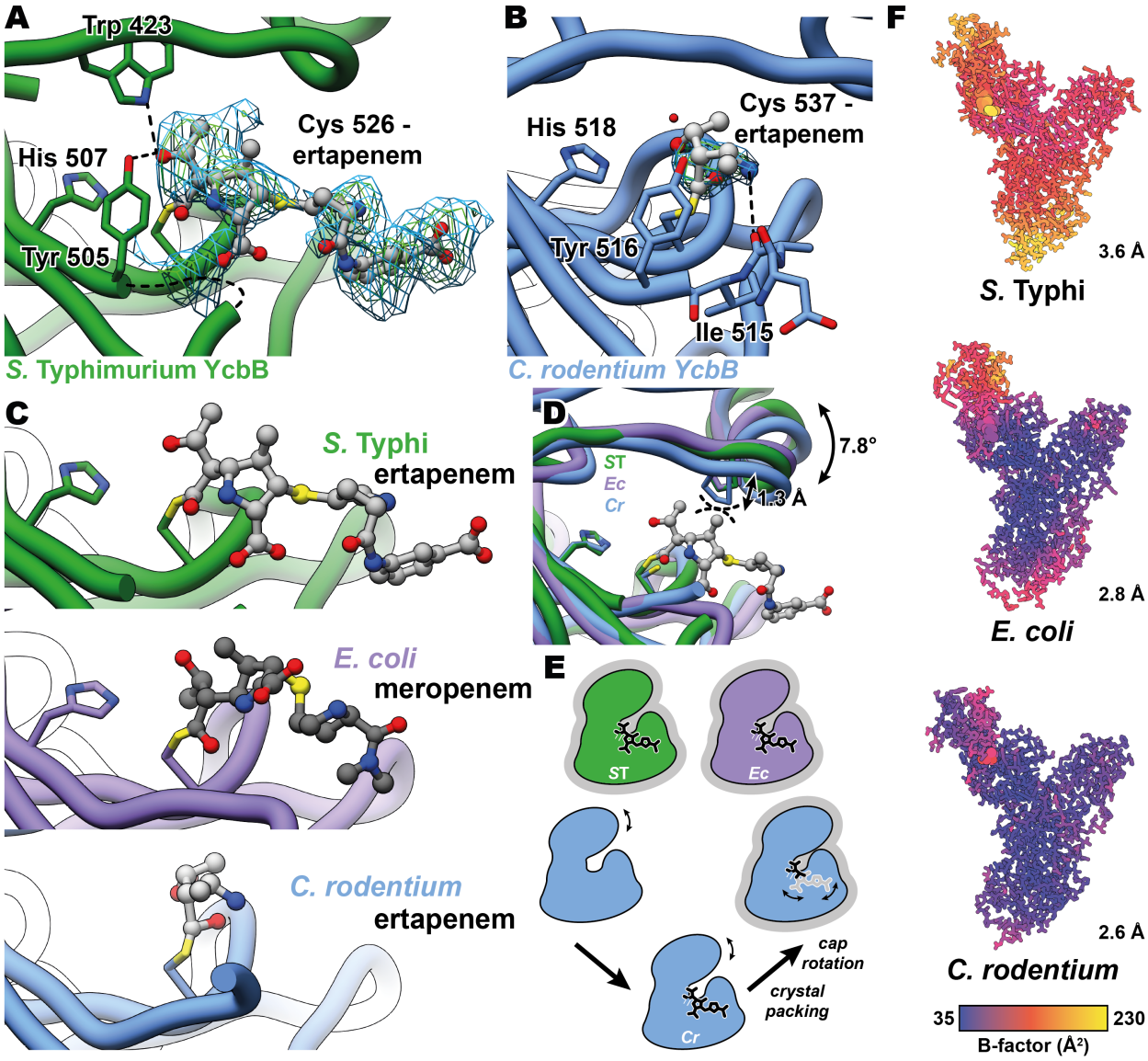

Figure 3.6 Carbapenem acylation of YcbB and movement of the capping loop.
(**A**) mF_o-DF_c simulated annealing omit map for the ertapenem-acylated Cys526 of *S.* Typhi YcbB, contoured at 2 and 2.5 σ in blue and green, respectively. *S.* Typhi YcbB is in green, ertapenem is in light grey, and selected residues and ertapenem are coloured by heteroatom. Hydrogen bonding between ertapenem, Tyr507, and Trp423 is represented with dashed lines. Some poorly resolved density is seen for residues 502-504, which are represented with a curved dashed line. (**B**) mF_o-DF_c simulated annealing omit map for the ertapenem-acylated Cys537 of *C. rodentium*, contoured at 2 and 2.5 σ in blue and green, respectively. *C. rodentium* YcbB is in blue and the remainder is coloured as in **A**. Hydrogen bonding between ertapenem and the backbone carbonyl of Ile515 is represented with dashed lines. (**C**) A comparison of ertapenem-*S.* Typhi YcbB (grey/green), ertapenem-*C. rodentium* YcbB (grey/blue), and meropenem-*E. coli* YcbB (grey/purple – PDB ID 6NTW (Caveney et al. 2019)). Acylated catalytic cystine and catalytic histidine residues are shown. Similar orientations of the active site residues are seen amongst all three homologues,

while the general position of both ertapenem and meropenem is conserved amongst the *S.* Typhi and *E. coli* structures, with the benzoic acid extension protruding away from the active site in the ertapenem-*S.* Typhi YcbB structure. (**D**) An overlay of *S.* Typhi (*S*T), *E. coli* (*Ec*), and *C. rodentium* (*Cr*) YcbB structures, highlighting capping loop rearrangement between the three. Modest rearrangements of the capping loop are seen to occlude the stability of ertapenem in the crystal structure of *C. rodentium* YcbB, likely through steric interference shown in dashed lines between an overlay of ertapenem and *C. rodentium* YcbB. (**E**) A schematic representation of the capping loop rearrangement and the impact on the acylation state during crystallization. Representations of states with structures are additionally outlined in grey. (**F**) B-factors of *S.* Typhi, *E. coli*, and *C. rodentium* YcbB structures, highlighting the increased B-factors of the capping loop within each model and the increased overall B-factors scaling with resolution (plotted in UCSF Chimera - Pettersen et al. 2004).

3.2.5 Conformational plasticity of YcbB capping loop sub-domain

In the structure of the ertapenem-*C. rodentium* YcbB acyl-enzyme complex, we see poor density for the bulk of the ertapenem-acylated catalytic cysteine (Figure 3.6 B). Due to the high sequence similarity amongst YcbB from *C. rodentium*, *S.* Typhi, and *E. coli*, and the acylated nature of the ligand, this observation is perhaps surprising. Due to the well resolved nature of the catalytic cysteine, which is observed to be rotated away from its conjugate base, His518, we propose that the *C. rodentium* YcbB is indeed in an acylated state (King et al. 2017; Caveney et al. 2019). Upon further observation, it is apparent that the capping loop is positioned in the lowest, most active site-occluding position in this structure (Figure 3.6 D). As we have previously proposed that these capping loop subdomains are likely motile in solution (Caveney et al. 2019), it is possible that the ertapenem formed key stabilizing interactions with *C. rodentium* YcbB in solution, prior to crystallization. In solution, there is likely an equilibrium between a stabilized acylated ertapenem and a lowered capping loop state with a destabilized ertapenem. The former stabilized state is likely favoured in this equilibrium (Figure 3.6 E). During the crystallization

process, this equilibrium could have been shifted toward the observed destabilized state during the crystallization process, with only the portion of the acylated ertapenem closest to the C7 acylation being stabilized, as observed in the density. We see minimal density beyond the acylation site, with some density for part of the secondary ring of the carbapenem, due in part to a hydrogen bond between N4 and the backbone carbonyl of Ile515, similar to the interaction seen to the backbone carbonyl of Ala505 in the *E. coli* YcbB structure.

With the structures provided here, we begin to see the potential dynamics of the capping loop sub-domain. Rotation of the latter is seen about the previously proposed hinge region (Caveney et al. 2019) with a modest rotation of 7.8°. Due to the conserved acylated and crystallized nature of these three YcbB structures, we see relatively similar slices of the potentially far greater landscape of motion that this capping loop can undergo. In all three structures observed to date, there is no potential pathway for the exit of the crosslinked substrate of the respective YcbBs, again eluding to the presence of an additional unobserved, further open state for the capping-loop as we have previously proposed (Caveney et al. 2019).

3.2.6 Implications in development of anti-YcbB therapeutics

Here, we have shown that YcbB does not act as a general virulence factor in a number of mouse models of bacterial infection. While this does not preclude the possibility that the general role of YcbB in bacterial outer envelope stress response could play a role in EPEC, EHEC, or non-typhoidal *Salmonella* infections, we believe this scenario would be unlikely, given the conserved mechanisms of bacterial infections and host responses between the mouse models used and human

infections. This leaves the previously discovered role of YcbB in the release of typhoid toxin in *S.* Typhi (Geiger et al. 2018) as the most attractive role of YcbB from a therapeutic standpoint.

Despite the wealth of research regarding the role of typhoid toxin in the virulence and physiology of *S.* Typhi, this toxin was only relatively recently discovered (Haghjoo and Galán 2004) within the broader context of research on typhoid infection, which is one of the oldest human diseases on written record. In the subsequent decade and a half, our understanding of the role of this toxin in the divergent symptoms of *S.* Typhi in comparison to the majority of other *S. enterica* serovars, which are limited to causing gastroenteritis, has greatly increased (Song, Gao, and Galán 2013; Del Bel Belluz et al. 2016; Yang et al. 2018; Stanaway et al. 2019). Despite the considerable evidence supporting the role of the typhoid toxin in the pathogenesis of *S.* Typhi, a recent human challenge study of typhoid infection found little to no role for the toxin in the early stages of *S.* Typhi infection (Gibani et al. 2019). Due to limitations on the severity of inflicted infections, for ethical reasons, the authors of the study note that the typhoid toxin may play a role in more severe cases of infection or in the development of persistent infection through modulation of the immune response. In addition, the authors note the study population was generally westernised, and likely had little prior immune priming, as may be seen in populations where *S.* Typhi infection is endemic. Clearly, there is a need to further dissect the role of typhoid toxin in the context of human infection. This provides additional rationale for the development and use of anti-YcbB therapeutic agents (in addition to existing, albeit non-specific, anti-YcbB carbapenem antibiotics), which could be used to help dissect the intricacies in the role of the typhoid toxin during infection.

With the additional structural insights provided in this work, we begin to see trends in the inhibition of these YcbBs. As first seen in the *E. coli* structure (Caveney et al. 2019), there are remarkably few factors which stabilize these carbapenems in the active site of each YcbB. This leads to the possibility of further design of evolved carbapenem antibiotics which can additionally extend into the active site of YcbB, as has been done with the Ldt enzymes from *Mycobacterium tuberculosis* (Kumar et al. 2017). In the *S.* Typhi structure of YcbB, which is acylated with ertapenem, we see additional extension of the C2 group away from the donor site of the enzyme, providing little to no benefit to the inhibitor (Figure 3.6). The possibility of extension at the C3 carboxylic acid group could potentially maximize the interaction of the inhibitor with the donor site, while extension at the C5 ethyl alcohol group could possibly begin to explore additional inhibition of the adjacent acceptor site.

In addition to the insights provided in this work for the potential evolution of carbapenem antibiotics which further explore the active site of YcbB, the additional understanding of the motion and steric hinderances of the capping loop will be of benefit to the development of novel anti-YcbB agents. There are two potential routes that could be pursued for the development of evolved carbapenems and other anti-YcbB agents. First, one could attempt to avoid interaction with the lower face of the capping loop, perhaps through removal of the C1 methyl group of the various carbapenems, to remove the steric hindrance proposed to have occurred during crystal formation in the *C. rodentium* YcbB structure. As the capping loop can likely only hinge and occlude so far before steric intervention by the residues along the edge of the active site, removal of the C1 methyl group may reduce binding interference between the capping loop and the drug, resulting in a more favourable binding event. Alternately, now that there is further understanding

of the hinge point for the rotation and movement of the capping loop, one could explore extension of the C1 methyl group to form specific contacts with the lower face of the capping loop. This could provide additional chemical space to explore in the evolution of carbapenem antibiotics to inhibit YcbB.

In this work, we have probed the role of *ycbB* in the infection of mice by *C. rodentium* and *S*. Typhimurium. We show that the general role of YcbB in PG reinforcement under bacterial outer envelope stress does not play a role in these models, and therefore does not likely play a profound role in *E. coli* or *Salmonella* infection of humans. This results in the limited, yet highly specific, potential for anti-YcbB therapeutic agents in treatment of *S*. Typhi infection. We determined the structures of both *Salmonella* Typhi and *Citrobacter rodentium* YcbB and from them observe the conserved structural components of YcbB across a variety of Gram-negative pathogens. Cumulatively, in this work we provide a foundation for the development of novel YcbB specific antibacterial therapeutics to assist in treatment of *S*. Typhi infection.

3.3 Methods

3.3.1 Generation of *ycbB* knockout strains

The *sacB* gene-based allelic exchange method and the suicide vector pRE112 were used to generate an in-frame deletion mutants of *ycbB* in both *S. enterica* serovar Typhimurium strain SL1344 and *C. rodentium* strain DBS100. Two DNA fragments flanking ~1 kb upstream and downstream of the coding region of *ycbB* were generated by PCR using the following primers:

TATAAGGTACCATAGCGTGCGGTTAAACGTCAACG – forward primer for upstream *S.* Typhimurium (KpnI site underlined), ATATTGAATTCCCCTTGCCCCCTGTTTTCG – reverse primer for upstream *S.* Typhimurium (EcoRI site underlined), TATAAGAATTCATGAAGAAGTTCTGGTAAATATGTTGTCC – forward primer for downstream *S.* Typhimurium (EcoRI site underlined), ATATTGAGCTCCGTGAGTAAAATTTGCATCAACG – reverse primer for downstream *S.* Typhimurium (SacI site underlined), TATAAGAGCTCACGCCAGCAAGCAGCGATACC – forward primer for upstream *C. rodentium* (SacI site underlined), ATATTGAATTCTATAGAAAGGCCAGAACCCTGTTGCC – reverse primer for upstream *C. rodentium* (EcoRI site underlined), TATAAGAATTCATGAAGACGTTCTGGTCATTATGG – forward primer for downstream *C. rodentium* (EcoRI site underlined), and ATATTGGTACCGTAACCAGAACTCATCTTCTTTTTCC – reverse primer for *C. rodentium* (KpnI site underlined). After digestion with KpnI/EcoRI or SacI/EcoRI, respectively, the DNA fragment pairs were gel-purified and cloned into KpnI/SacI-digested pRE112 in a three-way ligation, generating pRE112-Δ*S*T_*ycbB and* pRE112-Δ*Cr_ycbB.* These suicide vectors were transformed into *E. coli* strain MFD*pir* by electroporation and introduced into *S.* Typhimurium strain SL1344 or *C. rodentium* strain DBS100 by conjugation. After sucrose selection, colonies resistant to sucrose and sensitive to chloramphenicol were screened for *ycbB* deletion by PCR.

3.3.2 Secretion assays

For the type III secretion assay for *Citrobacter rodentium*, *C. rodentium* strains were grown overnight in LB broth at 37ºC in a shaker at 225 rpm. The overnight cultures were diluted 1:40

into 3 ml of pre-warmed Dulbecco's modified Eagle's medium (DMEM) (HyClone) supplemented with 4500 mg/L glucose, 4 mM L-glutamine and 110 mg/L sodium pyruvate in a 6-well tissue culture plate (Corning Inc.) and grown statically at 37°C for 6 hours in a tissue culture incubator containing 5% CO_2 (v/v) to induce type III secretion.

For SPI-1 secretion assays for *Salmonella enterica* serovar Typhimurium, *Salmonella* strains were grown overnight in LB broth containing 100 µg/ml of streptomycin sulfate at 37°C in a shaker at 225 rpm. The cultures were diluted 1:100 into 4 ml of fresh LB with 100 µg/ml of streptomycin sulfate and grown under the same conditions for 6 hours to induce SPI-1 type III secretion.

The bacterial cultures for either *C. rodentium* or *S.* Typhmurium were then centrifuged at 16,100 *g* for 10 min to pellet the bacteria. The culture supernatant was collected and passed through a Millex-GV 0.22 µm filter unit (Millipore) to remove any remaining bacteria, and the secreted proteins were precipitated with trichloroacetic acid (TCA) at a final concentration of 10% (v/v). The secreted proteins were then collected by centrifugation at 16,100 *g* for 30 min, and the protein pellet was dried in air and dissolved in SDS-PAGE sample buffer, with the residual TCA neutralized with 0.5 µl of saturated Tris. The amount of the sample buffer used to re-suspend the bacterial pellet or dissolve the precipitated proteins was normalized according to the A_{600} values of the cultures to ensure equal loading of the samples. The secreted proteins were analyzed in SDS-12% PAGE and stained with Coomassie Blue G250.

3.3.3 Mouse infections by *C. rodentium* wild-type strain DBS100 and its isogenic *ycbB* deletion mutant, *ΔycbB*

All mouse experiments were approved by the University of British Columbia (UBC) Animal Care Committee and performed in strict accordance with the guidelines of the Canadian Council on Animal Care and the UBC Animal Care Committee. Six-weeks-old, female C3H/HeJ mice were purchased from the Jackson Laboratory (Bar Harbor, ME) and housed in a specific pathogen-free facility at UBC. Groups of 5 mice were orally gavaged with ~3×10^8 CFU of bacteria in 100 µl of overnight cultures of *C. rodentium* DBS100 grown in LB at 37°C and 225 rpm. Bacterial shedding in stools was monitored by plating dilutions of fecal samples on MacConkey agar every two days throughout the infection. Mice were assessed daily for weight loss and clinical symptoms, and upon reaching the humane endpoint (typically weight loss of 20%, or moribund signs of bloody diarrhea, severe hunching, and/or rectal prolapse), mice were euthanized by isoflurane anesthesia followed by carbon dioxide inhalation, and this time point was taken as time of death.

3.3.4 Mouse infections by *Salmonella enterica* serovar Typhimurium and its isogenic *ycbB* deletion mutant

All mouse experiments were approved by the University of British Columbia (UBC) Animal Care Committee and performed in accordance with the ethical requirements of the Canadian Council on Animal Care and the UBC Animal Care Committee. Five-weeks-old, female C57BL/6 mice were purchased from the Jackson Laboratory (Bar Harbor, ME), and housed in a

specific pathogen-free facility at UBC. Two models of *Salmonella* infections were used, the typhoid model and the gastroenteritis model, which differ in that each mouse was given 20 mg of streptomycin by oral gavage 24 hours prior to *Salmonella* infection in the gastroenteritis model. *Salmonella enterica* serovar SL1344 strains were grown overnight in LB containing 100 µl of streptomycin at 37°C and 225 rpm and diluted 10-fold in phosphate-buffered saline (PBS). The mice were then infected with 100 µl of the diluted bacterial cultures containing ~5×10^7 CFU of bacteria. Mice were euthanized 3 days post infection by anaesthesia with isoflurane followed by CO_2 asphyxiation. Mouse organs (cecum, colon, ileum, spleen and liver) were dissected and collected in 1 mL of sterile PBS and homogenized in a FastPrep Homogenizer (MP Biochemicals). Serial dilutions in PBS were plated in LB agar plates containing 100 µg/mL of streptomycin for *Salmonella* CFU enumeration.

3.3.5 Cloning and protein expression

Salmonella Typhimurium and *Citrobacter rodentium* YcbB without their signal peptides (residues 31 and 48 onward, respectively) were cloned into the expression vector pET28a with a thrombin cleavable, N-terminal His-tag. Expression constructs were transformed into *E. coli* BL21 (DE3) for expression. Cells were cultured in ZYP-5052 autoinduction media for four hours at 37°C followed by overnight protein expression at 25°C. Cells were pelleted and stored at -80°C until required.

3.3.6 Protein purification

For purification of *S*. Typhimurium and *C. rodentium* YcbB, cell pellets were resuspended in lysis buffer (20 mM Hepes, pH 8.0, 300 mM NaCl, 10% glycerol) and lysed by processing twice with a homogenizer (15 kPa; Avestin). Cellular debris was pelleted by centrifugation at 125,000 x *g* for 1 hour. The resultant supernatant was loaded onto 10 mL of Ni-NTA Superflow resin (Qiagen), washed with 65 mM imidazole in Buffer A (20 mM Hepes, pH 8.0, 300 mM NaCl), and the protein was eluted with 300 mM imidazole in Buffer A. 1 U of thrombin was added per mg of protein to remove the N-terminal His-tag overnight at 4°C. Samples were purified further by size exclusion chromatography (SEC) with a Superdex 200 column (GE Lifesciences) equilibrated in Buffer B (20 mM Hepes, pH 8.0, 150 mM NaCl). Fractions containing purified protein were pooled and concentrated to 9 mg/mL for *S*. Typhimurium and 8.8 mg/mL for *C. rodentium*. Protein was frozen rapidly in liquid nitrogen and stored at -80°C until required.

3.3.7 X-ray crystallography and structure determination

S. Typhi YcbB was crystallized at 20°C by sitting drop vapour diffusion using 0.2 µL protein solution (9 mg/mL purified protein in Buffer A) and 1 µL of mother liquor (0.1 M Tris pH 8.5, 0.18 M $MgCl^2$, 17% PEG 8k, 2% ethanol) with the addition of 1mM ertapenem (Millipore Sigma). *C. rodentium* YcbB was crystallized at 20°C by sitting drop vapour diffusion using 0.2 µL protein solution (8.8 mg/mL purified protein in Buffer A) and 1 µL of mother liquor (0.16 M calcium acetate, 0.08 M Sodium Cacodylate pH 6.5, 14% (v/v) PEG 8k, 20% (v/v) glycerol) with the addition of 1mM ertapenem. Data for *S*. Typhi ertapenem-YcbB and *C. rodentium* ertapenem-

YcbB was collected on Advanced Photon Source beamline 23-ID-B and Canadian Light Source beamline 08B1-1, respectively. All datasets were processed with XDS (Kabsch 2010). For both YcbB datasets reported here, the structures were solved by molecular replacement using Phaser (McCoy et al. 2007). The previously reported structure of *E. coli* YcbB (6NTW (Caveney et al. 2019)) was divided into two parts, 1 - its capping loop-sub domain (residues 424-493) and 2 - the remainder of the protein (all modelled residues minus residues 422-495). The second part was placed first by manual methods and followed by the capping sub-domain. For phasing, all atom models were used with no sidechain modification, due to high levels of homology. These structures were then refined using Phenix (Adams et al. 2010) and Coot (Emsley and Cowtan 2004).

For the *S*. Typhi YcbB, the portions of the N-terminal face of the scaffolding domain and portions of the capping loop opposite the active site were manually trimmed from the phased model, as they could not reliably be fit into the density. The resulting model starts at residue 72, has the unmodelled regions 82-82, 107-108, 179-180, 201-204, 213-215 (lower portion of the scaffolding domain), 267-311, 331 (PG binding domain – disordered loop observed in *E. coli* YcbB), 451-456, 461-463, 480, 485-490, 502-503 (capping loop, opposite the active site), and ends at residue 609. The model has a MolProbity score of 2.69 and statistics that are in line with deposited models at this resolution (Figure 3.7 A). In addition, the interpretations we make from this structure are appropriate for the resolution and observed density, with the key observations centering around global architecture and structural conservation in comparison to the homologous structures of higher resolutions.

For the *C. rodentium* YcbB, the modelled residues are in line with the regions modelled for the *E. coli* YcbB. The resulting model starts at residue 72, has the unmodelled regions 288-322 (PG binding domain – disordered loop observed in *E. coli* YcbB), 512 (loop below active site),

466-467 (capping loop, opposite the active site), and ends at residue 622. The model has a MolProbity score of 2.26 and statistics that are in line with deposited models at this resolution (Figure 3.7 B). See Table 3.1 for data collection and refinement statistics.

3.4 Data availability

Atomic coordinates for the *Salmonella* Typhi YcbB-ertapenem and *C. rodentium* YcbB-ertapenem models will be forthcoming in the protein data bank.

Table 3.1 *S.* Typhi and *C. rodentium* YcbB data collection and refinement statistics.

	***S.* Typhi YcbB**	***C. rodentium* YcbB**
Data collection		
Space group	P 3_1 2	C 2 2 2_1
Cell dimensions		
a, *b*, *c* (Å)	75.309, 75.309, 194.370	89.997, 117.705, 125.185
a, b, g (°)	90, 90, 120	90, 90, 90
Resolution (Å)	45.96 – 3.6 (3.732 – 3.6)	35.97 – 2.6 (2.693 – 2.6)
R_{merge}	0.11 (2.01)	0.43 (4.62)
I / sI	10.30 (1.54)	3.57 (0.77)
Completeness (%)	98 (96)	99 (98)
Redundancy	9.3 (9.0)	6.6 (6.5)
Refinement		
Resolution (Å)	3.6	2.6
No. reflections	9261 (716)	20626 (1896)
R_{work} / R_{free}	28.07 (56.05) / 35.75 (71.61)	22.74 (37.41) / 28.27 (42.32)
No. atoms		
Protein	3661	4033
Ligand/ion	33	9
Water	-	10
B-factors (Å^2)		
Protein	135.2	61.6
Ligand/ion	161.1	115.8
Water	-	55.00
R.m.s deviations		
Bond lengths (Å)	0.01	0.01
Bond angles (°)	1.60	1.71

*Values in parentheses are for highest-resolution shell.

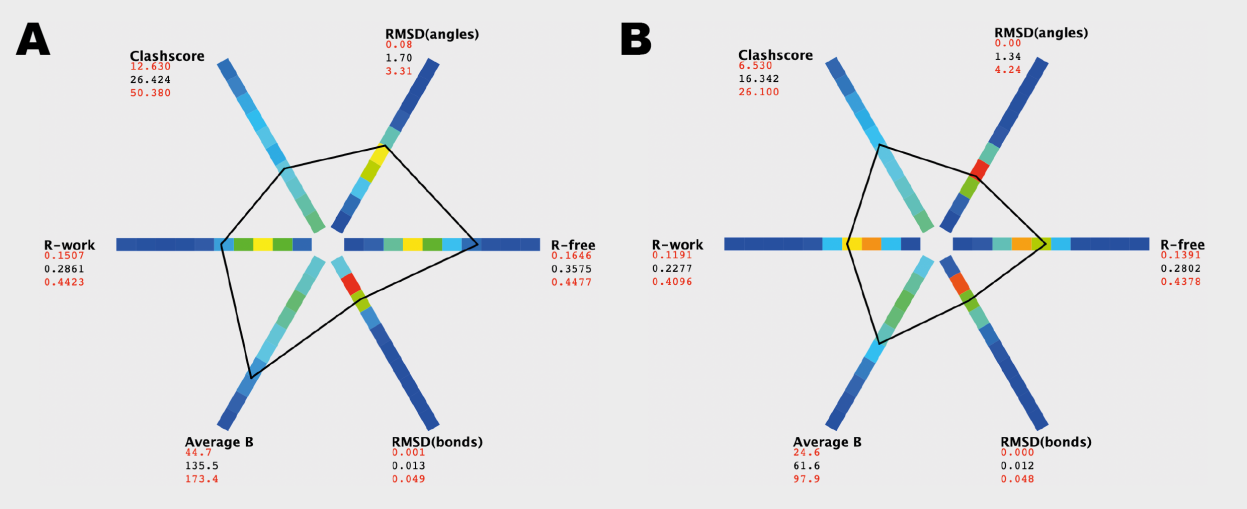

Figure 3.7 Polygon plots of model statistics for *S*. Typhi and *C. rodentium* YcbB.
(**A**) Polygon plot of *S*. Typhi YcbB clash score, RMSD (angles), R-free, RMSD (bonds), average B-factor, and R-work, showing comparison to deposited structures of similar resolutions. (**B**) Polygon plot of *C. rodentium* YcbB clash score, RMSD (angles), R-free, RMSD (bonds), average B-factor, and R-work, showing comparison to deposited structures of similar resolutions (Urzhumtseva et al. 2009).

Chapter 4: Structure of the peptidoglycan synthase activator LpoP in *Pseudomonas aeruginosa*

4.1 Introduction

The biosynthesis of the bacterial cell wall is an excellent target for antibacterial therapy, as is perhaps seen most clearly in the use of β-lactam antibiotics, which famously inhibit one of the final steps in the cell wall biosynthetic pathway. The bacterial cell wall is comprised of glycan strands of alternating β-1,4 linked *N*-acetylglucosamine and *N*-acetylmuramic acid which are connected by short peptides to form a mesh, called the peptidoglycan sacculus, that surrounds the cytoplasmic membrane. Peptidoglycan (PG) plays a crucial structural role in the bacterial cell envelope and defects in PG often result in bacterial lysis.

PG synthesis begins in the cytosol and leads to the membrane-attached precursor, lipid II, which is flipped across to the external leaflet of the cytosolic membrane for the polymerization of glycan strands and cross-linking of peptides by PG synthases. Most PG synthesis activity is provided by bifunctional penicillin binding proteins (class A PBPs). Recently, SEDS proteins were found to be PG glycosyltransferases that associate with monofunctional PBPs (class B PBPs) to synthesize cross-linked PG (Meeske et al. 2016), the role of another monofunctional glycosyltransferase, Mtg, has remained unclear. Despite the newly observed role for the SEDS-class B PBP complex, the canonical class A PBP PG synthase activity remains crucial in the maintenance of the bacterial cell envelope.

Class A PBPs perform both the glycosyltransferase (GTase) activity which polymerizes glycan strands from lipid II, and a DD-transpeptidase (TPase) activity which cleaves a D-Ala^4-D-Ala^5 peptide bond of the acyl donor and transfers the D-Ala^4 carbonyl to the primary amine of a diaminopimelic acid (DAP) residue on the acceptor peptide. In contrast, class B PBPs perform only the transpeptidase reaction. The DD-TPase activity is blocked by β-lactam antibiotics, which irreversibly acylate the catalytic serine of class A and B PBP (Caveney, Li, and Strynadka 2018).

Over the last years, it became evident that the activities of some class A PBPs are regulated by cognate outer membrane-anchored lipoprotein activators, LpoA and LpoB (Typas et al. 2010; Paradis-Bleau et al. 2010). Moreover, *E. coli* subjects the LpoB-mediated stimulation of PBP1B to regulation by CpoB, which functions together with members of the Tol system to coordinate outer membrane constriction with septal PG synthesis (Gray et al. 2015). These regulators were all identified in *Escherichia coli* and recent work provided insights into their structures, interface with the PBP and mechanisms of PBP activation (Egan et al. 2014; King, Lameignere, and Strynadka 2014; Jean et al. 2014; Egan et al. 2018; Kelley, Vijayalakshmi, and Saper 2019) These studies suggest that activators bind to a non-catalytic docking domain causing conformational changes in the PBP that ultimately affect active site residues (Greene, Fumeaux, and Bernhardt 2018).(Greene, Fumeaux, and Bernhardt 2018)(Greene, Fumeaux, and Bernhardt 2018)(Greene, Fumeaux, and Bernhardt 2018) *Pseudomonas aeruginosa* has a lipoprotein activator of PBP1B, termed LpoP, which likely functions in a similar way as LpoB in *E. coli* (Greene, Fumeaux, and Bernhardt 2018). However, while LpoP was shown to be essential for PBP1B function in the cell,

the structure of LpoP is not known and the previous work did not demonstrate the mechanism of activation of PBP1B by LpoP (Greene, Fumeaux, and Bernhardt 2018).

Here we show that LpoP shares structural organisation with LpoB, with both having a long, intrinsically disordered N-terminal region and a structured C-terminal region. Our crystal structure of the ordered C-terminal region revealed a tandem-tetratricopeptide repeat (tandem-TPR) structure. We probed the role of LpoP in activating *P. aeruginosa* PBP1B (^{Pa}PBP1B) and show that LpoP interacts with ^{Pa}PBP1B and stimulates its GTase and TPase activities *in vitro*. Additionally, we show that *P. aeruginosa* CpoB (^{Pa}CpoB) does not regulate ^{Pa}PBP1B/LpoP *in vitro*, contrary to its role in *E. coli*. To further dissect the ^{Pa}PBP1B-LpoP interaction, we show that the UB2H domain of ^{Pa}PBP1B interacts with the C-terminus of LpoP and use NMR to probe this interface. We propose a mechanism for the activation of PBP1B in *P. aeruginosa* that helps to understand similarities and differences in class A PBP activation across Gram-negative bacteria.

4.2 Results

4.2.1 Structural organization of full length LpoP

In order to obtain structural information about LpoP we used a multifaceted approach involving both NMR and crystallography. This was required due to the predicted mixture of both ordered and intrinsically disordered regions in LpoP, which could not be probed to the fullest extent by either technique alone. LpoP is a predicted lipoprotein with 259 amino acids and attached to the outer membrane via its N-terminal lipid modification at Cys19 (Greene, Fumeaux, and

Bernhardt 2018). To assess the structural organization of this protein by NMR, we first purified ^{15}N labeled LpoP (residues 20-259). The ^{1}H-^{15}N correlation spectrum of this construct displayed both dispersed peaks and intense narrow peaks with a very low ^{1}H chemical shift dispersion, indicating the presence of structured and unstructured regions (Figure 4.1 A). NMR data were then recorded on a [^{15}N-^{13}C]-LpoP sample and the backbone and sidechain ^{1}H-^{15}N-^{13}C -resonances were assigned using conventional tri-dimensional experiments. The assigned spectra revealed that residues Asp 154 to Ser 258 form a globular domain consisting of a succession of 6 helices (as determined by chemical shift index analysis – Figure 4.2) (Berjanskii and Wishart 2005). ^{1}H-^{15}N NOE relaxation measurements displayed positive NOE values (> 0.6) for residues 154 to 258, in agreement with the presence of a globular and stable domain (Figure 4.1 A). With the exception of the short stretch from residues 147-153 with intermediate NOE values (0.15 to 0.4), the rest of the residues produced low or negative NOE values which indicated fast motion (Figure 4.1 B). These resonances arise from the N-terminal intrinsically disordered domain (residues 20-146) that is connected by a short segment with reduced mobility (residues 147-153) to the C-terminal globular domain (residues 154-258) (Figure 4.1 C).

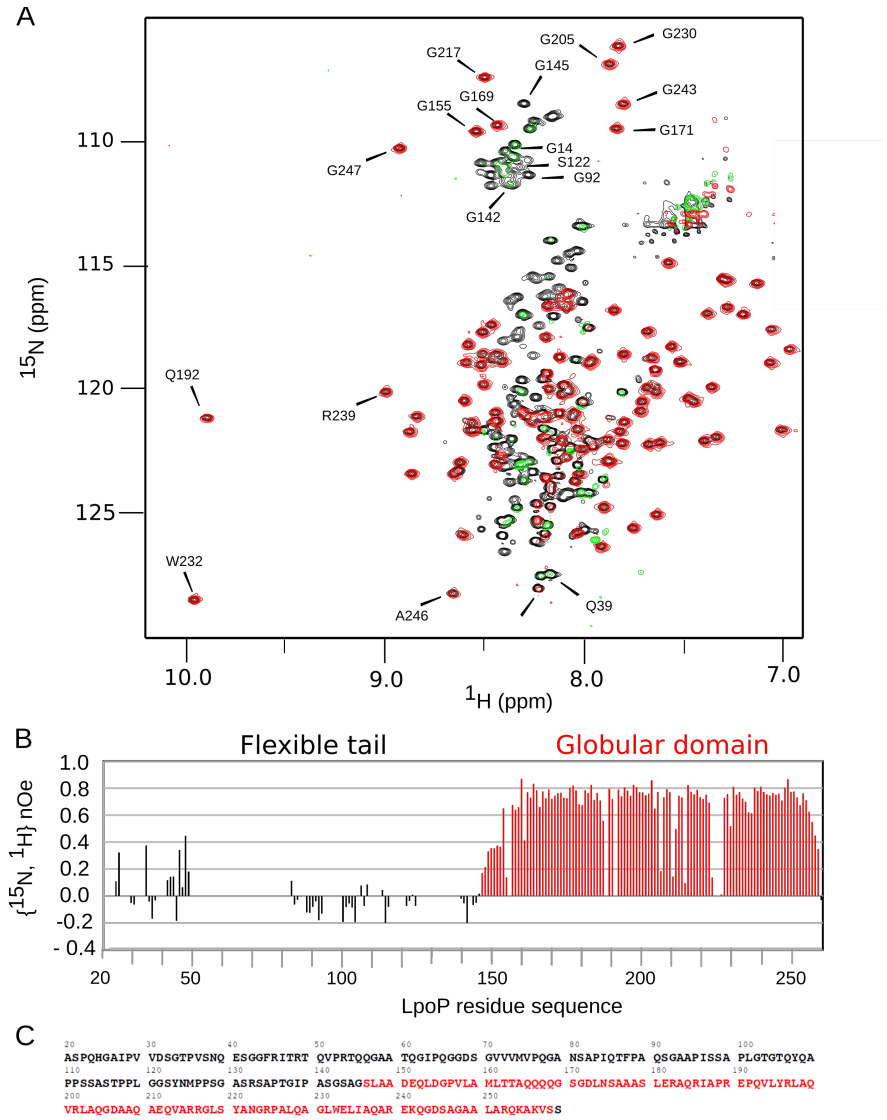

Figure 4.1 NMR of LpoP intrinsically disordered and globular domains.
(**A**) Overlay of the ^{1}H-^{15}N heteronuclear NOE recorded with and without initial proton saturation. Saturated experiment is plotted in red and green for positive and negative contour, respectively, whereas the reference experiment recorded without ^{1}H saturation is plotted in black. Both 2D ^{1}H-^{15}N experiments were collected on an 16.4 T NMR spectrometer at 25°C. Protein samples were prepared at 0.2 mM in 30 mM HEPES, 200 mM KCl buffer at pH 7.5. (**B**) Hetero-nuclear ^{1}H-^{15}N-NOE values calculated from the intensity ratio between the saturated and reference experiments. Regions with sequential positive ^{1}H-^{15}N-NOE values are colored in red and correspond to a structured domain. Errors in the intensity ratio were calculated from the signal-to-noise ratio of the NMR signal in each spectrum. The numbering begins at Ala20 just after the lipobox (residues 16-19). High, low, and negative ^{1}H-^{15}N-NOE values indicate low, medium, and high flexibility, respectively. (**C**) Sequence of the Lpop starting at residue Ala20 just after the lipobox segment, coloured as in **B**.

```
4           13        23        33        43          53
4   MASMTGGQQMGRGSEFASPQHGAIPVVDSGTPVSNQESGGFRITRTQVPR 53
4   CTTTTTTTCCCCCCCCTTTTCCTTTTCCCCCCCCCCCCTTTBBCCCTTT 53
4                                                       53

54          63        73        83        93          103
54  TQQGAATQGIPQGGDSGVVVMVPQGANSAPIQTFPAQSGAAPISSAPLGT 103
54  TCCTTTTCCCCCCCTTTTBBBTTTTCCCCCCCCCCCCCCCCCCCCCCCCC 103
54                                                      103

104         113       123       133       143         153
104 GTQYQAPPSSASTPPLGGSYNMPPSGASRSAPTGIPASGSAGSLAADEQL 153
104 CCCCCCCCCCCCCTTTTCCCTTTTTTTCCTTTTCCCCCCCCCCCCCCCCC 153
104                                                     153

154         163       173       183       193         203
154 DGPVLAMLTTAQQQQGSGDLNSAAASLERAQRIAPREPQVLYRLAQVRLA 203
154 CHHHHHHHHHHHHHHCCCHHHHHHHHHHHHHHTTTTHHHHHHHHHHHH 203
154                                                     203

204         213       223       233       243         253
204 QGDAAQAEQVARRGLSYANGRPALQAGLWELIAQAREKQGDSAGAALARQ 253
204 CCCHHHHHHHHHHHHHCCCCHHHHHHHHHHHHHHHCCCHHHHHHHHH 253
204                                                     253

254       259
254 KAKVSS 259
254 HCCCCC 259
254       259
```

Figure 4.2 Chemical shift index analysis of LpoP.
Secondary structures are determined, using the web server "CSI 3.0", by comparison of the assigned backbone NMR chemical shifts (Cα, CO, Cβ, N, Hα, NH) with reference chemical shift index.

4.2.2 Structure of the globular C-terminal domain of LpoP

To solve the structure of the globular region we purified and crystallized *P. aeruginosa* $LpoP_{143-259}$. Crystals of *P. aeruginosa* $LpoP_{143-259}$ displayed monoclinic $P2_1$ symmetry with unit cell dimensions of a = 48.8 Å, b = 154.6 Å, c = 54.1 Å, β = 90.1°, and diffracted with a resolution of 2.2 Å. There were eight molecules of LpoP in the asymmetric unit. The structure solution was phased using molecular replacement and a homology model of $LpoP_{143-259}$ and final refinement statistics were generated (Table 4.1). The resulting maps showed well resolved electron density for the majority of the protein chain, allowing near complete tracing of the ordered part from residues 152 onwards (see Methods). The structure indicated a monomeric form of the protein with no obvious crystallographic formation of larger oligomers. $LpoP_{143-259}$ is made up of 6 α-helices (H1–H6) of variable length that form helix-turn-helix motifs similar to those of tetratricopeptide repeats (TPR) and that are linked together through short loops (Figure 4.3 A,B) (Cortajarena et al. 2004; Zeytuni and Zarivach 2012). Numerous inter-helical hydrophobic contacts favored by the high percentage of Leu (12%) and Ala (22%) stabilize the core structure (Figure 4.4 A). LpoP has a striking structural similarity to protein domains formed by repetition of TPR domains (prosite PS50293 family). In particular, LpoP has a structure similar to the TPR domain of CpoB (PDB 2XEV (Krachler et al. 2010)) (RMSD of 1.17 Å over 59 residues and 2.534 Å over all 100 residues) despite a limited sequence identity of 18% (Figure 4.3 C) and varied electrostatic surface potential (Figure 4.4 B).

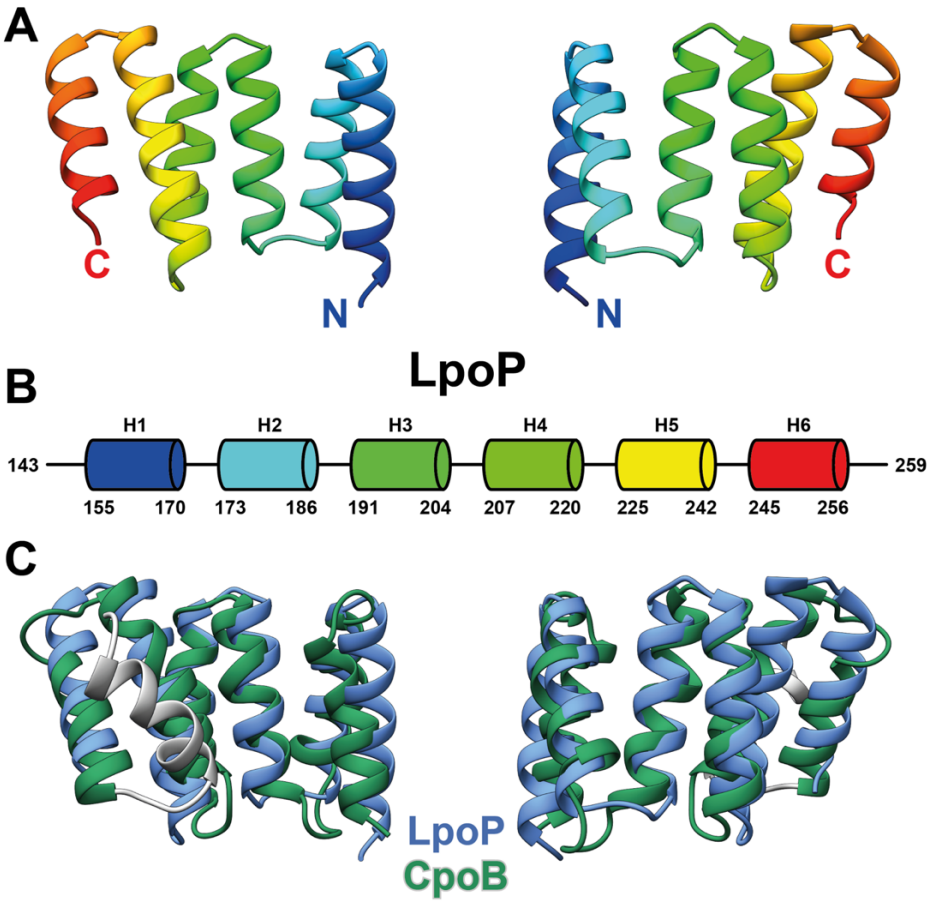

Figure 4.3 Structure of the globular domain of LpoP.
(**A**) Structure of $LpoP_{143-259}$ determined by X-ray crystallography. (**B**) Schematic representation of the $LpoP_{143-259}$ secondary structure. (**C**) Alignment of crystal structures of *P. aeruginosa* $LpoP_{143-259}$ and *Xanthomonas campestris* $CpoB_{3-124}$.

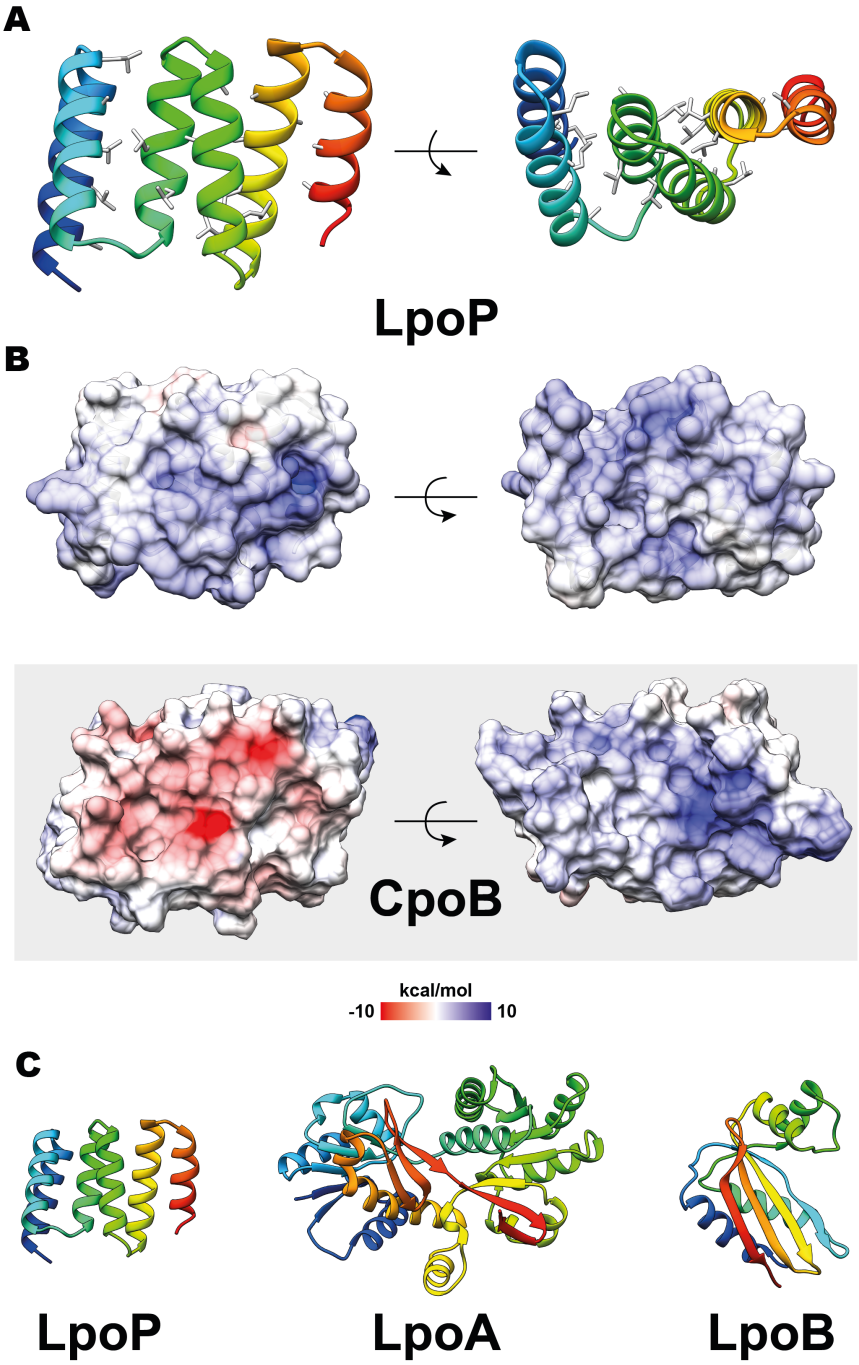

Figure 4.4 Hydrophobic core of LpoP, electrostatic surface potential of LpoP and CpoB, and structural comparison of LpoP, LpoA, and LpoB.
(**A**) The inter-helical Leu and Ala hydrophobic contacts which stabilize the core of LpoP. (**B**) The electrostatic surface potential of LpoP and CpoB (PDB 2XEV (Krachler et al. 2010)), highlighting the differences between the electropositive LpoP and the electropositive and electronegative faces of CpoB.

Table 4.1 LpoP data collection and refinement statistics.

	LpoP
Data collection	
Space group	P 1 2_1 1
Cell dimensions	
a, *b*, *c* (Å)	48.757, 154.584, 54.083
a, b, g (°)	90, 90.149, 90
Resolution (Å)	48.76 – 2.2 (2.279 - 2.2)*
R_{merge}	0.055 (0.372)
I / s*I*	13.16 (3.12)
Completeness (%)	98 (99)
Redundancy	3.2 (3.2)
Refinement	
Resolution (Å)	2.2
No. reflections	129749 (12773)
R_{work} / R_{free}	19.42 (26.90) / 22.99 (29.54)
No. atoms	
Protein	6210
Ligand/ion	85
Water	144
B-factors (Å^2)	
Protein	41.6
Ligand/ion	59.5
Water	42.3
R.m.s deviations	
Bond lengths (Å)	0.01
Bond angles (°)	0.99

*Values in parentheses are for highest-resolution shell.

4.2.3 Lpop interacts with ^{Pa}PBP1b and stimulates its activities *in vitro*

LpoP was identified as a potential ^{Pa}PBP1B activator (Greene, Fumeaux, and Bernhardt 2018)(Greene, Fumeaux, and Bernhardt 2018)(Greene, Fumeaux, and Bernhardt 2018)(Greene, Fumeaux, and Bernhardt 2018) based on the observation that LpoP is required for the function of ^{Pa}PBP1B in the cell (Greene, Fumeaux, and Bernhardt 2018). Contrary to the *E. coli* LpoB/PBP1B activator/synthase pair, until now there is no evidence for the activation of ^{Pa}PBP1B mediated by a direct physical interaction with LpoP. To test for a possible direct interaction, we purified both proteins and tested them in surface plasmon resonance (SPR) experiments. ^{Pa}PBP1B was covalently bound to a chip surface containing immobilized ampicillin and LpoP was then injected on the surface (Figure 4.5 A). LpoP bound to immobilized ^{Pa}PBP1B with a K_D of 4.2 ± 0.5 μM and approaching binding saturation at a concentration of approximately 10 μM. *E. coli* LpoB was previously shown to enhance the rate of lipid II consumption by ^{Ec}PBP1B 8-12 fold, stimulating the GTase and TPase activities of ^{Ec}PBP1B to produce a hyper-crosslinked PG *in vitro* (Typas et al. 2010; Egan et al. 2014, 2018)(Egan et al. 2018)(Egan et al. 2018)(Egan et al. 2018). Monitoring the rate of GTase activity in the presence and absence of LpoP in a continuous assay with a fluorescently labeled dansyl-lipid II as a substrate (Egan and Vollmer 2016) revealed that LpoP stimulated the GTase rate of ^{Pa}PBP1B by 4.5-fold (Figure 4.5 B). Additionally, an *in vitro* TPase activity assay showed a 2-fold increase in ^{Pa}PBP1b TPase activity in the presence of LpoP.

4.2.4 ^{Pa}CpoB is not a regulator of ^{Pa}PBP1b *in vitro*

In *E. coli,* CpoB acts to negatively regulate the stimulation of the TPase of PBP1B by LpoB in a NaCl concentration dependent manner, presumably to allow coordination of outer membrane constriction with PG synthesis during cell division (Gray et al. 2015; Egan et al. 2018). It was therefore of interest to explore the possible role of *P. aeruginosa* CpoB in regulation of PBP1B. Interestingly, in an *in vitro* assay of ^{Pa}PBP1B TPase activity, the addition of ^{Pa}CpoB to a reaction containing ^{Pa}PBP1B and LpoP did not alter cross-linking of the PG product (Figure 4.5 B, Figure 4.6 C). This result was consistent with our SPR analysis showing that ^{Pa}PBP1B did not interact with ^{Pa}CpoB over the concentration range tested (Figure 4.5 A). This is in contrast to the interaction of *E. coli* CpoB with PBP1B and its reduction of the stimulation of the TPase activity by LpoB.

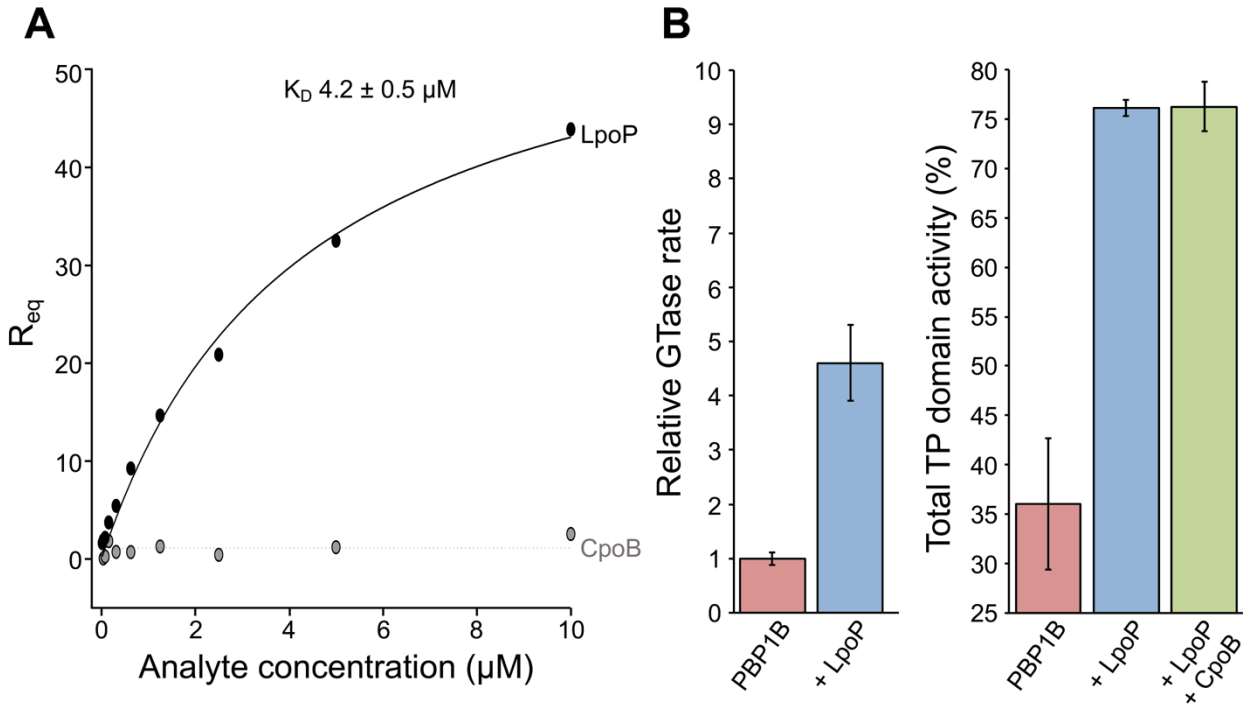

Figure 4.5 LpoP interaction and stimulation of ^{Pa}PBP1B.
(**A**) Representative SPR binding curves resulting from LpoP or ^{Pa}CpoB injection over immobilised ^{Pa}PBP1B. The concentration of analyte protein injected is plotted against the response its specific binding, or lack there-of, elicited at equilibrium. The protein injected is indicated next to the corresponding curve. Non-linear regression assuming one-site saturation was used to calculate the dissociation constant, K_D. The K_D shown is the mean with standard deviation (SD) for n = 4. (**B**) Quantification of relative GTase reaction rate and TPase domain activity (the sum of both peptide cross-linking and carboxypeptidase activity) of ^{Pa}PBP1B with and without LpoP and/or ^{Pa}CpoB. The data shown is the mean with SD for n = 4 and 3, respectively. Corresponding representative HPLC chromatograms and GTase data are shown in Figure 4.6 ^{1}H-^{15}N-NOE values.

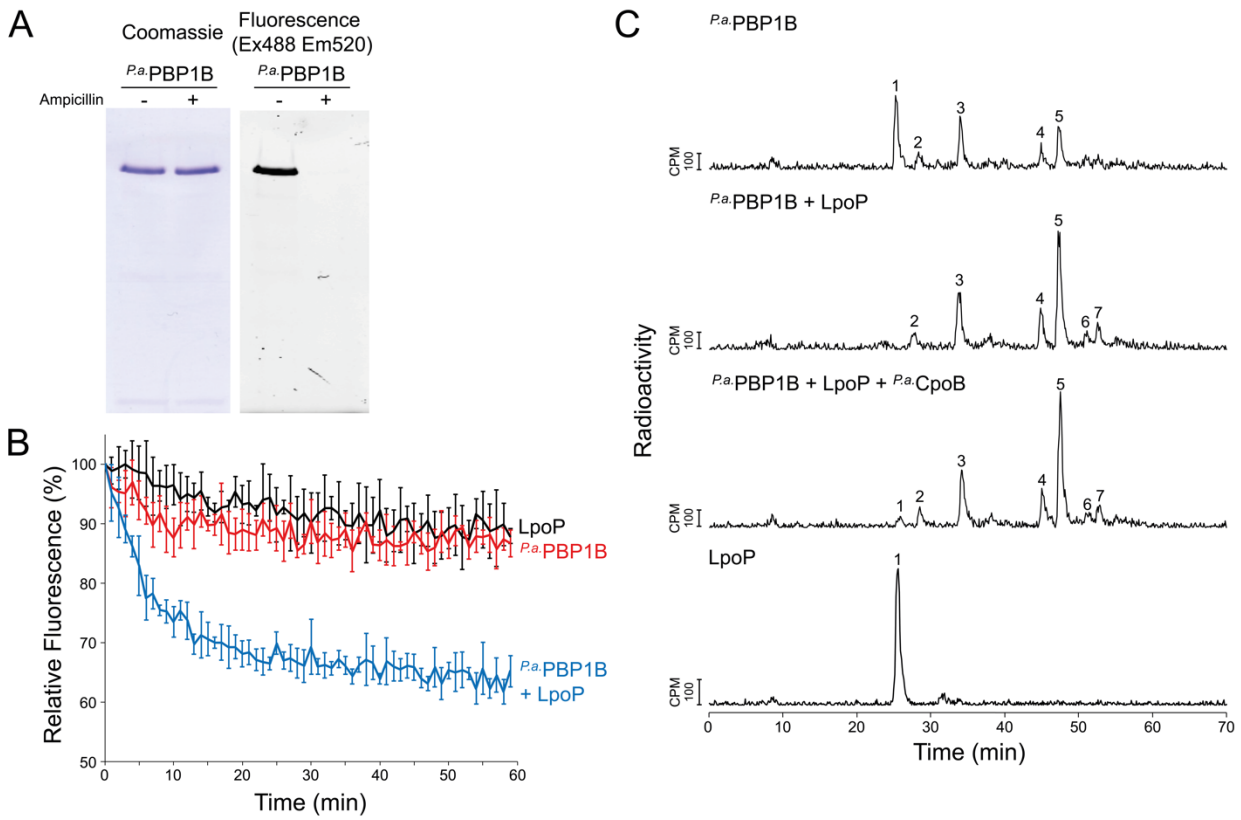

Figure 4.6 Folding and activity of ^{Pa}PBP1b.
(**A**) Fluorescence and coomassie stain images of an SDS-polyacrylamide gel on which Bocillin-bound ^{Pa}PBP1B was resolved. To ensure specificity of binding ^{Pa}PBP1B was incubated in duplicate at 37°C for 30 min, ampicillin was added to one of these duplicates (+). Bocillin was then added to both samples followed by further incubation at 37°C for 30 min. Specific binding of Bocillin shows the TPase domain, and presumably the entire protein, is correctly folded and functional. (**B**) GTase reaction rate data used to calculate relative rates shown in Figure 4.5 B. Mean relative fluorescence (%), using the start-point as 100%, is plotted against time in minutes (min). The protein component of each reaction is shown next to the corresponding curve in the same colour. Polymerisation of the fluorescently labelled lipid II causes a decrease in fluorescence signal. Thus, the slope of these plots gives a relative measure of the GTase rate (n = 4). Data is the mean ± SD. Photobleaching of the fluorophore also occurs over time. (**C**) Representative examples of HPLC chromatograms for TPase/CPase data shown in Figure 4.5 B. Peak 1; PentaP (remaining lipid II/glycan chain ends), peak 2; Tetra (GTase and CPase activity product), peak 3; Penta (GTase), peak 4; TetraTetra (GTase, TPase and CPase), peak 5; TetraPenta (GTase and TPase), peak 6, TetraTetraTetra (GTase, TPase and CPase), peak 7; TetraTetraPenta (GTase and Tpase).

4.2.5 The globular domain of LpoP interacts with the UB2H domain of ^{Pa}PBP1b

In *E. coli*, LpoB interacts with the regulatory UB2H domain of PBP1B. Since a similar domain is present in ^{Pa}PBPB1B (residues 66-159 – 24% identity to *E. coli*), we expressed and purified ^{Pa}UB2H to analyze its interaction with LpoP. We first used biolayer interferometry (BLI) to test for the interaction and quantify equilibrium dissociation constants (K_D) of the complex. Immobilized biotin labeled ^{Pa}UB2H samples were incubated with purified LpoP proteins and real-time association/dissociation curves were measured with concentration of LpoP ranging from 0 to 6 μM. The curves were subjected to BLI analysis and a K_D of 0.4 ± 0.1 μM was determined (Figure 4.7 A). This Kd is slightly lower than the one obtained for the full ^{Pa}PBP1B by SPR (4.2 ± 0.5 μM) but this difference could be due to the specific buffer required to measure the Kd by BLI using the truncated UB2H domain. However, the similarity between the two affinities suggest that the complex between LpoP and ^{Pa}PBP1B is largely stabilized by a direct interaction of LpoP with the UB2H domain.

To more precisely map the interface between LpoP and ^{Pa}UB2H, [^{1}H,^{15}N]-BEST-TROSY spectra were recorded on ^{15}N labelled LpoP alone and with a 1- and 2-fold molar excess of unlabelled ^{Pa}UB2H (Figure 4.7 B). Superimposition of the spectra readily identified perturbed LpoP amide resonances and the progressive shifts observed for the different concentration suggests a rapid exchange regime between the two domains in agreement with the moderate affinity constant measured for this complex. Chemical shift perturbation was determined for each amino acid resonance. The maximal chemical shift perturbations were mapped on the LpoP structure (Figure 4.7 C) and were found to concentrate mainly in the region connecting the extremities of

the helix 2 and the helix 3. As shown in Figure 4.7 D, this region also contains the most conserved amino acid residues as obtained by alignment of 150 sequences using CONSURF software.

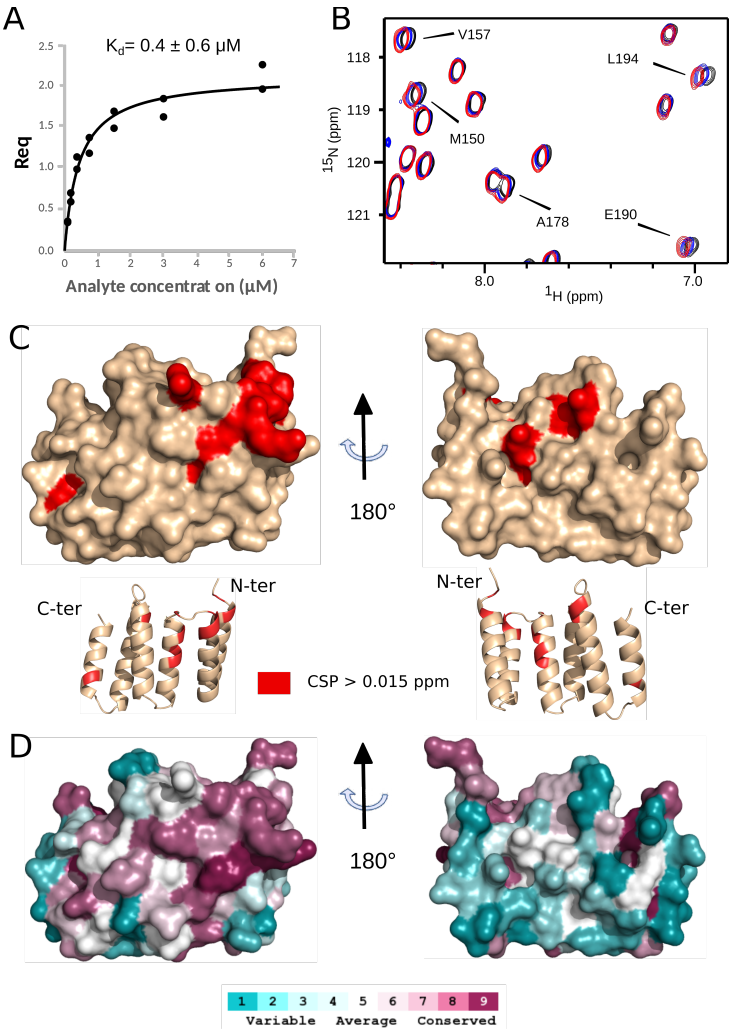

Figure 4.7 Interaction of LpoP with the ^{Pa}UB2H domain of ^{Pa}PBP1B.
(**A**) Quantified BLI binding data for biotin labeled ^{Pa}UB2H binding to LpoP (**B**) Region of ^{1}H–^{15}N correlation spectra showing chemical shift perturbations induced on ^{15}N labelled LpoP by addition of different ratios of ^{Pa}UB2H. The spectra plotted in black, blue and red correspond to a UB2H/LpoP ratio of 0, 1.2 and 1.8, respectively. The samples were prepared with 115 µM of ^{15}N,^{13}C LpoP in 50 mM HEPES buffer at pH 7 containing 150 mM NaCl. ^{Pa}UB2H was concentrated in the exact same buffer at a concentration of 150 µM and added to the NMR tube to reach the different ratios. The NMR experiments were recorded at 20 T spectrometer and 25°C. (***C***) Residues showing a perturbation higher than 0.015 ppm upon UB2H addition are mapped in red on the surface and cartoon representation of the LpoP structure. (**D**) Sequence conservation scores were calculated by the Consurf webserver (Landau et al. 2005) and displayed on the surface representation of LpoP using the same orientation as panel **C**. Scores range from 1 (not conserved, cyan) to 9 (highly conserved, magenta).

4.2.6 LpoP likely interacts between the GTase and UB2H domains of *Pa*PBP1b

We were unable to produce stable ^{15}N-labelled UB2H domain, which prevented us from performing further experiments on the interface residues in ^{Pa}PBP1B. Therefore, we turned to coevolutionary analysis of ^{Pa}PBP1B and LpoP (GREMLIN – (Ovchinnikov, Kamisetty, and Baker 2014)). While LpoP is not widely conserved amongst Gram-negative bacteria, there was a small subset of bacteria with both PBP1B and an LpoP homologue (Greene, Fumeaux, and Bernhardt 2018), resulting in medium to low confidence interface residues in ^{Pa}PBP1B (Figure 4.8 A,B). These data suggest that LpoP likely also associates with the GTase domain of ^{Pa}PBP1B, sitting between the UB2H and GTase domains, as has been proposed for the binding site for *E. coli* LpoB with ^{Ec}PBP1B.

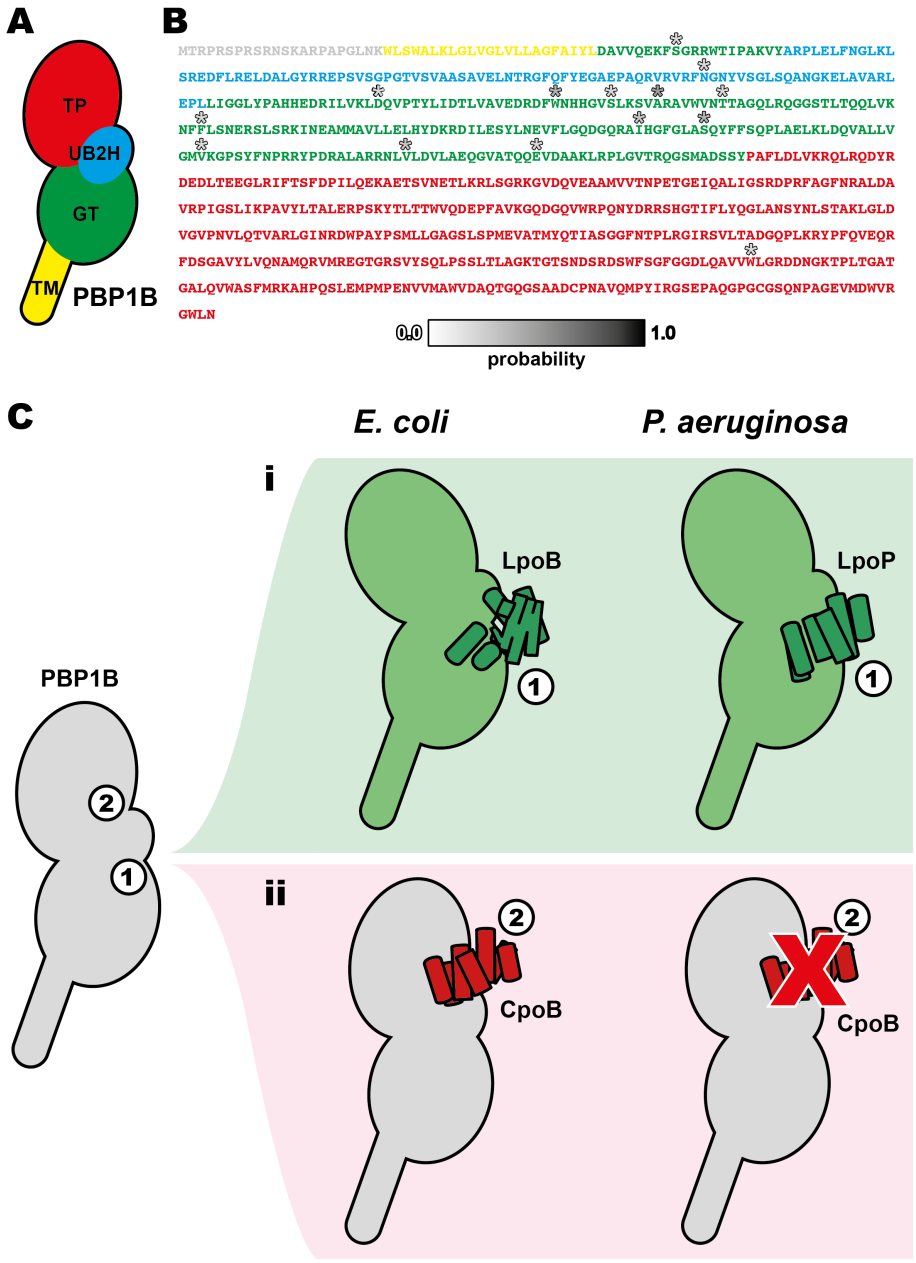

Figure 4.8 Interaction between LpoP and ^{Pa}PBP1B.
(**A**) A scheme of the domains of ^{Pa}PBP1B. (**B**) The sequence of ^{Pa}PBP1B with potential interacting residues labelled with an asterisk. Asterisks are coloured by probability scores from GREMLIN co-evolutionary analysis between LpoP and ^{Pa}PBP1B. (**C**) A schematic representation of the proposed model for ^{Pa}PBP1b activation and regulation, in comparison to ^{Ec}PBP1b. We propose a folding-independent activator binding site between the UB2H and GTase domains in ^{Pa}PBP1B (**i**) and the absence of an interaction between ^{Pa}CpoB and ^{Pa}PBP1 B in *P. aeruginosa* (**ii**).

4.3 Discussion

The recent identification of LpoP, which is required for cellular functionality of PBP1B in *Pseudomonas* and has been proposed to activate its activity (Greene, Fumeaux, and Bernhardt 2018), prompted this biochemical analysis of LpoP. In this work, we performed an in-depth investigation via *NMR*, biochemical assays, X-ray crystallography, and co-evolutionary analysis. We reveal the semi-conserved nature of class A PBP activation, highlighting the similarities and differences between LpoB and LpoP based systems.

4.3.1 Commonalities between LpoB and LpoP based systems

We show that the structure of LpoP is consistent with the model that it serves to activate ^{Pa}PBP1b in a similar manner by which LpoB activates ^{Ec}PBP1B. Using NMR, we show that the lipoprotein LpoP has an intrinsically disordered N-terminal extension, followed by a globular domain which specifically interacts with the UB2H domain of ^{Pa}PBP1B. This is similar to the previously found architecture of LpoB, which has been proposed to activate ^{Ec}PBP1B in response to the porosity of the PG layer (Typas et al. 2010, 2011) According to this model, LpoB activates the synthase at sites with stretched PG, and recent work showed that ^{Ec}PBP1B/LpoB also form a PG repair complex with the LD-transpeptidase LdtD and the DD-carboxypeptidase PBP6A, which was hypothesized to repair defects in PG that arise upon severe outer membrane assembly defect (Morè et al. 2019). Based on the similar architectures of LpoB and LpoP and the observed activation of ^{Pa}PBP1B, we hypothesize that LpoP has analogous roles in the *P. aeruginosa* pathogen.

We propose that LpoP would not only act to regulate ^{Pa}PBP1b at this broad mechanistic level, but also in a similar way at the protein level. We observed that LpoP interacts closely with the UB2H domain, and our coevolutionary analysis strongly suggests that this interaction interface is roughly spatially conserved with that of ^{Ec}PBP1b-LpoB (Figure 4.8). Together with previous data showing that it is possible to generate hyperactive PBP1B mutants that do not require activation by LpoB or LpoP in both species (Greene, Fumeaux, and Bernhardt 2018), this *s*upports the notion for a common mechanism for Lpo binding to conserved regions between the UB2H and GTase domains, leading to similar conformational rearrangements (Figure 4.8 B). These conformational rearrangements activate PBP1B in *E. coli* (Egan et al. 2014, 2018), and likewise, we see a similar, activation in the GTase and TPase activity of ^{Pa}PBP1b by LpoP, further reinforcing a conserved pathway of conformational activation.

4.3.2 Differences between LpoB and LpoP based systems

Despite the overarching conserved features between LpoB and LpoP based PBP1B activation mechanisms, there are also key differences. First, the globular domain of LpoP is distinct from the globular domain of LpoB. LpoP's C-terminal globular domain exclusively consists of three repeated TPR motifs, giving it primarily α-helical character and a structure greatly similar to the N-terminal domain of CpoB (Figure 4.3 C). This is in stark contrast to the C-terminal domain of LpoB, which consists of an internal four-strand β-sheet flanked by N- and C-terminal helices with an overall structural similarity to the N-terminal domain of TolB (Egan et al. 2014; King, Lameignere, and Strynadka 2014).

It appears that, despite the difference between the globular domains of LpoB and LpoP, the use of TPR motifs in the regulation of class A PBP proteins is a common theme. We see the use of TPR motifs in both the negative regulator CpoB, as well as in the LpoA activator of the elongasome. Interestingly in the case of LpoA, these TPR repeats are seen to be involved in the extension of the LpoA across the periplasm, instead of a direct interaction module as seen in LpoP and CpoB. Regardless, it is remarkable how activators and regulators of class A PBPs evolved from similar domain pieces in these distinct lineages.

Beyond the purely structural differences between the LpoP and LpoB systems, the different effects of CpoB on the two activators is of interest. Here we see that ^{Pa}CpoB does not reduce the activation of the TPase activity of ^{Pa}PBP1b by LpoP. This is explained by the lack of an interaction between ^{Pa}CpoB and ^{Pa}PBP1B. In *E. coli* the cpoB gene is adjacent to the genes for the Tol-Pal apparatus and CpoB has been proposed to act as a link between outer membrane constriction and PG synthesis activity. Perhaps CpoB primarily plays a role in the Tol-Pal apparatus, and interaction with PG synthases evolved downstream in a subset of Gammaproteobacteria. It would be of interest to further test this hypothesis, determine if there are alternate roles for CpoB, and see if this potential lack of a PG synthase regulatory function correlates to the presence of a LpoP.

4.4 Conclusion

We report the structure and organisation of LpoP and its interaction site with PBP1B from *P. aeruginosa*. We highlight the similarities and key differences between this activator-PG synthase system and the LpoB based PBP1B activation in *E. coli*. Our data suggest a semi-

conserved mechanism for PBP1B activation in *P. aeruginosa* and other LpoP based systems. Using this knowledge of the specificities of LpoP and LpoB based class A PBP regulation, it may be possible to target these via specific interface inhibiting compounds.

4.5 Methods

4.5.1 Plasmid construction

Expression vectors for ^{Pa}PBP1B (pAJFE52), LpoP lacking its lipoprotein sorting sequence (residues 20-259) (pAJFE57), and ^{Pa}CpoB lacking its periplasmic export sequence (residues 22-274) (pAJFE50) were prepared by Sequence and Ligase Independent Cloning (SLIC) following the procedure described previously (Jeong et al. 2012). Genes were inserted into pET28a, which had been linearized and amplified by PCR, opening the vector at the NdeI restriction site. Resulting proteins possessed an N-terminal hexa-Histidine tag followed by a thrombin cleavage sequence. pET28 linearization forward primer: ATGGCTAGCATGACTGGTGGAC. pET28 linearization reverse primer: ATGGCTGCCGCGCGGCACCAG. Gene inserts, with SLIC compatible complementary overhang sequences for insertion into the linearized pET28, were amplified from *P. aeruginosa* PA01 genomic DNA template. ^{Pa}PBP1B SLIC forward primer: TGGTGCCGCGCGGCAGCCATATGACGCGTCCCCGATCCC. ^{Pa}PBP1B SLIC reverse primer: TGTCCACCAGTCATGCTAGCCATTTATTCAATTCAGCCAGCCACGTAC. LpoP SLIC forward primer: CTGGTGCCGCGCGGCAGCCATGCCAGCCCGCAGCACGGGG. LpoP SLIC reverse primer: TGTC-CACCAGTCATGCTAGCCATTATCAGGAGCTGACCTTGGCCT. ^{Pa}CpoB SLIC forward

primer: CTGGTGCCGCGCGGCAGCCATATGCCCAAGCACCTGCGTGT. ^{Pa}CpoB SLIC reverse primer: TGTCCACCAGTCATGCTAGCCATTTAGCGAAGGTTCTTGAGATCGCGC.

4.5.2 Protein purification

4.5.2.1 LpoP protein purification

For LpoP purification, pAJFE57 was transformed into BL21(DE3). This strain was cultured in 1.5 L of LB at 30°C to an OD578 of 0.5, at which point 1 mM IPTG was added to induce protein overproduction for 3 h at 30°C. The culture was rapidly cooled before harvesting by centrifugation, cells were resuspended in 80 mL 25 mM Tris/HCl, 500 mM NaCl, 20 mM imidazole, 10% glycerol, pH 7.5. Sigma protease inhibitor cocktail (PIC) at 1 in 1000 dilution and 100 µM PMSF were added to the resuspension before cells were disrupted by sonication (Branson digital sonifier). Lysed cells were fractionated by ultracentrifugation (130,000 x *g*, 1 h, 4°C). The soluble fraction was applied to a 5 mL HisTrap column attached to an ÄKTA Prime+ equilibrated in resuspension buffer indicated above. The column was washed with 25 mM Tris/HCl, 1 M NaCl, 40 mM imidazole, 10% glycerol, pH 7.5 before elution of bound protein with 25 mM Tris/HCl, 500 mM NaCl, 400 mM imidazole, 10% glycerol, pH 7.5. His-LpoP containing fractions were pooled and 4 U/mL restriction grade thrombin (Novagen) was added. The sample was dialysed against 20 mM Tris/HCl, 200 mM NaCl, 10% glycerol, pH 7.5 for 20 h at 4°C. The sample was concentrated to <4 mL (using Sartorius Vivaspin turbo 15) and applied to a size exclusion chromatography column (HiLoad 16/600 Superdex200 pg) equilibrated in 20 mM HEPES/NaOH, 200 mM NaCl, 10% glycerol, pH 7.5 attached to an ÄKTA Prime+ system. The sample was

resolved at 0.8 mL/min. LpoP eluted in a single peak at 82 mL, corresponding fractions were collected and concentrated to 4 mL. This procedure yielded 28 mg of pure protein.

4.5.2.2 Labeled LpoP for NMR

For LpoP purification, pAJFE57 was transformed into BL21(DE3). This strain was cultured in 1 L of M9 containing 1g/L of ammonium chloride and 2g/L of glucose at 37°C to an OD600nm of 0.6, at which point 1 mM IPTG was added to induce protein overproduction for 4 h at 30°C. After harvesting, cells were resuspended in 15 mL 20 mM Tris pH8, 300 mM NaCl buffer supplemented with 1 tablet of cOmpleteTM EDTA-free (Roche) as protease inhibitor cocktail. Cells were disrupted by sonication (Sonics Vibra CellTM). Lysed cells were clarified by centrifugation (46 000 g, 40 min, 4°C). The soluble fraction was applied to a 4 mL Ni-NTA (Qiagen) column beforehand equilibrated in resuspension buffer. After sample application the column was washed with equilibration buffer containing 25 mM imidazole. Elution was performed using the same buffer supplemented with 500 mM imidazole. Fractions containing the protein were pooled and concentrated before to be injected to a size exclusion chromatography column (HiLoad 26/600 Superdex75 pg) equilibrated in 20 mM Tris pH8, 300 mM NaCl buffer. LpoP is eluted in a single peak at 149 mL, corresponding fractions were dialysed against 50 mM HEPES pH 7, 150 mM NaCl buffer for NMR or dialysed against 20 mM Tris, 150 mM NaCl, pH 8 for BLI interactions test.

4.5.2.3 LpoP$_{142-259}$ protein purification

For purification of LpoP$_{142-259}$, cell pellets were resuspended in lysis buffer (20 mM HEPES, pH 8.0, 300 mM NaCl, 10% glycerol) and lysed by processing twice with a homogenizer (15 kPa; Avestin). Cellular debris was pelleted by centrifugation at 125,000 x *g* for 1 hour. The resultant supernatant was loaded onto 10 mL Ni2+-saturated Ni-NTA superflow beads (Qiagen), washed with 65 mM imidazole in 20 mM HEPES, pH 8.0, 300 mM NaCl, and the protein was eluted with 300 mM imidazole in the previous buffer. 1 U of thrombin was added per mg of protein to remove the N-terminal His-tag overnight at 4°C). Samples were purified further by size exclusion chromatography (SEC) with a Superdex 200 column (GE Lifesciences) equilibrated in 20 mM HEPES, pH 8.0, 150 mM NaCl. Fractions containing pure LpoP were pooled and concentrated to 30 mg/mL. Protein was frozen rapidly in liquid nitrogen and stored at -80°C) until required.

4.5.2.4 ^{Pa}PBP1b protein purification

^{Pa}PBP1B was prepared by largely the same procedure as its *E. coli* homologue, described previously (Bertsche et al. 2006) with modifications. Plasmid pAJFE52 was transformed into *E. coli* BL21(DE3) expression strain. This strain was cultured in 1.5 L of LB at 30°C to an OD578 of 0.5, at which point 1 mM IPTG was added to induce protein overproduction for 3 h at 30°C. The culture was rapidly cooled before harvesting by centrifugation, cells were resuspended in 80 mL 25 mM Tris/HCl, 500 mM NaCl, 1 mM EGTA, 10% glycerol, pH 7.5. Sigma protease inhibitor cocktail (PIC) at 1 in 1000 dilution and 100 µM PMSF were added to the resuspension before cells

were disrupted by sonication (Branson digital sonifier). Lysed cells were fractionated by ultracentrifugation (130,000 x *g*, 1 h, 4C). Insoluble material was resuspended in 45 mL 25 mM Tris/HCl, 5 mM $MgCl_2$, 1 M NaCl, 20% glycerol, 2% Triton X-100, pH 7.5 plus 1/1000 PIC and 100 M phenylmethylsulphonylfluoride (PMSF) and mixed overnight at 4°C. Remaining insoluble material was pelleted by a second ultracentrifugation step, leaving solubilised membrane protein in the supernatant. The sample was diluted 1:1 with 25 mM Tris/HCl, 1 M NaCl, 40 mM imidazole, 20% glycerol, pH 7.5 before application to a 5 mL HisTrap column attached to an ÄKTA Prime+ equilibrated in 25 mM Tris/HCl, 2.5 mM $MgCl_2$, 1 M NaCl, 20 mM imidazole, 20% glycerol, 1% Triton X-100, pH 7.5. After binding the column was washed with 25 mM Tris/HCl, 1 M NaCl, 50 mM imidazole, 20% glycerol, 0.2% Triton X-100, pH 7.5 before elution of bound protein with 25 mM Tris/HCl, 1 M NaCl, 400 mM imidazole, 20% glycerol, 0.2% Triton X-100, pH 7.5. His-^{Pa}PBP1B containing fractions were pooled and 4 U/mL restriction grade thrombin (Novagen) was added. The sample was dialysed against 25 mM Tris/HCl, 1 M NaCl, 0.5 mM EGTA, 10% glycerol, pH 7.5 for 20 h at 4°C. The sample was then dialysed against a sequence of buffers in preparation for ion exchange chromatography. Firstly 4 h against 20 mM NaAc, 1 M NaCl, 10% glycerol, pH 5.0, followed by 16 h against 20 mM NaAc, 300 mM NaCl, 10% glycerol, pH 5.0. The sample was diluted 1:1 with 20 mM NaAc, 50 mM NaCl, 10% glycerol, 0.2% reduced Triton X-100, pH 5.0 before application to an equilibrated 1 mL HiTrap SP column attached to an ÄKTA Prime+ system. The column was equilibrated in buffer A (20 mM NaAc, 200 mM NaCl, 10% glycerol, 0.2% reduced Triton X-100, pH 5.0). ^{Pa}PBP1B was eluted by gradient from 100% buffer A to 100% buffer B (20 mM NaAc, 2 M NaCl, 10% glycerol, 0.2% reduced Triton X-100, pH 5.0) over 14 mL. ^{Pa}PBP1B containing fractions were pooled and dialysed against 20 mM NaAc, 500 mM NaCl, 20% glycerol, 0.2% reduced Triton X-100, pH 5.0. This procedure yielded 0.9 mg of

pure protein. To ensure correct folding, the protein's ability to bind to the fluorescent β-lactam Bocillin was assayed as previously described (Egan et al. 2018) (Figure 4.6).

4.5.2.5 *Pa*UB2H domain protein purification

Plasmid carrying UB2H domain of *Pseudomonas aeruginosa* PBP1b was transformed in Bl21(DE3) competent cells. This strain was cultured to an OD_{600nm} of 0.7, at which point 1 mM IPTG was added to induce protein overproduction for 3h at 37°C. After harvesting cells, pellet was resuspended in 20 mL 50 mM Tris pH 7.5 buffer. Cells were disrupted by sonication (Sonics Vibra CellTM) and lysate was centrifuged in a Beckman cold centrifuge (30 minutes, 46000g). The supernatant was discarded and inclusion bodies containing ^{Pa}UB2H was washed following cellular fractionation protocol alternating four washing steps in different buffer and centrifugations. The centrifugation steps were done at 4°C during 30 min at 46000g. Washing steps were done using 20 mL of 50 mM Tris pH 7.5, 2 M NaCl buffer, then 50 mM Tris pH 7.5, 1% Triton X100 buffer, finally two washes of 20mL 50 mM Tris pH7.5 . At the end inclusion bodies were solubilized in 80mL of 50 mM Tris pH 7.5, 6M Guanidium during an overnight incubation. After centrifugation (30 min at 46 000g, 4°C) the supernatant was loaded on 4 mL of Ni-NTA (Qiagen) column. Column was washed with 50mM Tris pH 7.5, 6M guanidium, 25 mM Imidazole buffer, and the protein was eluted with 50mM Tris pH 7.5, 6M guanidium, 500mM imidazole. The protein was refolded performing three baths of dialysis against 100mM sodium acetate pH5 buffer. After centrifugation the soluble protein was injected to a size exclusion chromatography column (HiLoad 26/600 Superdex75 pg) equilibrated in 100mM sodium acetate pH 5 buffer. ^{Pa}UB2H was eluted in a single peak at 206 mL corresponding to a monomer of the protein.

4.5.2.6 ^{Pa}CpoB protein purification

For ^{Pa}CpoB purification; protein overproduction, immobilised metal affinity chromatography (IMAC), and size exclusion chromatography (SEC) were performed by the same procedure as for LpoP described above. An additional ion exchange chromatography step, adapted from (Krachler et al. 2010), was included between IMAC and SEC. Post IMAC, His-^{Pa}CpoB containing fractions were pooled, 4 U/mL thrombin added, and dialysed against 20 mM Tris/HCl pH 8.0 for 20 h at 4°C. Some impurities carried from IMAC precipitate during this stage, these were removed after dialysis by centrifugation (4000 g, 15 min, 4C). The sample was applied to a 5 mL HiTrap SP column attached to an ÄKTA Prime+, equilibrated in buffer A (20 mM Tris/HCl pH 8.0). Bound ^{Pa}CpoB was eluted by gradient from 100% buffer A to 100% buffer B (20 mM Tris/HCl, 500 mM NaCl, pH 8.0) over 50 mL. ^{Pa}CpoB containing fractions were concentrated to <4 mL for SEC as above. In SEC, ^{Pa}CpoB eluted as a single peak at 65 mL, consistent with it existing as a trimer as reported for its *E. coli* homologue (Krachler et al. 2010). This procedure yielded 70 mg of pure protein.

4.5.3 *In vitro* protein interaction and activity assays

SPR experiments were performed as previously described (Egan et al. 2014). LpoP and ^{Pa}CpoB samples were prepared for injection over the ^{Pa}PBP1B surface by 1:1 serial dilution from 10 µM to 19.5 nM. Assays were performed at 25°C, at a flow rate of 75 µL/min and with an injection time of 5 min. The running buffer consisted of 10 mM Tris/HCl, 150 mM NaCl, 0.05% Triton X-100, pH 7.5. The dissociation constant (K_d) was calculated by non-linear regression using

SigmaPlot 13 software (Systat Software Inc.). Continuous fluorescence GTase assays were performed as described previously (Egan and Vollmer 2016) with slight modification. ^{Pa}PBP1B was assayed at a concentration of 0.5 µM 10 µM LpoP at 37°C for 1 h. Time points were taken every 1 min, instead of every 20 s to reduce photobleaching. Measurement of total PG synthesis activity using radiolabelled lipid II substrate was also performed as previously described (Biboy, Bui, and Vollmer 2013) using 0.5 M enzyme with 10 µM LpoP, 50 µM ^{Pa}CpoB at 37°C for 3 h. Total TPase activity was calculated as the percentage of muropeptide products known to be produced by this domain's function, including peptide cross-linking and DD-carboxypeptidase activity.

4.5.4 Biolayer interferometry experiments

Biolayer Interferometry Experiments (BLI) were recorded on an OctetRED96e (Fortebio) using biotinylated protein attached on streptavidin tips. For biotinylation of LpoP and ^{Pa}UB2H, 100µL of protein at 3.3 mg/mL an 5,2 mg/mL respectively for LpoP and ^{Pa}UB2H are mixed with 10µL of 1M MES pH 5,5, 2,7µL of Biotin-Hydrasin and 6,7µL of EDC (N-(3-Dimethylaminopropyl)-N′-ethylcarbodiimide). The reaction of biotinylation is performed 2h at 22°C under agitation. After biotinylation UB2H was dialysed in 50mM MES pH 6.5 and LpoP was dialysed in HBS buffer. Non-biotinylated LpoP and UB2H were prepared in 50mM MES pH6.5 buffer at 1,88 mg/mL and 5,37mg /mL respectively. UB2H-Biot (25µg/ml) was immobilised on Streptavidin coated -BLI biosensors to reach about 1 nm immobilisation in HBS-T (10 mM Hepes pH 7,5,150 mM NaCl and 0.02% Tween) Buffer. Tips loaded with UB2H were inserted into different LpoP concentrations (0 to 6µM) in HBS-T Buffer at 23°C. Kinetics were

recorded with 1200s for association and 1000sec for dissociation phases, experiments were reproduced twice with 10mM HCl pulses (3x) used for regeneration between cycles. Responses at equilibrium of the two series (end of the association phase) were simultaneously fitted with the equation $Req = \frac{Rmax \times conc}{Kd \times conc}$ by ForteBio data analysis software.

4.5.5 X-ray crystallography and structure determination

P. aeruginosa LpoP protein was crystallized at 20°C by sitting drop vapour diffusion using 0.2 µL protein solution (30 mg/mL purified protein in 20 mM HEPES, pH 8.0, 150 mM NaCl) and 1 µL of mother liquor (0.1 HEPES pH 7.5, 2.5 M $AmSO_4$, 1% PEG 400, 2.5% 1,2-butanediol). X-ray diffraction data of LpoP was collected on Advanced Light Source beamline 5.0.2. Diffraction data were processed using XDS (Kabsch 2010) and the structure was solved by molecular replacement using an ensemble of truncated Rosetta (Leaver-Fay et al. 2011) refined homology models in AMPLE (Bibby et al. 2012) based on a model from SWISS-MODEL (Waterhouse et al. 2018) and PDBID:5XW7 (Nojima et al. 2017). The structure was auto-built using Buccaneer (Cowtan 2006) and subsequently refined using Phenix (Adams et al. 2010) and Coot (Emsley and Cowtan 2004). There is excellent density for the majority of the $LpoP_{142\text{-}259}$ construct, with the absence of density for residues 142-153 – in line with the low and intermediate values seen in the ^{1}H-^{15}N-NOE (Figure 4.1). Density for a triethylene glycol portion of the precipitant, PEG 400, was seen at one interface between two of the LpoP proteins in the crystal lattice. See Table 4.1 for data collection and refinement statistics.

4.5.6 NMR resonance assignments

The 2D- and 3D-NMR experiments were collected on 200 µM ^{13}C,^{15}N-labeled LpoP NMR samples in 30 mM HEPES, 200 mM KCl buffer at pH 7.5 containing 10%D_2O. Backbone resonance assignments were carried out using a combination of 2D ^{1}H-^{15}N-BEST-TROSY and 3D HN(CO)CACB, iHNCACB, HNCO, HN(CA)CO, H(NCACO)NH. In order to limit the number of overlaps, BEST-TROSY version of the above listed experiments was used (Solyom et al. 2013; Brutscher et al. 2015). For the assignment of side-chains aliphatic carbons, 2D ^{1}H-^{13}C-HSQC and 3D (H)C(CO)NH, (H)CCH-TOCSY, and H(C)CH-TOCSY experiments were collected. All spectra were recorded at 25°C using Bruker AVANCE spectrometers operating at 800 and 850 MHz proton frequency equipped with TCI cryoprobes.

The NMR spectra were processed using the TopSpin™ software by Bruker in its 3.2 version and were analyzed using the CcpNmr Analysis software (Vranken et al. 2005). The ^{1}H chemical shifts were referenced to the internal standard 4,4-dimethyl-4-silapentane-1- sulfonic acid (DSS) methyl resonance. ^{13}C and ^{15}N chemical shifts were referenced indirectly using the IUPAC-IUB protocol (Markley et al. 1998).

4.5.7 NMR titration experiments

Interaction studies were performed with ^{13}C,^{15}N-labeled LpoP at 115 µM prepared in a buffer containing 50 mM HEPES buffer, pH 7, 150 mM NaCl and 5% (vol/vol) D_2O. Unlabelled ^{Pa}UB2H were dialyzed in the same buffer at a concentration of 150 µM and successively added to

the NMR tube to reach the protein-to-protein ratio of 0, 0.6, 1.2 and 1.8. [^{1}H,^{15}N]-BEST-TROSY-HSQC spectra were collected at 298K for each protein ratio using Bruker AVANCE spectrometers equipped with a TCI cryoprobe and operating at 850 MHz proton frequency. Analysis software CcpNmr 2.2 was used to monitor protein chemical shift perturbations for every assigned amide resonance by superimposition of the ^{15}N-BEST-TROSY spectra and automatic peak picking. Chemical shift perturbations ($\Delta\delta$) were calculated on a per-residue basis for the highest substrate-to-protein ratio as described previously (Egan et al. 2018).

4.5.8 Co-evolutionary analysis

The Baker lab's GREMLIN software (Ovchinnikov, Kamisetty, and Baker 2014) was used to probe the interface between LpoP and ^{Pa}PBP1b. Input sequences were that of the globular domain of LpoP and all residues of ^{Pa}PBP1b. For alignment, the HHBlits server (Zimmermann et al. 2018) was used and E-value cut-offs for both sequences were set at 10^{-2} and the alignments were run for 8 iterations so as to align with LpoP sequences and avoid a majority of unrelated proteins of similar sequence identity. Alignments were performed 08/10/2019.

Table 4.2 Co-evolutionary sequences and GREMIN raw results.

LpoP Sequence
SRSAPTGIPASGSAGSLAADEQLDGPVLAMLTTAQQQQGSGDLNSAAASLERAQRIAPREPQV
LYRLAQVRLAQGDAAQAEQVARRGLSYANGRPALQAGLWELIAQAREKQGDSAGAALARQKAK
VS

PBP1b Sequence
MTRPRSPRSRNSKARPAPGLNKWLSWALKLGLVGLVLLAGFAIYLDAVVQEKFSGRRWTIPAK
VYARPLELFNGLKLSREDFLRELDALGYRREPSVSGPGTVSVAASAVELNTRGFQFYEGAEPA
QRVRVRFNGNYVSGLSQANGKELAVARLEPLLIGGLYPAHHEDRILVKLDQVPTYLIDTLVAV
EDRDFWNHHGVSLKSVARAVWVNTTAGQLRQGGSTLTQQLVKNFFLSNERSLSRKINEAMMAV
LLELHYDKRDILESYLNEVFLGQDGQRAIHGFGLASQYFFSQPLAELKLDQVALLVGMVKGPS
YFNPRRYPDRALARRNLVLDVLAEQGVATQQEVDAAKLRPLGVTRQGSMADSSYPAFLDLVKR
QLRQDYRDEDLTEEGLRIFTS

LpoP	PBP1b	r score	s score	probability
193_Q	206_A	0.032	1.377	0.501
199_A	195_W	0.031	1.327	0.461
156_G	288_S	0.03	1.284	0.427
207_D	281_I	0.027	1.171	0.342
205_Q	213_T	0.025	1.058	0.267
206_G	134_N	0.024	1.044	0.258
185_Q	213_T	0.024	1.026	0.247
247_A	176_D	0.023	1.008	0.237
165_A	54_S	0.023	0.995	0.229
164_T	176_D	0.023	0.994	0.229
165_A	201_S	0.023	0.993	0.228
179_A	234_F	0.023	0.992	0.228
181_L	311_V	0.023	0.987	0.225
218_G	64_V	0.023	0.973	0.217
193_Q	210_W	0.022	0.966	0.213
199_A	382_Q	0.022	0.964	0.212
181_L	185_T	0.022	0.962	0.211
90_Y	288_S	0.061	0.975	0.515
67_L	333_V	0.052	0.819	0.343
75_G	347_E	0.046	0.73	0.258
41_G	679_L	0.044	0.699	0.232

4.6 Data availability

Atomic coordinates for the *Pseudomonas aeruginosa* LpoP model have been deposited in the protein data bank as PDB ID 6W5Q.

Chapter 5: Summary and future directions

5.1 Summary

The bacterial cell wall proves one of the most fascinating and impactful systems to study to this day. Despite a relatively longstanding identification of the components of the core biosynthetic pathway, the countless modifications and additional regulatory networks that feed in (and out) of the peptidoglycan biosynthetic pathway have kept scientists captivated for decades. Coupled to this, there is no time of greater importance to further our understanding of the bacterial cell well, as we enter into uncertain times regarding the use and efficacy of our current antibiotics amid an increasing presence of multidrug resistant bacteria in the clinic.

Study of the bacterial cell wall can lead to the development of novel and targeted antibiotic therapies, which can help combat these emerging multidrug resistant strains. One area which shows huge promise for the development of new antibiotic therapies, is the use of structure guided drug design for the modulation of existing therapeutics (Kumar et al. 2017). The foundation for this work are the structures of the many enzymes that make up the peptidoglycan biosynthetic pathway, with the entirety of the core biosynthetic pathway (Mur → PBPs) being structurally characterized with the publication of the structure of MurJ in 2017 (Kuk, Mashalidis, and Lee 2017). Despite this wealth of structural knowledge, many of the core enzymes have not been characterized with substrates or products bound or from relevant pathogenic species. Additionally, the inherent complexity of the pathway lends to potential for targeting of noncanonical targets –

from peripheral proteins, such as the stress regulated YcbB, to targets from clinically relevant targets, such as the PBP1b activator LpoP in *Pseudomonas aeruginosa*.

To this end, my thesis has used a largely structural approach to study the modulation of bacterial peptidoglycan synthase activity. In particular I have focused on the aforementioned proteins YcbB and LpoP, which both form complexes with canonical class A PBPs to modulate their function. Here, we present the structure of YcbB from *E. coli*, *S.* Typhi, and *C. rodentium* to provide a more comprehensive understanding of this tightly conserved protein across a handful of clinically important bacteria. We have discovered that these proteins have a novel domain architecture consisting of a putative scaffolding domain, a peptidoglycan binding domain, and a canonical L,D-transpeptidase catalytic domain. Furthermore, observe for the first time the interesting addition of an extended capping-loop sub-domain on the catalytic domain of these enzymes and have captured this sub-domain in three distinct orientations. Additionally, we see three liganded states for this class of enzyme, leading to insights into the rather poor inhibition observed for L,D-transpeptidases by carbapenem antibiotics. We have also explored both the role of the unique structural features of YcbB in *in vivo* β-lactam resistance in *E. coli*, as well as its role in acute bacterial infections in mouse models of both *S.* Typhi and EPEC infection. Collectively we have advanced our understanding of the structure and role of YcbB in the modulation of canonical peptidoglycan synthase activity and provide a foundation for future work in the development of YcbB inhibiting anti-typhoidal therapeutic agents.

Additionally, we report the structure of the activator of PBP1b in *P. aeruginosa*, LpoP. Given the presumed structural differences between LpoP and the canonical LpoB seen in *E. coli*,

it was of interest to pursue the characterization of LpoP to provide insight into the differences and similarities in activation of class A PBPs across diverse bacterial systems. We see that the structure of LpoP consists of a tandem-TPR fold, more similar to the negative regulator of PBP1b in *E. coli*, CpoB, than the positive regulator, LpoB. To further probe the regulation of PBP1b in *P. aeruginosa*, we dissected both the modulation of GTase and TPase activity by both LpoP and CpoB in *in vitro* assays. Here, we see additional differences between regulation in *P. aeruginosa* and *E. coli*, with the role of CpoB in negative regulation of PBP1b not being observed in *P. aeruginosa*. This work lays the foundation for further study of the activation of class A PBP activation in noncanonical systems.

Together this work of this thesis provides crucial structural and biological insights into the modulation of peptidoglycan synthase activity through both alteration of canonical activity, through YcbB, and stimulation of canonical activity, through LpoP.

5.2 Future directions

5.2.1 YcbB

We have determined the structure of acylated YcbB from a variety of bacterial species and probed the role of YcbB in both β-lactam resistance and acute bacterial infections; however, a few pressing questions still stand.

From a structural standpoint, there are two key structures of YcbB that are outstanding. The first being a deacylated structure of YcbB. This has been a challenge as a crystallographic pursuit, due to the apparent necessity of acylation in the stabilization of YcbB for crystallographic purposes. This could potentially be overcome with additional and extensive screening of crystallization conditions, yet there are alternate methods that could potentially be more fruitful. One such method would be the use of NMR to solve the apo structure of the catalytic domain of YcbB. NMR is well known for its amenability with flexible samples, and apo structures of L,D-transpeptidases have been solved previously using this methodology (Lecoq et al. 2012, 2013). The NMR structure of the catalytic domain of YcbB has previously eluded characterization, mostly due to the difficulty in construct design given the overall structure of YcbB. With the structure of YcbB solved via X-ray crystallography, we hope that new, informed, constructs of stable YcbB catalytic domain can be generated and allow for the determination of the apo-YcbB state.

Additionally, as it was recently shown that copper can inhibit Ldts (Peters et al. 2018), there is interest in the determination of any potential complex formed between YcbB and copper. As this effect is seen across a variety of Ldts, and the only conserved domain is the catalytic domain of YcbB, one could likely pursue this via X-ray crystallography of the full-length protein or via NMR of the catalytic domain alone.

As we have shown that both PBP1b and PBP5 interact with YcbB in the context of the *E. coli* system, it would also be of interest to determine the structure of the potential tripartite complex between all three enzymes. Due to the complexity in the crystallization of such a complex, it would likely be more amenable for structural determination via cryogenic electron microscopy (cryoEM).

Significant work will need to be invested in the formation of a stable complex between these proteins, the successful vitrification of the complex, and the collection of this data would likely require significant microscope time. That being said, the determination of this complex sits firmly within the feasibility of the technique at this current time and the technique is advancing rapidly in both hardware and software.

The final future direction of the YcbB project, which is perhaps most enticing, is in the structure guided drug design of anti-YcbB compounds for potential use in treatment of typhoid infection. With the bulk of structural data provided in this thesis, there is significant insight into the inhibition of these enzymes by carbapenem antibiotics, specifically meropenem and ertapenem. From this, we know that there is room for significant improvement in the design of downstream modifications to these existing antibiotics to increase their specificity and affinity for YcbB. The development of such specific antibiotics could aid in the treatment of typhoid infections and assist in further deconvolution of the role of the typhoid toxin in human infection.

5.2.2 LpoP

We have determined the structure of the PBP1b activator in *P. aeruginosa*, LpoP and provided insight into the similarities and differences between the canonical LpoB-PBP1b system and the LpoP-PBP1b system; however, a few pressing questions still stand.

From a structural standpoint, it would certainly be of interest to pursue the complex structure between PBP1b and LpoP. This would provide insight into the activation of PBP1b in *P.*

aeruginosa and the activation of class A PBPs in general, as no such complex structure exists, even for the canonical LpoB-PBP1b complex. That being said, it would likely be of interest to pursue the structures of LpoP-PBP1b and LpoB-PBP1b in tandem, to allow for comparison between the two distinct systems. Similar to the methodology proposed for the characterization of the YcbB-PBP1b-PBP5 complex, these complexes would likely be most amenable to structural determination via cryoEM. Despite being on the smaller end of the spectrum when it comes to cryoEM, the complex masses are ~100 kDa and are certainly within the realm of feasibility using current technology.

From a non-structural standpoint, further experimentation could be performed to try and understand the differences between the roles of CpoB in *E. coli* and *P. aeruginosa*. It could be of interest to dissect the phenotypes of bacterium with deletion and modifications in CpoB under a variety of stress conditions, to see if the role of CpoB has more recently evolved to include a role in modulation of class A PBPs, as seen in *E. coli*. *P. aeruginosa* would also perhaps be a reasonable model organism to study the role of CpoB in perhaps its more fundamental non-PG related functions, as it presumably does not play a role in PG modulation, as seen in *E. coli*. This would allow a clearer "background" for the determination and exploration of these roles and could then be tested in organisms such as *E. coli* to see if these alternate roles are conserved.

Clearly, these are exciting times in the field of peptidoglycan biosynthesis, and particularly the study of the modulation of peptidoglycan synthase activity. It will be fascinating to see how the work provided in this thesis is able to help shape this future research and assist in further advancing our understanding of bacterial biology.

References

Abraham, Mark James, Teemu Murtola, Roland Schulz, Szilárd Páll, Jeremy C. Smith, Berk Hess, and Erik Lindahl. 2015. "GROMACS: High Performance Molecular Simulations through Multi-Level Parallelism from Laptops to Supercomputers." *SoftwareX* 1–2 (September): 19–25. https://doi.org/10.1016/j.softx.2015.06.001.

Adams, Paul D., Pavel V. Afonine, Gábor Bunkóczi, Vincent B. Chen, Ian W. Davis, Nathaniel Echols, Jeffrey J. Headd, et al. 2010. "PHENIX: A Comprehensive Python-Based System for Macromolecular Structure Solution." *Acta Crystallographica. Section D, Biological Crystallography* 66 (Pt 2): 213–21. https://doi.org/10.1107/S0907444909052925.

Al-Dabbagh, Bayan, Xavier Henry, Meriem El Ghachi, Geneviève Auger, Didier Blanot, Claudine Parquet, Dominique Mengin-Lecreulx, and Ahmed Bouhss. 2008. "Active Site Mapping of MraY, a Member of the Polyprenyl-Phosphate N-Acetylhexosamine 1-Phosphate Transferase Superfamily, Catalyzing the First Membrane Step of Peptidoglycan Biosynthesis." *Biochemistry* 47 (34): 8919–28. https://doi.org/10.1021/bi8006274.

Al-Dabbagh, Bayan, Samir Olatunji, Muriel Crouvoisier, Meriem El Ghachi, Didier Blanot, Dominique Mengin-Lecreulx, and Ahmed Bouhss. 2016. "Catalytic Mechanism of MraY and WecA, Two Paralogues of the Polyprenyl-Phosphate N-Acetylhexosamine 1-Phosphate Transferase Superfamily." *Biochimie* 127 (August): 249–57. https://doi.org/10.1016/j.biochi.2016.06.005.

Alexander, J. Andrew N., Som S. Chatterjee, Stephanie M. Hamilton, Lindsay D. Eltis, Henry F. Chambers, and Natalie C J Strynadka. 2018. "Structural and Kinetic Analysis of Penicillin-Binding Protein 4 (PBP4)-Mediated Antibiotic Resistance in Staphylococcus Aureus." *The Journal of Biological Chemistry* 4 (1): jbc.RA118.004952.

https://doi.org/10.1074/jbc.RA118.004952.

Aoki, Hatsuo, Hei Ichi Sakai, Masanobu Kohsaka, Toshio Konomi, Junji Hosoda, Eiko Iguchi, Hiroshi Imanaka, and Yoshiaki Kubochi. 1976. "Nocardicin a, a New Monocyclic β-Lactam Antibiotic I. Discovery, Isolation and Characterization." *The Journal of Antibiotics* 29 (5): 492–500. https://doi.org/10.7164/antibiotics.29.492.

Bel Belluz, Lisa Del, Riccardo Guidi, Ioannis S. Pateras, Laura Levi, Boris Mihaljevic, Syed Fazle Rouf, Marie Wrande, et al. 2016. "The Typhoid Toxin Promotes Host Survival and the Establishment of a Persistent Asymptomatic Infection." *PLoS Pathogens* 12 (4): 1–25. https://doi.org/10.1371/journal.ppat.1005528.

Benson, Timothy E., Christopher T. Walsh, and James M. Hogle. 1996. "The Structure of the Substrate-Free Form of MurB, an Essential Enzyme for the Synthesis of Bacterial Cell Walls." *Structure (London, England : 1993)* 4 (1): 47–54. https://doi.org/10.1016/S0969-2126(96)00008-1.

Benson, Timothy E, Christopher T Walsh, and James M Hogle. 1997. "X-Ray Crystal Structures of the S229A Mutant and Wild-Type MurB in the Presence of the Substrate Enolpyruvyl-UDP-N-Acetylglucosamine at 1.8-A Resolution." *Biochemistry* 36 (4): 806–11. https://doi.org/10.1021/bi962221g.

Berjanskii, Mark V., and David S. Wishart. 2005. "A Simple Method To Predict Protein Flexibility Using Secondary Chemical Shifts." *Journal of the American Chemical Society* 127 (43): 14970–71. https://doi.org/10.1021/ja054842f.

Bernal-Cabas, Margarita, Juan Alfonso Ayala, and Tracy L. Raivio. 2015. "The Cpx Envelope Stress Response Modifies Peptidoglycan Cross-Linking via the l,d-Transpeptidase LdtD and the Novel Protein YgaU." *Journal of Bacteriology* 197 (3): 603–14.

https://doi.org/10.1128/jb.02449-14.

Bertrand, Jay A, Eric Fanchon, Lydie Martin, Didier Blanot, Jean Van Heijenoort, and Otto Dideberg. 1997. "Crystal Structure of UDP-N-Acetylmuramoyl- L - Alanine : D -Glutamate Ligase from Escherichia Coli" 16 (12): 3416–25.

Bertsche, Ute, Thomas Kast, Benoit Wolf, Claudine Fraipont, Mirjam E. G. Aarsman, Kai Kannenberg, Moritz von Rechenberg, et al. 2006. "Interaction between Two Murein (Peptidoglycan) Synthases, PBP3 and PBP1B, in Escherichia Coli." *Molecular Microbiology* 61 (3): 675–90. https://doi.org/10.1111/j.1365-2958.2006.05280.x.

Best, Robert B., Xiao Zhu, Jihyun Shim, Pedro E M Lopes, Jeetain Mittal, Michael Feig, and Alexander D Mackerell. 2012. "Optimization of the Additive CHARMM All-Atom Protein Force Field Targeting Improved Sampling of the Backbone φ, ψ and Side-Chain χ(1) and χ(2) Dihedral Angles." *Journal of Chemical Theory and Computation* 8 (9): 3257–73. https://doi.org/10.1021/ct300400x.

Bianchet, Mario A., Ying H. Pan, Leighanne A.Brammer Basta, Harry Saavedra, Evan P. Lloyd, Pankaj Kumar, Rohini Mattoo, Craig A. Townsend, and Gyanu Lamichhane. 2017. "Structural Insight into the Inactivation of Mycobacterium Tuberculosis Non-Classical Transpeptidase LdtMt2by Biapenem and Tebipenem." *BMC Biochemistry* 18 (1): 1–14. https://doi.org/10.1186/s12858-017-0082-4.

Biarrotte-Sorin, Sabrina, Jean Emmanuel Hugonnet, Vanessa Delfosse, Jean Luc Mainardi, Laurent Gutmann, Michel Arthur, and Claudine Mayer. 2006. "Crystal Structure of a Novel β-Lactam-Insensitive Peptidoglycan Transpeptidase." *Journal of Molecular Biology* 359 (3): 533–38. https://doi.org/10.1016/j.jmb.2006.03.014.

Bibby, Jaclyn, Ronan M. Keegan, Olga Mayans, Martyn D. Winn, and Daniel J. Rigden. 2012.

"AMPLE : A Cluster-and-Truncate Approach to Solve the Crystal Structures of Small Proteins Using Rapidly Computed Ab Initio Models." *Acta Crystallographica Section D Biological Crystallography* 68 (12): 1622–31. https://doi.org/10.1107/S0907444912039194.

Biboy, Jacob, Nhat Khai Bui, and Waldemar Vollmer. 2013. "In Vitro Peptidoglycan Synthesis Assay with Lipid II Substrate." In , 273–88. https://doi.org/10.1007/978-1-62703-245-2_17.

Bielnicki, Jakub, Yancho Devedjiev, Urszula Derewenda, Zbigniew Dauter, Andrzej Joachimiak, and Zygmunt S. Derewenda. 2006. "B. Subtilis YkuD Protein at 2.0 Å Resolution: Insights into the Structure and Function of a Novel, Ubiquitous Family of Bacterial Enzymes." *Proteins: Structure, Function and Genetics* 62 (1): 144–51. https://doi.org/10.1002/prot.20702.

Birnbaum, Jerome, Frederick M. Kahan, Helmut Kropp, and J S MacDonald. 1985. "Carbapenems, a New Class of Beta-Lactam Antibiotics. Discovery and Development of Imipenem/Cilastatin." *The American Journal of Medicine* 78 (6A): 3–21. https://doi.org/10.1016/0002-9343(85)90097-X.

Bouhss, Ahmed, Muriel Crouvoisier, Didier Blanot, and Dominique Mengin-Lecreulx. 2004. "Purification and Characterization of the Bacterial MraY Translocase Catalyzing the First Membrane Step of Peptidoglycan Biosynthesis." *The Journal of Biological Chemistry* 279 (29): 29974–80. https://doi.org/10.1074/jbc.M314165200.

Bricogne, G., C. Vonrhein, C. Flensburg, M. Schiltz, and W. Paciorek. 2003. "Generation, Representation and Flow of Phase Information in Structure Determination: Recent Developments in and around SHARP 2.0." *Acta Crystallographica. Section D, Biological Crystallography* 59 (Pt 11): 2023–30. https://doi.org/10.1107/S0907444903017694.

Browne, Annie J., Bahar H. Kashef Hamadani, Emmanuelle A.P. Kumaran, Puja Rao, Joshua

Longbottom, Eli Harriss, Catrin E. Moore, et al. 2020. “Drug-Resistant Enteric Fever Worldwide, 1990 to 2018: A Systematic Review and Meta-Analysis.” *BMC Medicine* 18 (1): 1–22. https://doi.org/10.1186/s12916-019-1443-1.

Brutscher, Bernhard, Isabella C. Felli, Sergio Gil-Caballero, Tomáš Hošek, Rainer Kümmerle, Alessandro Piai, Roberta Pierattelli, and Zsófia Sólyom. 2015. “NMR Methods for the Study of Instrinsically Disordered Proteins Structure, Dynamics, and Interactions: General Overview and Practical Guidelines.” *Advances in Experimental Medicine and Biology* 870: 49–122. https://doi.org/10.1007/978-3-319-20164-1_3.

Bush, Larry, and Maria Perez. 2018a. “Escherichia Coli Infections.” In *Merck Manual*. Merck.

———. 2018b. “Pseudomonas and Related Infections.” In *Merck Manual*. Merck.

Caveney, Nathanael A., Guillermo Caballero, Henri Voedts, Ana Niciforovic, Liam J. Worrall, Marija Vuckovic, Matthieu Fonvielle, Jean-Emmanuel Hugonnet, Michel Arthur, and Natalie C. J. Strynadka. 2019. “Structural Insight into YcbB-Mediated Beta-Lactam Resistance in Escherichia Coli.” *Nature Communications* 10 (1): 1849. https://doi.org/10.1038/s41467-019-09507-0.

Caveney, Nathanael A, Franco KK Li, and Natalie CJ Strynadka. 2018. “Enzyme Structures of the Bacterial Peptidoglycan and Wall Teichoic Acid Biogenesis Pathways.” *Current Opinion in Structural Biology*. Elsevier Ltd. https://doi.org/10.1016/j.sbi.2018.05.002.

Chen, Ming Wei, Bernhard Lohkamp, Robert Schnell, Julien Lescar, and Gunter Schneider. 2013. “Substrate Channel Flexibility in Pseudomonas Aeruginosa MurB Accommodates Two Distinct Substrates.” *PloS One* 8 (6): e66936. https://doi.org/10.1371/journal.pone.0066936.

Chung, Ben C., Ellene H. Mashalidis, Tetsuya Tanino, Mijung Kim, Akira Matsuda, Jiyong

Hong, Satoshi Ichikawa, and Seok-Yong Lee. 2016. “Structural Insights into Inhibition of Lipid I Production in Bacterial Cell Wall Synthesis.” *Nature* 533 (7604): 557–60. https://doi.org/10.1038/nature17636.

Chung, Ben C, Jinshi Zhao, Robert A Gillespie, Do-Yeon Kwon, Ziqiang Guan, Jiyong Hong, Pei Zhou, and Seok-Yong Lee. 2013. “Crystal Structure of MraY, an Essential Membrane Enzyme for Bacterial Cell Wall Synthesis.” *Science (New York, N.Y.)* 341 (6149): 1012–16. https://doi.org/10.1126/science.1236501.

Cortajarena, Aitziber L., Tommi Kajander, Weilan Pan, Melanie J. Cocco, and Lynne Regan. 2004. “Protein Design to Understand Peptide Ligand Recognition by Tetratricopeptide Repeat Proteins.” *Protein Engineering, Design and Selection* 17 (4): 399–409. https://doi.org/10.1093/protein/gzh047.

Cowtan, Kevin. 2006. “The Buccaneer Software for Automated Model Building. 1. Tracing Protein Chains.” *Acta Crystallographica Section D: Biological Crystallography* 62 (9): 1002–11. https://doi.org/10.1107/S0907444906022116.

Curtis, N A, David Orr, Gordon W Ross, and Michael G Boulton. 1979. “Affinities of Penicillins and Cephalosporins for the Penicillin-Binding Proteins of Escherichia Coli K-12 and Their Antibacterial Activity.” *Antimicrobial Agents and Chemotherapy* 16 (5): 533–39. https://doi.org/10.1128/AAC.16.5.533.

Dam, Vincent van, Robert Sijbrandi, Matthijs Kol, Ewa Swiezewska, Ben de Kruijff, and Eefjan Breukink. 2007. “Transmembrane Transport of Peptidoglycan Precursors across Model and Bacterial Membranes.” *Molecular Microbiology* 64 (4): 1105–14. https://doi.org/10.1111/j.1365-2958.2007.05722.x.

Decuyper, Lena, Sari Deketelaere, Lore Vanparys, Marko Jukič, Izidor Sosič, Eric Sauvage, Ana

Maria Amoroso, et al. 2018. “In Silico Design and Enantioselective Synthesis of Functionalized Monocyclic 3-Amino-1-Carboxymethyl-β-Lactams as Inhibitors of Penicillin-Binding Proteins of Resistant Bacteria.” *Chemistry - A European Journal* 24 (57): 15254–66. https://doi.org/10.1002/chem.201801868.

Delhaye, Antoine, Jean François Collet, and Géraldine Laloux. 2016. “Fine-Tuning of the Cpx Envelope Stress Response Is Required for Cell Wall Homeostasis in Escherichia Coli.” *MBio* 7 (1): 1–10. https://doi.org/10.1128/mBio.00047-16.

Deng, Wanyin, Natalie C. Marshall, Jennifer L. Rowland, James M. McCoy, Liam J. Worrall, Andrew S. Santos, Natalie C. J. Strynadka, and B. Brett Finlay. 2017. “Assembly, Structure, Function and Regulation of Type III Secretion Systems.” *Nature Reviews. Microbiology* 15 (6): 323–37. https://doi.org/10.1038/nrmicro.2017.20.

DiMaio, Frank, Yifan Song, Xueming Li, Matthias J. Brunner, Chunfu Xu, Vincent Conticello, Edward Egelman, Thomas Marlovits, Yifan Cheng, and David Baker. 2015. “Atomic-Accuracy Models from 4.5-Å Cryo-Electron Microscopy Data with Density-Guided Iterative Local Refinement.” *Nature Methods* 12 (4): 361–65. https://doi.org/10.1038/nmeth.3286.

Egan, Alexander J. F., and Waldemar Vollmer. 2016. “Continuous Fluorescence Assay for Peptidoglycan Glycosyltransferases.” *Methods in Molecular Biology (Clifton, N.J.)* 1440: 171–84. https://doi.org/10.1007/978-1-4939-3676-2_13.

Egan, Alexander J.F., Roberto Maya-Martinez, Isabel Ayala, Catherine M. Bougault, Manuel Banzhaf, Eefjan Breukink, Waldemar Vollmer, and Jean Pierre Simorre. 2018. “Induced Conformational Changes Activate the Peptidoglycan Synthase PBP1B.” *Molecular Microbiology* 110 (3): 335–56. https://doi.org/10.1111/mmi.14082.

Egan, Alexander J F, Jacob Biboy, Inge van't Veer, Eefjan Breukink, and Waldemar Vollmer. 2015. "Activities and Regulation of Peptidoglycan Synthases." *Philosophical Transactions of the Royal Society B: Biological Sciences* 370 (1679): 20150031. https://doi.org/10.1098/rstb.2015.0031.

Egan, Alexander J F, Nicolas L Jean, Alexandra Koumoutsi, Catherine M Bougault, Jacob Biboy, Jad Sassine, Alexandra S Solovyova, et al. 2014. "Outer-Membrane Lipoprotein LpoB Spans the Periplasm to Stimulate the Peptidoglycan Synthase PBP1B." *Proceedings of the National Academy of Sciences of the United States of America* 111 (22): 8197–8202. https://doi.org/10.1073/pnas.1400376111.

Emami, Kaveh, Aurelie Guyet, Yoshikazu Kawai, Jenny Devi, Ling J. Wu, Nick Allenby, Richard A. Daniel, and Jeff Errington. 2017. "RodA as the Missing Glycosyltransferase in Bacillus Subtilis and Antibiotic Discovery for the Peptidoglycan Polymerase Pathway." *Nature Microbiology* 2 (January): 16253. https://doi.org/10.1038/nmicrobiol.2016.253.

Emsley, Paul, and Kevin Cowtan. 2004. "Coot: Model-Building Tools for Molecular Graphics." *Acta Crystallographica Section D: Biological Crystallography* 60 (12 I): 2126–32. https://doi.org/10.1107/S0907444904019158.

Erdemli, Sabri B., Radhika Gupta, William R. Bishai, Gyanu Lamichhane, L. Mario Amzel, and Mario A. Bianchet. 2012. "Targeting the Cell Wall of Mycobacterium Tuberculosis: Structure and Mechanism of L,D-Transpeptidase 2." *Structure (London, England : 1993)* 20 (12): 2103–15. https://doi.org/10.1016/j.str.2012.09.016.

Eschenburg, Susanne, Wolfgang Kabsch, Martha L Healy, and Ernst Schonbrunn. 2003. "A New View of the Mechanisms of UDP-N-Acetylglucosamine Enolpyruvyl Transferase (MurA) and 5-Enolpyruvylshikimate-3-Phosphate Synthase (AroA) Derived from X-Ray Structures

of Their Tetrahedral Reaction Intermediate States." *The Journal of Biological Chemistry* 278 (49): 49215–22. https://doi.org/10.1074/jbc.M309741200.

Fakhar, Zeynab, Thavendran Govender, Glenn E. M. Maguire, Gyanu Lamichhane, Ross C. Walker, Hendrik G. Kruger, and Bahareh Honarparvar. 2017. "Differential Flap Dynamics in l,d-Transpeptidase2 from Mycobacterium Tuberculosis Revealed by Molecular Dynamics." *Molecular BioSystems* 13 (6): 1223–34. https://doi.org/10.1039/C7MB00110J.

Fiser, A., and A. Sali. 2003. "ModLoop: Automated Modeling of Loops in Protein Structures." *Bioinformatics* 19 (18): 2500–2501. https://doi.org/10.1093/bioinformatics/btg362.

Fleming, Alexander. 1929. "On the Antibacterial Action of Cultures of a Penicillium, with Special Reference to Their Use in the Isolation of B. Influenzæ." *Br. J. Exp. Pathol.* 10 (3): 226–36.

Fodje, Michel, Pawel Grochulski, Kathryn Janzen, Shaunivan Labiuk, James Gorin, and Russ Berg. 2014. "08B1-1: An Automated Beamline for Macromolecular Crystallography Experiments at the Canadian Light Source." *Journal of Synchrotron Radiation* 21 (3): 633–37. https://doi.org/10.1107/S1600577514005578.

Fokine, Andrei, Konstantin A. Miroshnikov, Mikhail M. Shneider, Vadim V. Mesyanzhinov, and Michael G. Rossmann. 2008. "Structure of the Bacteriophage ΦKZ Lytic Transglycosylase Gp144." *Journal of Biological Chemistry* 283 (11): 7242–50. https://doi.org/10.1074/jbc.M709398200.

Fraipont, Claudine, Svetlana Alexeeva, Benoît Wolf, René van der Ploeg, Marie Schloesser, Tanneke den Blaauwen, and Martine Nguyen-Distèche. 2011. "The Integral Membrane FtsW Protein and Peptidoglycan Synthase PBP3 Form a Subcomplex in Escherichia Coli." *Microbiology (Reading, England)* 157 (Pt 1): 251–59.

https://doi.org/10.1099/mic.0.040071-0.

Fujihashi, M, Y W Zhang, Y Higuchi, X Y Li, T Koyama, and K Miki. 2001. "Crystal Structure of Cis-Prenyl Chain Elongating Enzyme, Undecaprenyl Diphosphate Synthase." *Proceedings of the National Academy of Sciences of the United States of America* 98 (8): 4337–42. https://doi.org/10.1073/pnas.071514398.

Galán, Jorge E. 2016. "Typhoid Toxin Provides a Window into Typhoid Fever and the Biology of Salmonella Typhi." *Proceedings of the National Academy of Sciences of the United States of America* 113 (23): 6338–44. https://doi.org/10.1073/pnas.1606335113.

García-del Portillo, Francisco. 2020. "Building Peptidoglycan inside Eukaryotic Cells: A View from Symbiotic and Pathogenic Bacteria." *Molecular Microbiology* 113 (3): 613–26. https://doi.org/10.1111/mmi.14452.

Geiger, Tobias, Manuel Pazos, Maria Lara-Tejero, Waldemar Vollmer, and Jorge E. Galán. 2018. "Peptidoglycan Editing by a Specific Ld-Transpeptidase Controls the Muramidase-Dependent Secretion of Typhoid Toxin." *Nature Microbiology* 3 (11): 1243–54. https://doi.org/10.1038/s41564-018-0248-x.

Ghachi, Meriem El, Nicole Howe, Chia-Ying Huang, Vincent Olieric, Rangana Warshamanage, Thierry Touzé, Dietmar Weichert, et al. 2018. "Crystal Structure of Undecaprenyl-Pyrophosphate Phosphatase and Its Role in Peptidoglycan Biosynthesis." *Nature Communications* 9 (1): 1078. https://doi.org/10.1038/s41467-018-03477-5.

Gibani, Malick M., Carl Britto, and Andrew J. Pollard. 2018. "Typhoid and Paratyphoid Fever: A Call to Action." *Current Opinion in Infectious Diseases* 31 (5): 440–48. https://doi.org/10.1097/QCO.0000000000000479.

Gibani, Malick M., Elizabeth Jones, Amber Barton, Celina Jin, Juliette Meek, Susana Camara,

Ushma Galal, et al. 2019. “Investigation of the Role of Typhoid Toxin in Acute Typhoid Fever in a Human Challenge Model.” *Nature Medicine* 25 (7): 1082–88. https://doi.org/10.1038/s41591-019-0505-4.

Gokulan, Kuppan, Sangeeta Khare, Carl E. Cerniglia, Steven L. Foley, and Kottayil I. Varughese. 2018. “Structure and Inhibitor Specificity of L,D-Transpeptidase (LdtMt2) from Mycobacterium Tuberculosis and Antibiotic Resistance: Calcium Binding Promotes Dimer Formation.” *The AAPS Journal* 20 (2): 44. https://doi.org/10.1208/s12248-018-0193-x.

Gordon, Elspeth, Bernard Flouret, Laurent Chantalat, J van Heijenoort, Dominique Mengin-Lecreulx, and Otto Dideberg. 2001. “Crystal Structure of UDP-N-Acetylmuramoyl-L-Alanyl-D-Glutamate: Meso-Diaminopimelate Ligase from Escherichia Coli.” *The Journal of Biological Chemistry* 276 (14): 10999–6. https://doi.org/10.1074/jbc.M009835200.

Gray, Andrew N, Alexander JF Egan, Inge L van’t Veer, Jolanda Verheul, Alexandre Colavin, Alexandra Koumoutsi, Jacob Biboy, et al. 2015. “Coordination of Peptidoglycan Synthesis and Outer Membrane Constriction during *Escherichia Coli* Cell Division.” *ELife* 4: 1–29. https://doi.org/10.7554/eLife.07118.

Greene, Neil G., Coralie Fumeaux, and Thomas G. Bernhardt. 2018. “Conserved Mechanism of Cell-Wall Synthase Regulation Revealed by the Identification of a New PBP Activator in Pseudomonas Aeruginosa.” *Proceedings of the National Academy of Sciences of the United States of America* 115 (12): 3150–55. https://doi.org/10.1073/pnas.1717925115.

Haghjoo, Erik, and Jorge E. Galán. 2004. “Salmonella Typhi Encodes a Functional Cytolethal Distending Toxin That Is Delivered into Host Cells by a Bacterial-Internalization Pathway.” *Proceedings of the National Academy of Sciences of the United States of America* 101 (13): 4614–19. https://doi.org/10.1073/pnas.0400932101.

Hakulinen, Jonna K, Jenny Hering, Gisela Brändén, Hongming Chen, Arjan Snijder, Margareta Ek, and Patrik Johansson. 2017. "MraY-Antibiotic Complex Reveals Details of Tunicamycin Mode of Action." *Nature Chemical Biology* 13 (3): 265–67. https://doi.org/10.1038/nchembio.2270.

Heijenoort, Y van, M Gómez, M Derrien, J Ayala, and J van Heijenoort. 1992. "Membrane Intermediates in the Peptidoglycan Metabolism of Escherichia Coli: Possible Roles of PBP 1b and PBP 3." *Journal of Bacteriology* 174 (11): 3549–57. http://www.ncbi.nlm.nih.gov/pubmed/1592809.

Holm, Liisa, and Päivi Rosenström. 2010. "Dali Server: Conservation Mapping in 3D." *Nucleic Acids Research* 38 (SUPPL. 2): 545–49. https://doi.org/10.1093/nar/gkq366.

Hu, Yanan, Lan Chen, Sha Ha, Ben Gross, Brian Falcone, Deborah Walker, Maryam Mokhtarzadeh, and Suzanne Walker. 2003. "Crystal Structure of the MurG:UDP-GlcNAc Complex Reveals Common Structural Principles of a Superfamily of Glycosyltransferases." *Proceedings of the National Academy of Sciences of the United States of America* 100 (3): 845–49. https://doi.org/10.1073/pnas.0235749100.

Huang, C.-Y., H.-W. Shih, L.-Y. Lin, Y.-W. Tien, T.-J. R. Cheng, W.-C. Cheng, C.-H. Wong, and C. Ma. 2012. "Crystal Structure of Staphylococcus Aureus Transglycosylase in Complex with a Lipid II Analog and Elucidation of Peptidoglycan Synthesis Mechanism." *Proceedings of the National Academy of Sciences* 109 (17): 6496–6501. https://doi.org/10.1073/pnas.1203900109.

Hugonnet, Jean-Emmanuel, Dominique Mengin-Lecreulx, Alejandro Monton, Tanneke den Blaauwen, Etienne Carbonnelle, Carole Veckerlé, Yves V Brun, et al. 2016. "Factors Essential for L,D-Transpeptidase-Mediated Peptidoglycan Cross-Linking and β-Lactam

Resistance InEscherichia Coli." *ELife* 5 (OCTOBER2016): 1–22. https://doi.org/10.7554/eLife.19469.

Humphrey, William, Andrew Dalke, and Klaus Schulten. 1996. "VMD: Visual Molecular Dynamics." *Journal of Molecular Graphics* 14 (1): 33–38, 27–28. https://doi.org/10.1016/0263-7855(96)00018-5.

Jean, Nicolas L., Catherine M. Bougault, Adam Lodge, Adeline Derouaux, Gilles Callens, Alexander J.F. Egan, Isabel Ayala, Richard J. Lewis, Waldemar Vollmer, and Jean Pierre Simorre. 2014. "Elongated Structure of the Outer-Membrane Activator of Peptidoglycan Synthesis LpoA: Implications for PBP1A Stimulation." *Structure* 22 (7): 1047–54. https://doi.org/10.1016/j.str.2014.04.017.

Jeong, Jae Yeon, Hyung Soon Yim, Ji Young Ryu, Hyun Sook Lee, Jung Hyun Lee, Dong Seung Seen, and Sung Gyun Kang. 2012. "One-Step Sequence-and Ligation-Independent Cloning as a Rapid and Versatile Cloning Method for Functional Genomics Studies." *Applied and Environmental Microbiology* 78 (15): 5440–43. https://doi.org/10.1128/AEM.00844-12.

Jo, Sunhwan, Taehoon Kim, Vidyashankara G. Iyer, and Wonpil Im. 2008. "CHARMM-GUI: A Web-Based Graphical User Interface for CHARMM." *Journal of Computational Chemistry* 29 (11): 1859–65. https://doi.org/10.1002/jcc.20945.

Kabsch, Wolfgang. 2010. "XDS." *Acta Crystallographica. Section D, Biological Crystallography* 66 (Pt 2): 125–32. https://doi.org/10.1107/S0907444909047337.

Kelley, Aaron, J. Vijayalakshmi, and Mark A. Saper. 2019. "Crystal Structures of the Amino-Terminal Domain of LpoA from Escherichia Coli and Haemophilus Influenzae." *Acta Crystallographica Section F: Structural Biology Communications* 75: 368–76. https://doi.org/10.1107/S2053230X19004011.

King, Dustin T., Emilie Lameignere, and Natalie C J Strynadka. 2014. "Structural Insights into the Lipoprotein Outer Membrane Regulator of Penicillin-Binding Protein 1B." *Journal of Biological Chemistry* 289 (27): 19245–53. https://doi.org/10.1074/jbc.M114.565879.

King, Dustin T., Solmaz Sobhanifar, and Natalie C. J. Strynadka. 2016. "One Ring to Rule Them All: Current Trends in Combating Bacterial Resistance to the β-Lactams." *Protein Science : A Publication of the Protein Society* 25 (4): 787–803. https://doi.org/10.1002/pro.2889.

King, Dustin T., Gregory A. Wasney, Michael Nosella, Anita Fong, and Natalie C. J. Strynadka. 2017. "Structural Insights into Inhibition of Escherichia Coli Penicillin-Binding Protein 1B." *The Journal of Biological Chemistry* 292 (3): 979–93. https://doi.org/10.1074/jbc.M116.718403.

Kouidmi, Imène, Roger C. Levesque, and Catherine Paradis-Bleau. 2014. "The Biology of Mur Ligases as an Antibacterial Target." *Molecular Microbiology* 94 (2): 242–53. https://doi.org/10.1111/mmi.12758.

Krachler, Anne Marie, Amit Sharma, Anna Cauldwell, Grigorios Papadakos, and Colin Kleanthous. 2010. "TolA Modulates the Oligomeric Status of YbgF in the Bacterial Periplasm." *Journal of Molecular Biology* 403 (2): 270–85. https://doi.org/10.1016/j.jmb.2010.08.050.

Kuk, Alvin C Y, Ellene H Mashalidis, and Seok-yong Lee. 2017. "Crystal Structure of the MOP Flippase MurJ in an Inward-Facing Conformation." *Nature Structural & Molecular Biology* 24 (2): 171–76. https://doi.org/10.1038/nsmb.3346.

Kumar, Pankaj, Amit Kaushik, Evan P Lloyd, Shao-Gang Li, Rohini Mattoo, Nicole C Ammerman, Drew T Bell, et al. 2017. "Non-Classical Transpeptidases Yield Insight into New Antibacterials." *Nature Chemical Biology* 13 (1): 54–61.

https://doi.org/10.1038/nchembio.2237.

Landau, Meytal, Itay Mayrose, Yossi Rosenberg, Fabian Glaser, Eric Martz, Tal Pupko, and Nir Ben-Tal. 2005. "ConSurf 2005: The Projection of Evolutionary Conservation Scores of Residues on Protein Structures." *Nucleic Acids Research* 33 (SUPPL. 2): 299–302. https://doi.org/10.1093/nar/gki370.

Leaver-Fay, Andrew, Michael Tyka, Steven M. Lewis, Oliver F. Lange, James Thompson, Ron Jacak, Kristian Kaufman, et al. 2011. "Rosetta3: An Object-Oriented Software Suite for the Simulation and Design of Macromolecules." *Methods in Enzymology* 487 (C): 545–74. https://doi.org/10.1016/B978-0-12-381270-4.00019-6.

Leclercq, Sophie, Adeline Derouaux, Samir Olatunji, Claudine Fraipont, Alexander J. F. Egan, Waldemar Vollmer, Eefjan Breukink, and Mohammed Terrak. 2017. "Interplay between Penicillin-Binding Proteins and SEDS Proteins Promotes Bacterial Cell Wall Synthesis." *Scientific Reports* 7 (January): 43306. https://doi.org/10.1038/srep43306.

Lecoq, Lauriane, Catherine Bougault, Jean Emmanuel Hugonnet, Carole Veckerlé, Ombeline Pessey, Michel Arthur, and Jean Pierre Simorre. 2012. "Dynamics Induced by β-Lactam Antibiotics in the Active Site of Bacillus Subtilis l,d-Transpeptidase." *Structure* 20 (5): 850–61. https://doi.org/10.1016/j.str.2012.03.015.

Lecoq, Lauriane, Vincent Dubée, Sébastien Triboulet, Catherine Bougault, Jean-Emmanuel Hugonnet, Michel Arthur, and Jean-Pierre Simorre. 2013. "Structure of Enterococcus Faecium l , d -Transpeptidase Acylated by Ertapenem Provides Insight into the Inactivation Mechanism." *ACS Chemical Biology* 8 (6): 1140–46. https://doi.org/10.1021/cb4001603.

Lee, Jumin, Xi Cheng, Jason M. Swails, Min Sun Yeom, Peter K. Eastman, Justin A. Lemkul, Shuai Wei, et al. 2016. "CHARMM-GUI Input Generator for NAMD, GROMACS,

AMBER, OpenMM, and CHARMM/OpenMM Simulations Using the CHARMM36 Additive Force Field." *Journal of Chemical Theory and Computation* 12 (1): 405–13. https://doi.org/10.1021/acs.jctc.5b00935.

Lees, Watson J, Timothy E Benson, James M Hogle, and Christopher T Walsh. 1996. "(E)-Enolbutyryl-UDP-N-Acetylglucosamine as a Mechanistic Probe of UDP-N-Acetylenolpyruvylglucosamine Reductase (MurB)." *Biochemistry* 35 (5): 1342–51. https://doi.org/10.1021/bi952287w.

Lim, Daniel, and Natalie C J Strynadka. 2002. "Structural Basis for the Beta Lactam Resistance of PBP2a from Methicillin-Resistant Staphylococcus Aureus." *Nature Structural Biology* 9 (11): 870–76. https://doi.org/10.1038/nsb858.

Liu, Hans H., and Alexander Tomasz. 1985. "Penicillin Tolerance in Multiply Drug-Resistant Natural Isolates of Streptococcus Pneumoniae." *Journal of Infectious Diseases* 152 (2): 365–72. https://doi.org/10.1093/infdis/152.2.365.

Lovering, Andrew L., Liza H. de Castro, Daniel Lim, and Natalie C. J. Strynadka. 2007. "Structural Insight into the Transglycosylation Step of Bacterial Cell-Wall Biosynthesis." *Science (New York, N.Y.)* 315 (5817): 1402–5. https://doi.org/10.1126/science.1136611.

Lovering, Andrew L, Susan S Safadi, and Natalie C J Strynadka. 2012. "Structural Perspective of Peptidoglycan Biosynthesis and Assembly." *Annual Review of Biochemistry* 81 (1): 451–78. https://doi.org/10.1146/annurev-biochem-061809-112742.

Maciejewska, Barbara, Karol Źrubek, Akbar Espaillat, Magdalena Wiśniewska, Krzysztof P. Rembacz, Felipe Cava, Grzegorz Dubin, and Zuzanna Drulis-Kawa. 2017. "Modular Endolysin of Burkholderia AP3 Phage Has the Largest Lysozyme-like Catalytic Subunit Discovered to Date and No Catalytic Aspartate Residue." *Scientific Reports* 7 (1): 1–12.

https://doi.org/10.1038/s41598-017-14797-9.

Magnet, Sophie, Lionel Dubost, Arul Marie, Michel Arthur, and Laurent Gutmann. 2008. "Identification of the L,D-Transpeptidases for Peptidoglycan Cross-Linking in Escherichia Coli." *Journal of Bacteriology* 190 (13): 4782–85. https://doi.org/10.1128/JB.00025-08.

Mahasenan, Kiran V., Rafael Molina, Renee Bouley, María T. Batuecas, Jed F. Fisher, Juan A. Hermoso, Mayland Chang, and Shahriar Mobashery. 2017. "Conformational Dynamics in Penicillin-Binding Protein 2a of Methicillin-Resistant Staphylococcus Aureus, Allosteric Communication Network and Enablement of Catalysis." *Journal of the American Chemical Society* 139 (5): 2102–10. https://doi.org/10.1021/jacs.6b12565.

Manat, Guillaume, Sophie Roure, Rodolphe Auger, Ahmed Bouhss, Hélène Barreteau, Dominique Mengin-Lecreulx, and Thierry Touzé. 2014. "Deciphering the Metabolism of Undecaprenyl-Phosphate: The Bacterial Cell-Wall Unit Carrier at the Membrane Frontier." *Microbial Drug Resistance (Larchmont, N.Y.)* 20 (3): 199–214. https://doi.org/10.1089/mdr.2014.0035.

Markley, John L., Ad Bax, Yoji Arata, C. W. Hilbers, Robert Kaptein, Brian D. Sykes, Peter E. Wright, and Kurt Wüthrich. 1998. "Recommendations for the Presentation of NMR Structures of Proteins and Nucleic Acids." *Journal of Molecular Biology* 280 (5): 933–52. https://doi.org/10.1006/jmbi.1998.1852.

McCoy, Airlie J., Ralf W. Grosse-Kunstleve, Paul D. Adams, Martyn D. Winn, Laurent C. Storoni, and Randy J. Read. 2007. "Phaser Crystallographic Software." *Journal of Applied Crystallography* 40 (4): 658–74. https://doi.org/10.1107/S0021889807021206.

Meeske, Alexander J., Eammon P. Riley, William P. Robins, Tsuyoshi Uehara, John J. Mekalanos, Daniel Kahne, Suzanne Walker, Andrew C. Kruse, Thomas G. Bernhardt, and

David Z. Rudner. 2016. “SEDS Proteins Are a Widespread Family of Bacterial Cell Wall Polymerases.” *Nature* 537 (7622): 634–38. https://doi.org/10.1038/nature19331.

Mohammadi, Tamimount, Vincent van Dam, Robert Sijbrandi, Thierry Vernet, André Zapun, Ahmed Bouhss, Marlies Diepeveen-de Bruin, Martine Nguyen-Distèche, Ben de Kruijff, and Eefjan Breukink. 2011. “Identification of FtsW as a Transporter of Lipid-Linked Cell Wall Precursors across the Membrane.” *The EMBO Journal* 30 (8): 1425–32. https://doi.org/10.1038/emboj.2011.61.

Morè, Niccolò, Alessandra M Martorana, Jacob Biboy, Christian Otten, Matthias Winkle, Carlos K Gurnani Serrano, Alejandro Montón Silva, et al. 2019. “Peptidoglycan Remodeling Enables Escherichia Coli To Survive Severe Outer Membrane Assembly Defect.” *MBio* 10 (1): 16–18. https://doi.org/10.1128/mBio.02729-18.

Nicola, George, Joshua Tomberg, R. F. Pratt, Robert A. Nicholas, and Christopher Davies. 2010. “Crystal Structures of Covalent Complexes of β-Lactam Antibiotics with Escherichia Coli Penicillin-Binding Protein 5: Toward an Understanding of Antibiotic Specificity.” *Biochemistry* 49 (37): 8094–8104. https://doi.org/10.1021/bi100879m.

Nojima, Shingo, Ayumi Fujishima, Koji Kato, Kayoko Ohuchi, Nobutaka Shimizu, Kento Yonezawa, Kenji Tajima, and Min Yao. 2017. “Crystal Structure of the Flexible Tandem Repeat Domain of Bacterial Cellulose Synthesis Subunit.” *Scientific Reports* 7 (1): 1–10. https://doi.org/10.1038/s41598-017-12530-0.

Otero, L. H., A. Rojas-Altuve, L. I. Llarrull, C. Carrasco-Lopez, M. Kumarasiri, E. Lastochkin, J. Fishovitz, et al. 2013. “How Allosteric Control of Staphylococcus Aureus Penicillin Binding Protein 2a Enables Methicillin Resistance and Physiological Function.” *Proceedings of the National Academy of Sciences* 110 (42): 16808–13.

https://doi.org/10.1073/pnas.1300118110.

Ovchinnikov, Sergey, Hetunandan Kamisetty, and David Baker. 2014. "Robust and Accurate Prediction of Residue-Residue Interactions across Protein Interfaces Using Evolutionary Information." *ELife* 2014 (3): 1–21. https://doi.org/10.7554/eLife.02030.

Ovchinnikov, Sergey, Lisa Kinch, Hahnbeom Park, Yuxing Liao, Jimin Pei, David E. Kim, Hetunandan Kamisetty, Nick V. Grishin, and David Baker. 2015. "Large-Scale Determination of Previously Unsolved Protein Structures Using Evolutionary Information." *ELife* 4 (September): e09248. https://doi.org/10.7554/eLife.09248.

Paradis-Bleau, Catherine, Monica Markovski, Tsuyoshi Uehara, Tania J Lupoli, Suzanne Walker, Daniel E Kahne, and Thomas G Bernhardt. 2010. "Lipoprotein Cofactors Located in the Outer Membrane Activate Bacterial Cell Wall Polymerases." *Cell* 143 (7): 1110–20. https://doi.org/10.1016/j.cell.2010.11.037.

Pazos, Manuel, Katharina Peters, and Waldemar Vollmer. 2017. "Robust Peptidoglycan Growth by Dynamic and Variable Multi-Protein Complexes." *Current Opinion in Microbiology* 36 (April): 55–61. https://doi.org/10.1016/j.mib.2017.01.006.

Peters, Katharina, Manuel Pazos, Zainab Edoo, Jean-Emmanuel Hugonnet, Alessandra M Martorana, Alessandra Polissi, Michael S VanNieuwenhze, Michel Arthur, and Waldemar Vollmer. 2018. "Copper Inhibits Peptidoglycan LD-Transpeptidases Suppressing β-Lactam Resistance Due to Bypass of Penicillin-Binding Proteins." *Proceedings of the National Academy of Sciences of the United States of America* 115 (42): 10786–91. https://doi.org/10.1073/pnas.1809285115.

Petersen, Thomas Nordahl, Søren Brunak, Gunnar von Heijne, and Henrik Nielsen. 2011. "SignalP 4.0: Discriminating Signal Peptides from Transmembrane Regions." *Nature*

Methods 8 (10): 785–86. https://doi.org/10.1038/nmeth.1701.

Pettersen, Eric F., Thomas D. Goddard, Conrad C. Huang, Gregory S. Couch, Daniel M. Greenblatt, Elaine C. Meng, and Thomas E. Ferrin. 2004. "UCSF Chimera - A Visualization System for Exploratory Research and Analysis." *Journal of Computational Chemistry* 25 (13): 1605–12. https://doi.org/10.1002/jcc.20084.

Raivio, Tracy L., Shannon K.D. Leblanc, and Nancy L. Price. 2013. "The Escherichia Coli Cpx Envelope Stress Response Regulates Genes of Diverse Function That Impact Antibiotic Resistance and Membrane Integrity." *Journal of Bacteriology* 195 (12): 2755–67. https://doi.org/10.1128/JB.00105-13.

Rojas, Enrique R., Gabriel Billings, Pascal D. Odermatt, George K. Auer, Lillian Zhu, Amanda Miguel, Fred Chang, Douglas B. Weibel, Julie A. Theriot, and Kerwyn Casey Huang. 2018. "The Outer Membrane Is an Essential Load-Bearing Element in Gram-Negative Bacteria." *Nature* 559 (7715): 617–21. https://doi.org/10.1038/s41586-018-0344-3.

Ruiz, Natividad. 2008. "Bioinformatics Identification of MurJ (MviN) as the Peptidoglycan Lipid II Flippase in Escherichia Coli." *Proceedings of the National Academy of Sciences of the United States of America* 105 (40): 15553–57. https://doi.org/10.1073/pnas.0808352105.

Sabe, Victor T., Gideon F. Tolufashe, Collins U. Ibeji, Sibusiso B. Maseko, Thavendran Govender, Glenn E.M. Maguire, Gyanu Lamichhane, Bahareh Honarparvar, and Hendrik G. Kruger. 2019. "Identification of Potent L,D-Transpeptidase 5 Inhibitors for Mycobacterium Tuberculosis as Potential Anti-TB Leads: Virtual Screening and Molecular Dynamics Simulations." *Journal of Molecular Modeling* 25 (11). https://doi.org/10.1007/s00894-019-4196-z.

Sathiyamoorthy, Karthik, J. Vijayalakshmi, Bhramara Tirupati, Lixin Fan, and Mark A. Saper.

2017. “Structural Analyses of the Haemophilus Influenzaepeptidoglycan Synthase Activator LpoA Suggest Multiple Conformations in Solution.” *The Journal of Biological Chemistry* 292 (43): 17626–42. https://doi.org/10.1074/jbc.M117.804997.

Schanda, Paul, Sébastien Triboulet, Cédric Laguri, Catherine M. Bougault, Isabel Ayala, Morgane Callon, Michel Arthur, and Jean Pierre Simorre. 2014. “Atomic Model of a Cell-Wall Cross-Linking Enzyme in Complex with an Intact Bacterial Peptidoglycan.” *Journal of the American Chemical Society* 136 (51): 17852–60. https://doi.org/10.1021/ja5105987.

Schönbrunn, Ernst, Stefan Sack, Susanne Eschenburg, Anastassis Perrakis, Florian Krekel, Nikolaus Amrhein, and Eckhard Mandelkow. 1996. “Crystal Structure of UDP-N-Acetylglucosamine Enolpyruvyltransferase, the Target of the Antibiotic Fosfomycin.” *Structure (London, England : 1993)* 4 (9): 1065–75. https://doi.org/10.1016/S0969-2126(96)00113-X.

Sjodt, Megan, Kelly Brock, Genevieve Dobihal, Patricia D.A. Rohs, Anna G. Green, Thomas A. Hopf, Alexander J. Meeske, et al. 2018. “Structure of the Peptidoglycan Polymerase RodA Resolved by Evolutionary Coupling Analysis.” *Nature* 556 (7699): 118–21. https://doi.org/10.1038/nature25985.

Skarzynski, Tadeusz, Anil Mistry, Alan Wonacott, Susan E Hutchinson, Valerie A Kelly, and Kenneth Duncan. 1996. “Structure of UDP-N-Acetylglucosamine Enolpyruvyl Transferase, an Enzyme Essential for the Synthesis of Bacterial Peptidoglycan, Complexed with Substrate UDP-N-Acetylglucosamine and the Drug Fosfomycin.” *Structure (London, England : 1993)* 4 (12): 1465–74. https://doi.org/10.1016/S0969-2126(96)00153-0.

Sobhanifar, Solmaz, Dustin T King, and Natalie C J Strynadka. 2013. “Fortifying the Wall: Synthesis, Regulation and Degradation of Bacterial Peptidoglycan.” *Current Opinion in*

Structural Biology 23 (5): 695–703. https://doi.org/10.1016/j.sbi.2013.07.008.

Solyom, Zsofia, Melanie Schwarten, Leonhard Geist, Robert Konrat, Dieter Willbold, and Bernhard Brutscher. 2013. "BEST-TROSY Experiments for Time-Efficient Sequential Resonance Assignment of Large Disordered Proteins." *Journal of Biomolecular NMR* 55 (4): 311–21. https://doi.org/10.1007/s10858-013-9715-0.

Song, Jeongmin, Xiang Gao, and Jorge E. Galán. 2013. "Structure and Function of the Salmonella Typhi Chimaeric A 2 B 5 Typhoid Toxin." *Nature* 499 (7458): 350–54. https://doi.org/10.1038/nature12377.

Spraggon, Glen, Robert Schwarzenbacher, Andreas Kreusch, Christian C Lee, Polat Abdubek, Eileen Ambing, Tanya Biorac, et al. 2004. "Crystal Structure of an Udp-n-Acetylmuramate-Alanine Ligase MurC (TM0231) from Thermotoga Maritima at 2.3 A Resolution." *Proteins* 55 (4): 1078–81. https://doi.org/10.1002/prot.20034.

Stanaway, Jeffrey D., Robert C. Reiner, Brigette F. Blacker, Ellen M. Goldberg, Ibrahim A. Khalil, Christopher E. Troeger, Jason R. Andrews, et al. 2019. "The Global Burden of Typhoid and Paratyphoid Fevers: A Systematic Analysis for the Global Burden of Disease Study 2017." *The Lancet Infectious Diseases* 19 (4): 369–81. https://doi.org/10.1016/S1473-3099(18)30685-6.

Stankeviciute, Gabriele, Amanda V Miguel, Atanas Radkov, and Seemay Chou. 2019. "Differential Modes of Crosslinking Establish Spatially Distinct Regions of Peptidoglycan in Caulobacter Crescentus" 111 (February): 995–1008. https://doi.org/10.1111/mmi.14199.

Stickgold, R A, and Francis C. Neuhaus. 1967. "On the Initial Stage in Peptidoglycan Synthesis. Effect of 5-Fluorouracil Substitution on Phospho-N-Acetylmuramyl-Pentapeptide Translocase (Uridine 5'-Phosphate)." *The Journal of Biological Chemistry* 242 (6): 1331–

37. https://doi.org/10.1021/bi00865a012.

Sung, Ming-ta, Yen-ting Lai, Chia-Ying Huang, Lien-yang Chou, Hao-Wei Shih, Wei-Chieh Cheng, Chi-Huey Wong, and Che Ma. 2009. "Crystal Structure of the Membrane-Bound Bifunctional Transglycosylase PBP1b from Escherichia Coli." *Proceedings of the National Academy of Sciences of the United States of America* 106 (22): 8824–29. https://doi.org/10.1073/pnas.0904030106.

Terwilliger, Thomas C., Ralf W. Grosse-Kunstleve, Pavel V. Afonine, Nigel W. Moriarty, Peter H. Zwart, Li Wei Hung, Randy J. Read, and Paul D. Adams. 2007. "Iterative Model Building, Structure Refinement and Density Modification with the PHENIX AutoBuild Wizard." *Acta Crystallographica Section D: Biological Crystallography* 64 (1): 61–69. https://doi.org/10.1107/S090744490705024X.

Tomasz, Alexander. 1986. "Penicillin-Binding Proteins and the Antibacterial Effectiveness of β-Lactam Antibiotics." *Reviews of Infectious Diseases* 8 (August): 260–78. https://doi.org/10.1093/clinids/8.Supplement_3.S260.

Torres, Alfredo G., Xin Zhou, and James B. Kaper. 2005. "Adherence of Diarrheagenic Escherichia Coli Strains to Epithelial Cells." *Infection and Immunity* 73 (1): 18–29. https://doi.org/10.1128/IAI.73.1.18-29.2005.

Triboulet, Sébastien, Vincent Dubée, Lauriane Lecoq, Catherine Bougault, Jean-Luc Mainardi, Louis B. Rice, Mélanie Ethève-Quelquejeu, et al. 2013. "Kinetic Features of L,D-Transpeptidase Inactivation Critical for β-Lactam Antibacterial Activity." *PloS One* 8 (7): e67831. https://doi.org/10.1371/journal.pone.0067831.

Typas, Athanasios, Manuel Banzhaf, Bart van den Berg van Saparoea, Jolanda Verheul, Jacob Biboy, Robert J Nichols, Matylda Zietek, et al. 2010. "Regulation of Peptidoglycan

Synthesis by Outer-Membrane Proteins." *Cell* 143 (7): 1097–1109. https://doi.org/10.1016/j.cell.2010.11.038.

Typas, Athanasios, Manuel Banzhaf, Carol a. Gross, and Waldemar Vollmer. 2011. "From the Regulation of Peptidoglycan Synthesis to Bacterial Growth and Morphology." *Nature Reviews Microbiology* 10 (2): 123–36. https://doi.org/10.1038/nrmicro2677.

Urzhumtseva, Ludmila, Pavel V. Afonine, Paul D. Adams, and Alexandre Urzhumtsev. 2009. "Crystallographic Model Quality at a Glance." *Acta Crystallographica Section D: Biological Crystallography* 65 (3): 297–300. https://doi.org/10.1107/S0907444908044296.

Vancouver Coastal Health. 2016. "Antimicrobial Stewardship Programme - Treatment Guidelines For Vancouver General Hospital." http://www.vhpharmsci.com/Resources/Pocket/ASP Card (14MAR16)-FINAL.pdf.

Voss, Neil R., and Mark Gerstein. 2010. "3V: Cavity, Channel and Cleft Volume Calculator and Extractor." *Nucleic Acids Research* 38 (SUPPL. 2): 555–62. https://doi.org/10.1093/nar/gkq395.

Vranken, Wim F., Wayne Boucher, Tim J. Stevens, Rasmus H. Fogh, Anne Pajon, Miguel Llinas, Eldon L. Ulrich, John L. Markley, John Ionides, and Ernest D. Laue. 2005. "The CCPN Data Model for NMR Spectroscopy: Development of a Software Pipeline." *Proteins: Structure, Function and Genetics* 59 (4): 687–96. https://doi.org/10.1002/prot.20449.

Waterhouse, Andrew, Martino Bertoni, Stefan Bienert, Gabriel Studer, Gerardo Tauriello, Rafal Gumienny, Florian T. Heer, et al. 2018. "SWISS-MODEL: Homology Modelling of Protein Structures and Complexes." *Nucleic Acids Research* 46 (W1): W296–303. https://doi.org/10.1093/nar/gky427.

WHO. 2017. "Global Priority List of Antibiotic-Resistant Batceria to Guide Research,

Discovery, and Development of New Antibiotics." *Who*, 7. https://www.who.int/news-room/detail/27-02-2017-who-publishes-list-of-bacteria-for-which-new-antibiotics-are-urgently-needed.

Workman, Sean D., Liam J. Worrall, and Natalie C. J. Strynadka. 2018. "Crystal Structure of an Intramembranal Phosphatase Central to Bacterial Cell-Wall Peptidoglycan Biosynthesis and Lipid Recycling." *Nature Communications* 9 (1): 1159. https://doi.org/10.1038/s41467-018-03547-8.

Worrall, L J, C Hong, M Vuckovic, W. Deng, J. R. C. Bergeron, D. D Majewski, R. K. Huang, et al. 2016. "Near-Atomic-Resolution Cryo-EM Analysis of the Salmonella T3S Injectisome Basal Body." *Nature* 540 (7634): 597–601. https://doi.org/10.1038/nature20576.

Yan, Youwei, Sanjeev Munshi, Barbara Leiting, Matt S Anderson, John Chrzas, and Zhongguo Chen. 2000. "Crystal Structure of Escherichia Coli UDPMurNAc-Tripeptide d-Alanyl-d-Alanine-Adding Enzyme (MurF) at 2.3 A Resolution." *Journal of Molecular Biology* 304 (3): 435–45. https://doi.org/10.1006/jmbi.2000.4215.

Yang, Yi An, Sohyoung Lee, Jun Zhao, Andrew J. Thompson, Ryan McBride, Buyankhishig Tsogtbaatar, James C. Paulson, Ruth Nussinov, Lingquan Deng, and Jeongmin Song. 2018. "In Vivo Tropism of Salmonella Typhi Toxin to Cells Expressing a Multiantennal Glycan Receptor." *Nature Microbiology* 3 (2): 155–63. https://doi.org/10.1038/s41564-017-0076-4.

Yoo, Jiho, Ellene H. Mashalidis, Alvin C. Y. Kuk, Kazuki Yamamoto, Benjamin Kaeser, Satoshi Ichikawa, and Seok-Yong Lee. 2018. "GlcNAc-1-P-Transferase-Tunicamycin Complex Structure Reveals Basis for Inhibition of N-Glycosylation." *Nature Structural & Molecular Biology* 25 (3): 217–24. https://doi.org/10.1038/s41594-018-0031-y.

Zeytuni, Natalie, and Raz Zarivach. 2012. "Structural and Functional Discussion of the Tetra-

Trico-Peptide Repeat, a Protein Interaction Module." *Structure* 20 (3): 397–405. https://doi.org/10.1016/j.str.2012.01.006.

Zhu, Jin-yi, Yan Yang, Huijong Han, Stephane Betzi, Sanne H Olesen, Frank Marsilio, and Ernst Schönbrunn. 2012. "Functional Consequence of Covalent Reaction of Phosphoenolpyruvate with UDP-N-Acetylglucosamine 1-Carboxyvinyltransferase (MurA)." *The Journal of Biological Chemistry* 287 (16): 12657–67. https://doi.org/10.1074/jbc.M112.342725.

Zimmermann, Lukas, Andrew Stephens, Seung Zin Nam, David Rau, Jonas Kübler, Marko Lozajic, Felix Gabler, Johannes Söding, Andrei N. Lupas, and Vikram Alva. 2018. "A Completely Reimplemented MPI Bioinformatics Toolkit with a New HHpred Server at Its Core." *Journal of Molecular Biology* 430 (15): 2237–43. https://doi.org/10.1016/j.jmb.2017.12.007.